13:18:44 OCA PAD AMENDMENT - PROJECT HEADER INFORMATION 11/16/91

Active

Project #: E-25-645 Cost share #: Rev #: 4
Center # : R6635-0A0 Center shr #: OCA file #:
Work type : RES
Contract#: AX0867554 Mod #: MOD 2 Document : PO
Prime #: Contract entity: GTRC

Subprojects ? : N CFDA:
Main project #: PE #:

Project unit: MECH ENGR Unit code: 02.010.126
Project director(s):
ABDEL-KHALIK S I MECH ENGR (404)894-3719

Sponsor/division names: SAVANNAH RIVER COMPANY / WESTINGHOUSE
Sponsor/division codes: 240 / 004

Award period: 881101 to 920930 (performance) 920930 (reports)

Sponsor amount	New this change	Total to date
Contract value	0.00	74,500.00
Funded	0.00	74,500.00
Cost sharing amount		0.00

Does subcontracting plan apply ?: N

Title: SUPPRESSION OF MOLTEN ALUMINUM - WATER EXPLOSIONS

PROJECT ADMINISTRATION DATA

OCA contact: Mildred S. Heyser 894-4820

Sponsor technical contact	Sponsor issuing office
M.L. HYDER	M.B. SPLETZER
(803)725-3122	(803)725-3016
WESTINGHOUSE SAVANNAH RIVER COMPANY	WESTINGHOUSE SAVANNAH RIVER COMPANY
P.O. BOX 616	P.O. BOX 616
AIKEN, SC 29802	AIKEN, SC 29802

Security class (U,C,S,TS) : U ONR resident rep. is ACO (Y/N): N
Defense priority rating : N/A N/A supplemental sheet
Equipment title vests with: Sponsor X GIT
TITLE TO EQUIP. PURCHASED HAVING A COST OF > $1000 VESTS WITH THE GOVERMENT.
Administrative comments -
MOD 2 EXTENDS PERFORMANCE ENDING DATE TO 9/30/92 . ALL OTHER TERMS AND CONDITIONS REMAIN UNCHANGED.

GEORGIA INSTITUTE OF TECHNOLOGY
OFFICE OF CONTRACT ADMINISTRATION

NOTICE OF PROJECT CLOSEOUT

Closeout Notice Date 04/21/92

Project No. E-25-645 Center No. R6635-0A0

Project Director ABDEL-KHALIK S I School/Lab MECH ENGR

Sponsor SAVANNAH RIVER COMPANY/WESTINGHOUSE

Contract/Grant No. AX0867554 Contract Entity GTRC

Prime Contract No. _____

Title SUPPRESSION OF MOLTEN ALUMINUM - WATER EXPLOSIONS

Effective Completion Date 920930 (Performance) 920930 (Reports)

Closeout Actions Required:	Y/N	Date Submitted
Final Invoice or Copy of Final Invoice	Y	911021
Final Report of Inventions and/or Subcontracts	Y	_____
Government Property Inventory & Related Certificate	Y	_____
Classified Material Certificate	N	_____
Release and Assignment	Y	_____
Other _____	N	_____

Comments_____

Subproject Under Main Project No. _____

Continues Project No. _____

Distribution Required:

Project Director	Y
Administrative Network Representative	Y
GTRI Accounting/Grants and Contracts	Y
Procurement/Supply Services	Y
Research Property Managment	Y
Research Security Services	N
Reports Coordinator (OCA)	Y
GTRC	Y
Project File	Y
Other _____	N
_____	N

NOTE: Final Patent Questionnaire sent to PDPI.

E-25-645

Georgia Tech

THE GEORGE W. WOODRUFF SCHOOL OF
MECHANICAL ENGINEERING

Georgia Institute of Technology
Atlanta, Georgia 30332-0405

S. I. Abdel-Khalik
Georgia Power Professor
and Associate Director

March 18, 1992

Mr. M. Lee Hyder
Westinghouse Savannah River Company
Centennial Corporate Building
1991 South Centennial Avenue
Aiken, SC 29803

Subject: Final Report for Contract #AX 867554

Dear Lee:

Attached are four copies of the final report for the above referenced contract. We appreciate WSRC's long standing support for our research.

Best regards.

Sincerely,

Said Abdel-Khalik

Attachments

cc: OCA, Georgia Tech (2)
P. Dawkins

GTRSR-0012

Effects of Polymeric Additives on the Likelihood and/or Severity of Vapor Explosions

Submitted to
Westinghouse Savannah River Company
Savannah River Laboratory
(Contract #AX-867554)

By

Michael F. Dowling, Bill M. Ip and
Said I. Abdel-Khalik

Georgia Institute of Technology
Nuclear Engineering Program

March, 1992

Abstract

Aqueous solutions of four water-soluble polymers and glycerol were tested for their ability to suppress spontaneous vapor explosions. Poly-(ethylene oxide) (MW 4×10^6), a copolymer of sodium acrylate and acrylamide (Percol 1011), hydroxyethyl cellulose (Natrosol 250HHR), and guar gum (Galactosol 211) were used to make aqueous solutions with viscosity ratios (η_r) of approximately 1.25, 1.50, and 2.00 at 25°C. Twelve grams of tin at 1000°C was poured from a height of 60 cm into a cylindrical plexiglass vessel (I.D. 12.5 cm) containing one liter of each of the listed solutions. The resulting pressure signals were detected with a lithium niobate pressure transducer, amplified, and digitally sampled at 25 μsec intervals. The experiment was repeated ten times with each solution to check consistency and repeatability. The metal fragmented violently every time when pure deionized water was the coolant. The maximum pressures recorded for each experiment were used to compare the relative violence of spontaneous vapor explosions in each solution. Debris particle size distributions were determined for representative experiments with each coolant solution.

Experiments with pure water were carried out to provide a reference of comparison for the other solutions. In fifty experiments using pure water with the molten tin ranging in temperature from 600 to 1000°C only one peak pressure above 100 kPa was recorded (123.4 kPa for an experiment with T_{tin}=900°C). In the polymer solutions the observed frequency of explosions generally decreased as the solution viscosity increased. Poly(ethylene oxide) was the most effective at suppressing the explosions based on pressure records and examination of the debris. No explosions at all were seen when tin at 900 and 1000°C was poured into poly(ethylene oxide) solutions with $\eta_r \approx 2.00$ The other three additives had less effective, approximately similar performance. For all of the coolant additives, however, peak pressures much larger than any recorded in pure water (more than twice as large) occurred occasionally when the solution was only slightly more viscous than pure water. This trend was also observed when glycerol was the coolant additive.

In summary, the data suggest that dilute solutions of polymeric additives, particularly poly(ethylene oxide), may be used to suppress vapor explosions if, and only if, it can be assured that the concentration can be maintained above a threshold value. At lower concentrations, more violent, albeit less frequent, explosions may result.

Contents

List of Figures

Results

Transient Pressure Signals:

Particle Size Distributions:

List of Tables

1 Introduction

Vapor explosions are violent interactions involving a high temperature melt and a cold volatile liquid. Rapid heat transfer from the melt can cause explosive vaporization of the liquid and highly destructive shock waves. Steam explosions are a hazard in any industry where hot metals must be handled near a volatile coolant like water, e.g., the aluminum industry. [1]

The nuclear industry is a potential setting for steam explosion accidents; in this context they are commonly referred to as "fuel-coolant interactions" or FCIs. Failure of the normal and emergency coolant flow in a light water reactor could result in a melt-down of the fuel and cladding. If this melt were to contact residual cooling water, energetic steam explosions could occur with possible damage to the vessel and containment structures and release of radioactivity. (Cronenberg and Benz [2] review the hazard of steam explosions in the nuclear industry.) Situations which could lead to FCIs are considered to be unlikely. For example, the German Risk Study Phase B released in 1990 estimates the likelihood of a total core melt with low containment pressure at 3.2×10^{-6} per year per reactor for the German Pressurized Water Reactor considered in the study (quoted in [3]). Nevertheless, FCIs are regarded as a potential hazard.

One possibility for reducing the FCI risks is to identify an additive for the emergency coolant water which prevents steam explosions or makes them less violent. In the present work we report on the ability of aqueous solutions of high molecular weight, water-soluble polymers to suppress explosions (see Table 1.1 for a list of the polymers used). Polymer additives are attractive because extremely low concentrations (in the range of hundreds of parts per million) cause marked shifts in solution heat transfer and flow characteristics such as the turbulent friction factor (the additives are all drag-reducing).

Numerous studies of steam explosion phenomena have been conducted

Table 1.1: Polymer Additives Used in the Present Investigation

Polymeric Additive	Brand Name	Source
Guar Gum	Galactosol 211	Aqualon Company (Wilmington, DE)
Poly(acrylamide/ sodium acrylate)	Percol 1011	Allied Colloids (Suffolk, VA)
Hydroxyethyl Cellulose	Natrosol 250HHR	Aqualon Company (Wilmington, DE)
Poly(ethylene oxide)	M_W 4×10^6	Aldrich Chemical Co. (Milwaukee, WI)

in the past. In general, this work divides into two groups: "small-scale" laboratory experiments similar to the one described in the present report which involve a few grams of molten metal, and "large-scale" experiments using tens or hundreds of kilograms. (See Farawila and Abdel-Khalik [4] for an extensive review.) Large-scale steam explosions are generally divided into four stages:

- coarse mixing of the melt and coolant, [1]
- local triggering of the interaction,
- propagation of the explosion throughout the melt,
- rapid expansion of the generated coolant vapor.

Small-scale experiments do not completely replicate all four of these stages, but they provide a good model of the triggering phase of a full-size explosion and provide an easily reproducible way of examining the experimental parameters independently. Coarse mixing generates small "cells" of melt surrounded by coolant which are similar to the small melt masses used in the small-scale experiment described below. Initially, these extremely hot drops are separated from the coolant by a stable film boiling layer which prevents explosively rapid heat transfer—when this vapor layer remains intact the metal droplet can solidify without violence. The collapse of film boiling leads to explosive fragmentation of the melt droplet and generates shock waves. These local shock waves are assumed to trigger coherent explosions throughout large volumes of melt during a full-scale FCI. [7, 8] Details of the fragmentation indicate that coolant boiling characteristics, viscosity, and surface tension all play a fundamental role.

---

[1] A few large explosions have been observed without evidence of such mixing ([5], page 28), but it usually occurs and is assumed to be a necessary step [6].

1.1 The Fragmentation Process in Small Melt Drops

The explosive fragmentation of small drops has been studied intensively in recent years using high speed photography, and several theories explaining the collapse of film boiling have been advanced ([8], [5] and references therein). Small drop explosions have a characteristic repeating cycle of growth and collapse [9, 10, 13] which appear to be the result of "coolant jets" penetrating the vapor film layer. The two models below describe different ways these jets could develop and explain the cyclical growth of the vapor "bubble" around the drop.

Model 1: Nelson *et al.* [5] propose an augmented Assymetric Bubble Collapse (ABC) mechanism based on high-speed photographs and pressure signals from explosions of iron oxide (Nelson and Duda [10, 9, 12]) and tin (Frölich and Anderle [13]) triggered by applied shock waves. Their deduced fragmentation mechanism is depicted in Figure 1.

In stage 2 of Figure 1 the film boiling layer expands due to the slight rarefaction following the applied shock wave. As it cools it shrinks again, and the inertia of the surrounding water causes it to collapse (stage 3). The standard ABC model assumes that this process is generally assymetric (stage 3a), so that the mechanical action of the collapse creates jets impinging on the melt surface at high velocities. Nelson *et al.* suggest that collapsing cavitation bubbles (created by the rarefaction) can also give rise to jets, even when the film boiling layer collapses symmetrically (stage 3b). The jets embed small volumes of water under the melt surface which vaporize (stage 4, the next growth cycle) and fragment the outer shell (stage 5). The suddenly increased heat transfer area causes the next cycle of vapor expansion and melt fragmentation.

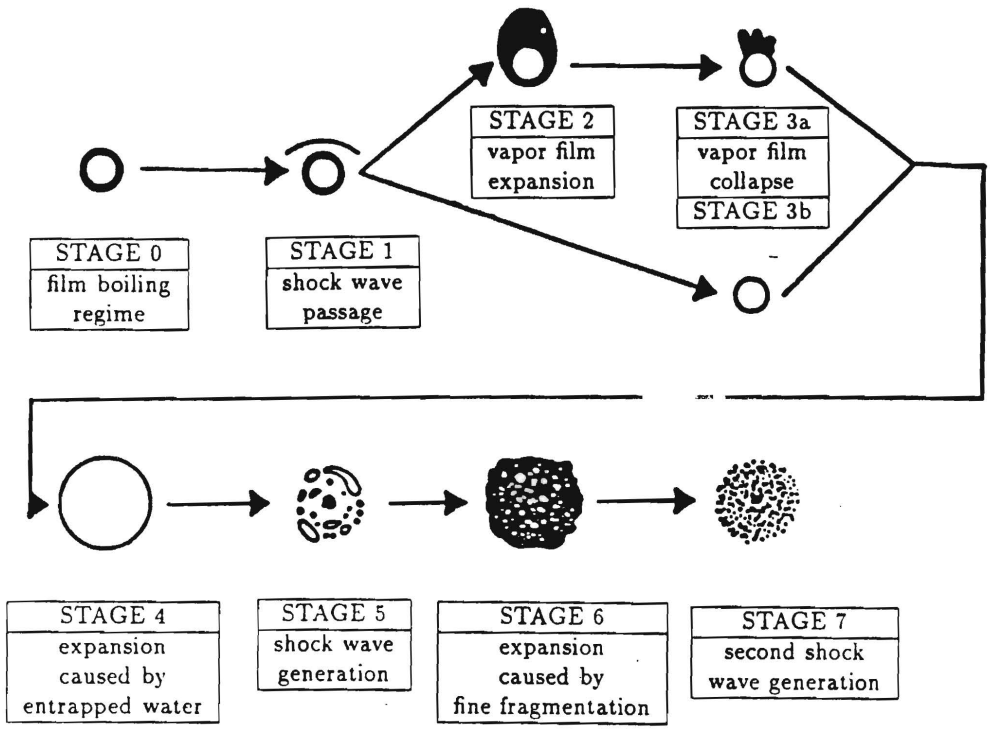

Figure 1.1: Droplet Fragmentation: the Assymetric Bubble Collapse model from [5].

Model 2: Corradini (Corradini [14]) suggests that Rayleigh-Taylor instabilities may also be a source of coolant jets. This mechanism is shown in Figure 2.

The vapor surface moves in response to the applied pulse, and the layer's local thermal resistance changes: As it moves out into the liquid the thermal resistance increases, the vapor begins to cool and condense, and the layer accelerates inward. As it presses inward the thermal resistance drops, the vapor warms and expands, and the layer accelerates outward. The instability grows as neighboring regions begin oscillating in opposite directions (stage 2) and grow into longer "fingers" of intertwined water and vapor. The oscillating fingers grow into jets and eventually penetrate the melt (stage 3). Stages 4a and 4b correspond to stage 4 of Figure 1; fragmentation of the outer shell is caused by the rapid vaporization of the embedded water. The boiling layer is reestablished above the newly exposed surface of the melt, and the same type of instability recurs; the cycle continues.

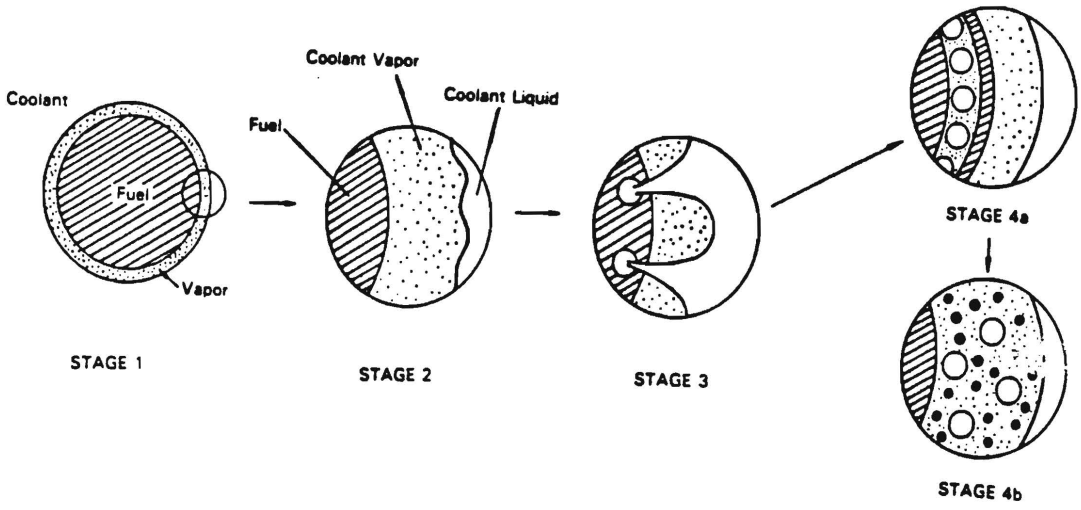

Figure 1.2: Droplet Fragmentation: the Raleigh-Taylor Instability model from [8].

The two models above and the experimental data on which they are based suggest that there are several important parameters in a melt/coolant interaction. The viscosities and surface tensions of the melt and coolant (and their temperature dependence) and the coolant's ability to wet the melt surface will control mixing properties, interface properties, and the formation of jets. The coolant's boiling point, boiling curve (heat flux as a function of $T_{surface} - T_{liquid}$), critical heat flux, and homogeneous nucleation temperature (the temperature at which vapor bubbles can spontaneously form in bulk liquid) will affect the heat transfer from melt to coolant. Additionally, both models attribute the fine fragmentation to "flash vaporization" of water droplets embedded by jets within the melt, which requires that the drops reach the homogeneous nucleation temperature for water, ≈543 K. Nelson *et al.* propose that only droplets below a critical diameter are able to flash vaporize. Otherwise, a new film boiling layer can grow and inhibit heat transfer long enough for the embedded water drops to reach the surface again without fragmenting the melt. ([5], pp. 48–52) The surface tensions and viscosities of the molten metal and coolant will also determine how the coolant jets break up and will affect the size of the embedded water droplets. Coolant heat transfer properties will determine the time needed to heat embedded droplets to the nucleation temperature.

1.2 Previous Experiments Involving Viscous Coolants

In general, viscous coolants suppress explosions. They cause falling droplets of melt to entrain more air upon entry into the coolant (which stabilizes film boiling [15]), and they tend to damp out oscillations in the boiling layer. Several studies have reported that viscous coolants suppress explosions, for example, Kim [16], Nelson and Guay [15], and Flory [17].

Table 1.2 gives a brief summary of the results of these experiments.

Kim [16] studied triggered explosions of iron oxide in aqueous solutions of cellulose gum and determined the efficiency of explosions following applied trigger pressures of 200 and 400 kPa. For the 400 kPa case, the efficiency clearly drops from approximately 6% to almost 0% as the solution viscosity increased from 40 centipoise to 240 centipoise (corresponding to solution viscosity ratios from approximately 40 to 240). Nelson and Guay [15] used aqueous solutions of glycerol and cellulose gum to increase the viscosity of the coolant. They observed that the depth at which spontaneous explosions of tin occurred increased as the solution viscosity increased. When the viscosity of the cellulose gum solutions exceeded approximately 25 centipoise at room temperature the molten tin fell to the bottom without exploding. (The viscosity value at the solution boiling point was much lower: 15 centipoise) Flory *et al.* [17] used carboxymethyl cellulose to increase the viscosity of water by approximately 5 times and found that the fragmentation of tin and other metals was greatly reduced or totally prevented.

On the other hand, McCracken observed more complicated behavior. He estimated the percentage of the metal which was finely fragmented due to spontaneous vapor explosions and used these figures to compare the violence of explosions in aqueous solutions of sugar and glycerol. In McCracken's experiment the weight percentage of sugar or glycerol was held constant while the solution viscosity varied with coolant temperature. When the coolants were at 20°C explosions in viscous solutions of sugar and glycerol had less fragmentation than explosions in pure water. At higher coolant temperatures there was more fragmentation in the viscous solutions than in water. He also observed that when explosions did occur in the viscous solutions, they appeared to be more violent than those in water. Nevertheless, McCracken concluded that coolant viscosity was not an important parameter in vapor explosion phenomema. Detergent added to lower the surface tension of the coolant also had a negligible effect in his experiments.

Table 1.2 also includes results from Nelson and Duda [12], who examined the importance of coolant composition by comparing results for pure water, pure n-pentadecane (a paraffin hydrocarbon), and an aqueous solution of ammonium sulfate. Their triggered experiments with molten iron oxide were performed with the same apparatus used by Kim (Ref. [16] above). The paraffin hydrocarbon was flammable, and the resulting noncondensible gas stabilized film boiling as the molten metal descended and completely prevented explosions. Ammonium sulfate, a soluble salt which has reportedly suppressed vapor explosions in a system of molten salt/water [19], did not suppress triggered explosions of the iron oxide when used in a 20 $^{w}/_{o}$ solution.

Obviously, extremely viscous solutions can suppress spontaneous explosions. Experimental data and hypothetical models of the fragmentation process indicate that several other coolant parameters should influence steam explosions (see Ref. [5] and references therein), including boiling heat transfer properties and surface tension. The fragmentation observed during a vapor explosion is believed to be caused by the rapid expansion of coolant embedded beneath the surface of the molten metal by liquid jets [5]. The viscosities and surface tensions of the melt and coolant (and their temperature dependence) and the coolant's ability to wet the melt surface will control mixing properties, interface properties, and the formation of jets. The coolant's boiling heat transfer characteristics will affect the heat transfer from melt to coolant. The dilute solutions of polymeric additives used in the present investigation had relatively low viscosities; however, the polymer concentration was sufficiently high to affect significantly the solution boiling heat transfer characteristics.

As Table 1.2 indicates, many of the previously tested solutions were extremely viscous and impractical for use as a reactor emergency coolant. The dilute polymer solutions examined in the present study had viscosity ratios ($\eta_r \equiv \eta_{solution}/\eta_{solvent}$) of less than 4.00 at room temperature.

Table 1.2: Previous Reports of Coolant Viscosity Effects

Author and Reference	Melt Material	Coolant	Viscosity Ratio (25°C)	Results and Comments
Kim [16]	Iron oxide	Cellulose Gum (aqueous solution)	40–240	Explosion efficiency decreased as viscosity increased. Weak explosions could be initiated even at $\eta_r \approx 240$ if the applied trigger pressure was strong enough.
Nelson and Guay [15]	Tin	Glycerol, Cellulose Gum (aqueous solutions)	1–24	No spontaneous explosions seen in a glycerol solution above $\eta_r \approx 15$. Depth of melt when it exploded increased with viscosity.
Flory *et al.* [17]	Tin, Lead	Carboxymethyl Cellulose (aqueous solution)	5	Explosions completely suppressed.
Nelson and Duda [12]	Iron oxide	Ammonium Sulfate (20 $^w/_o$ aqueous solution)	Not given	Results similar to those with pure water, with a well-developed explosion and fine fragmentation.
"		n-pentadecane, (n-$C_{15}H_{32}$) (pure solution)	Not given	Pyrolysis of the coolant created copious amounts of noncondensable gas stabilized film boiling layer. Explosions could not be triggered at all due to pyrolysis of the coolant.
McCracken [18]	Tin	Sucrose, Glycerol (aqueous solutions)	1–4	Results similar to those with pure water. Explosions when they did occur were the most violent. Critical coolant temperature (above which no explosions occur) increased about 5–10°C.

1.3 Boiling Heat Transfer in Polymer Solutions

The coolants used in the present study are all dilute aqueous solutions of drag-reducing, high molecular weight, nonvolatile polymers. In laminar flow such solutions obey the heat transfer correlations for Newtonian liquids; however, for turbulent flow the heat transfer coefficients and friction factors are reduced dramatically ([20], pp 6–9). These additives also affect boiling heat transfer, but published data are rather limited. In general, they leave the boiling point nearly unchanged because of their low concentration and nonvolatility [20], but they shift the boiling curve along the ΔT axis, and they can affect the critical heat flux value.

Kotchaphakdee and Williams [21] studied the effects of hydroxyethyl cellulose and polyacrylamide on nucleate boiling in water using samples of various average molecular weights for each polymer. With a flat plate for the heat source, they found that for a given temperature difference polymeric additives all increased the heat flux—in some cases as much as 250%. A non-polymeric additive (acrylamide monomer) decreased the heat flux slightly. Their data indicated that the peak heat flux for hydroxyethyl cellulose would probably not be significantly different from that of pure water whereas the polyacrylamides probably would increase it, however, they could not measure the peak flux values. The boiling curves which they obtained are shown in Figure 1.3. Surface tension effects were not significant.

Paul [20] examined steady-state nucleate boiling behavior for all four of the polymeric additives used in the present study.[2]For nucleate boiling on a heated platinum wire, he found that for a given temperature difference every additive decreased the heat flux (Figure 1.4). This result is opposite that of

[2]The copolymer of acrylamide and sodium acrylate used by Paul was Separan AP-30, formerly manufactured by DuPont. DuPont specified Percol 1011, made by Allied Colloids, as the closest replacement when it ceased production.

Kotchaphakdee and Williams. For each polymeric additive Paul found that the shift in the boiling curve could be explained using a standard correlation for the effects of viscosity and surface tension. He concluded that other factors (polymer type, molecular weight, concentration) were important only for their effect on the viscosity and surface tension.

Transient boiling data for dilute polymer solutions were obtained by Rouai,[22] who quenched a hot brass ball in an isothermal pool and calculated the transient boiling curve by solving the inverse heat conduction problem. He was able to obtain the entire boiling curve including the critical heat flux and minimum film boiling temperature values. Poly(ethylene oxide) and guar gum solutions increased the critical heat flux as much as 1.8 times. The heat flux in the film boiling regime was also larger than that for pure water. Poly(ethylene oxide) also increased the Leidenfrost temperature significantly. Similar concentrations of polyacrylamide and graphite gave results almost identical to those for water.

These data suggest that polymeric additives may significantly affect the transient boiling phenomena inherent in steam explosions. They also affect the coolant viscosity at relatively low concentrations. To this end, the present investigation was undertaken to examine the competing effects of enhanced heat transfer and increased solution viscosity produced by small concentrations of polymeric additives.

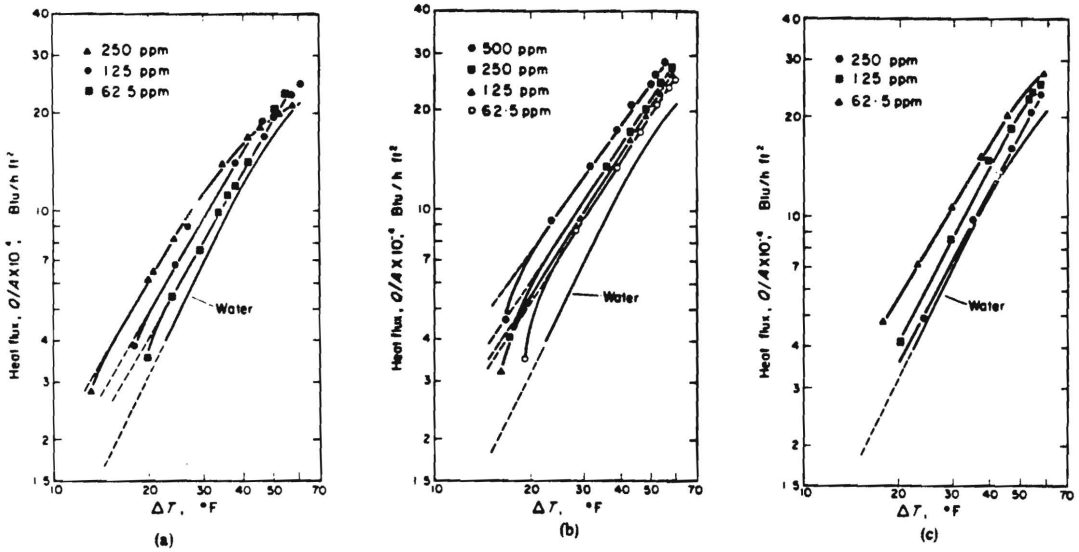

Figure 1.3: The Effect of Nonvolatile Drag-Reducing Agents on the Boiling Curve of Water: Flat Plate Boiling (from [21]). Aqueous solutions of the following polymers: (a) Hydroxyethyl Cellulose, (b) Polyacrylamide (Separan NP10), (c) Polyacrylamide (Separan NP20).

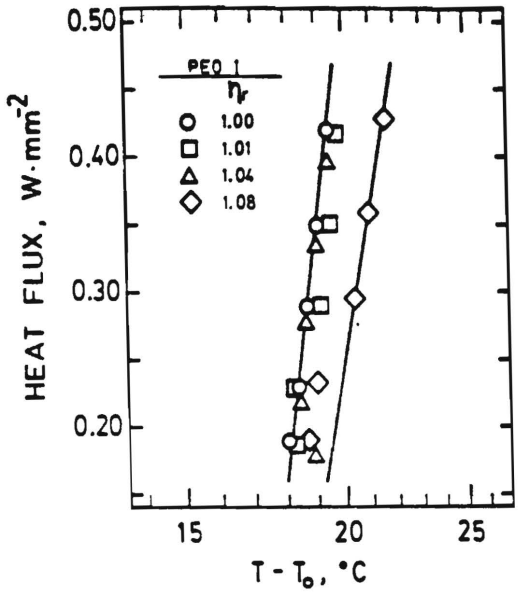

a) Poly(ethylene oxide)
($Mw = 10^6$)

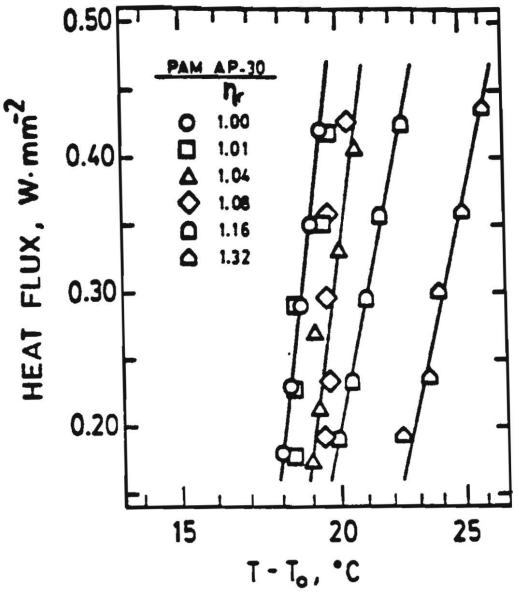

b) Polyacrylamide
(Separan AP-30)

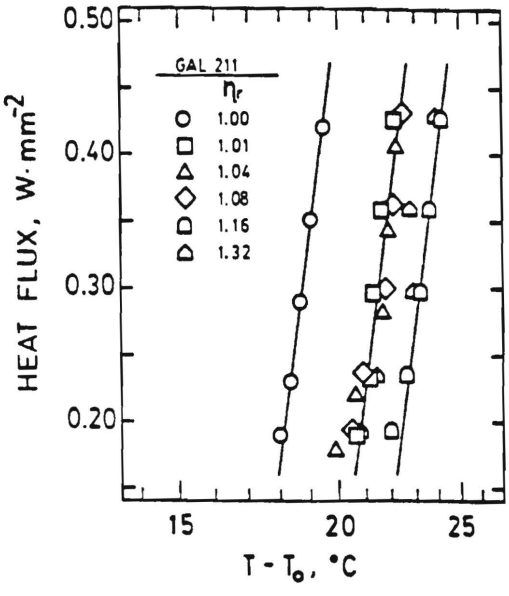

c) Guar Gum (Galactosol 211)

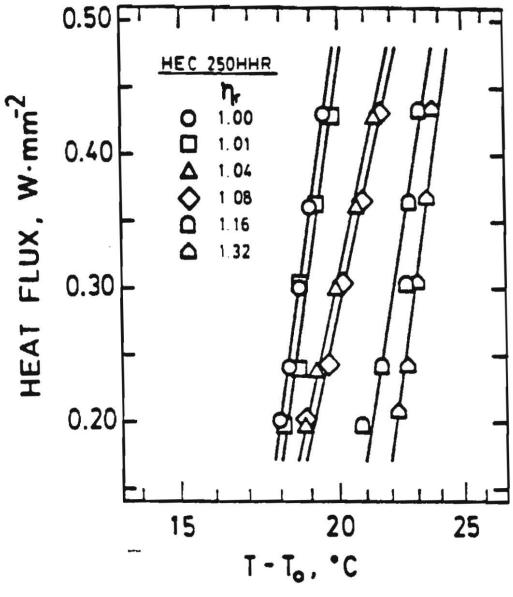

d) Hydroxyethyl Cellulose
(Natrosol 250HHR)

Figure 1.4: The Effect of Nonvolatile Drag-Reducing Agents on the Boiling Curve of Water: Platinum Wire Boiling (from [20]).

2 Physical Properties of the Polymers

2.1 Description and Molecular Structures

The comments on each of the polymers were culled from Paul [20] and information supplied by the manufacturers.

NATROSOL Hydroxyethylcellulose 250HHR A modified natural polymer subject to biological degradation. Long mixing times needed (6–8 hours). Virtually insensitive to shear degradation. A non-ionic surfactant.

GALACTOSOL 211 (Guar Gum) A galactomannan polysaccharide derived from the guar plant. Subject to biological degradation. Solubility in water is limited by viscosity. (For more viscous solutions a fine suspension may be the best that can be achieved.) Virtually insensitive to shear degradation. Exposure to boric acid causes gel formation. A non-ionic non-surfactant.

PERCOL 1011 (Poly(acrylamide/sodium acrylate)) A polyacrylamide derivative. Average molecular weight 10– 20 million (unofficial company estimate). Subject to chemical degradation from Fe_6^{+3} ions in solution (from rust). Attack by residual persulfate polymerization initiator can occur as solutions age, but small amounts of added alcohol can prevent this. Percol 1011 is similar to Separan AP-30 (formerly manufactured by Dow and used in the study by Paul [20].) An anionic non-surfactant.

POLY(ETHYLENE OXIDE) Average molecular weight 4 million. A linear polyer with poor shear stability. Extreme care should be used in preparing these solutions. A non-ionic surfactant. Poly(ethylene oxide) has a negative solubility coeffiecient in water; it becomes less soluble as the temperature increases. Near the boiling point it precipitates and clouds the solution [23].

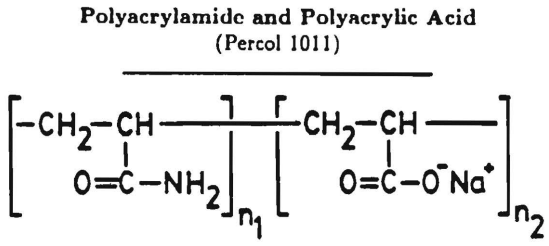

Figure 2.1: Molecular Structure of the Poly(acrylamide/sodium acrylate) (Percol 1011)

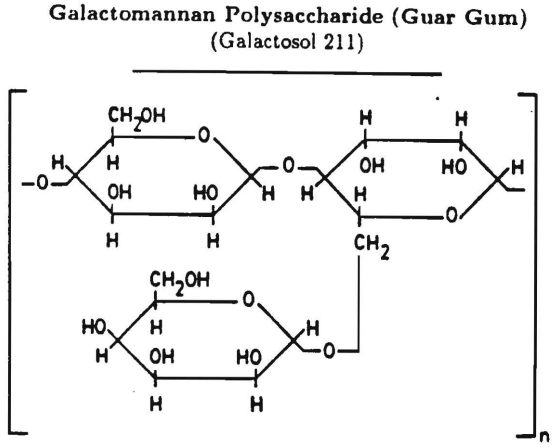

Figure 2.2: Molecular Structure of Guar Gum (Galactosol 211)

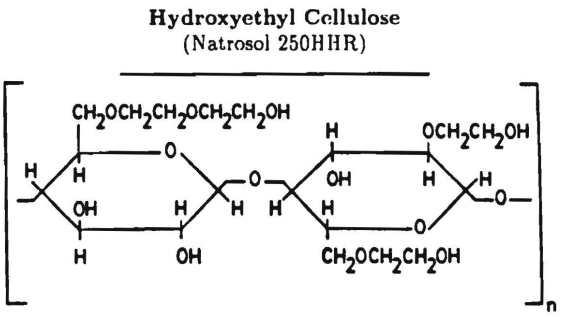

Figure 2.3: Molecular Structure Hydroxyethyl Cellulose (Natrosol 250HHR)

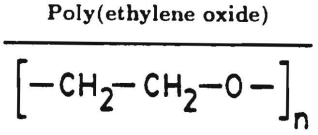

Figure 2.4: Molecular Structure of Poly(ethylene oxide)

2.2 Relation of Polymer Concentration to Viscosity

High molecular weight polymers have the property of increasing the viscosity of aqueous solutions. The viscosity characteristics for a given type of polymer in solution are extremely sensitive to the length of these chains—longer chains affect the solution viscosity more than short ones. Thus, in addition to the chemical identity of the polymer, information about the average length of the chains and the distribution of lengths in the sample must be known to predict viscosity properties. Some polymers are commercially available in different "lengths" which have different viscosity properties in solution.

For dilute solutions of non-ionic polymers the viscosity ratio, (η_r, where $\eta_r = \eta_{solution}/\eta_{solvent}$), may be obtained from a Taylor series expansion in the polymer concentration (c):

$$\eta_r = 1 + [\eta]c + H[\eta]^2c^2 + \ldots \tag{2.1}$$

In equation 2.1 $[\eta]$ is called the intrinsic viscosity, and H is referred to as the Huggins constant. (For the range of viscosities examined in this investigation a second order expansion was sufficiently accurate.) The polymers are supplied in a fine, powdery form, and polymer concentrations in solution are most conveniently measured in weight parts per million (wppm), so that the units of intrinsic viscosity are $(\text{wppm})^{-1}$ and the Huggins constant is unitless. The intrinsic viscosity is determined experimentally for each polymer: viscosity ratios are determined for solutions of known concentration, and the data is plotted on a graph of $(\ln \eta_r)/c$ *vs.* c. The result is a straight line in most cases, and the intrinsic viscosity is then defined as the limit of $(\ln \eta_r)/c$ as $c \rightarrow 0$. Once $[\eta]$ is known, the Huggins constant H is determined by fitting the experimental data to the parabola in equation 2.1. The constants for the polymers used in the present investigation are given in Table 2.1 below. The data and the curves calculated using equation 2.1 are shown in Figure 2.5.

Table 2.1: Intrinsic Viscosities and Huggins Constants for Polymers used in the Present Investigation (Parameters for Equation 2.1)

Polymeric Additive	Brand Name	Intrinsic Viscosity $(\text{wppm})^{-1}$	Huggins Constant
Guar Gum	Galactosol 211	0.00100	1.49
Poly(acrylamide/ sodium acrylate)	Percol 1011[a]	0.00820	0.37
Hydroxyethyl Cellulose	Natrosol 250HHR	0.00135	0.87
Poly(ethylene oxide)	M_W 4×10^6	0.00121	0.79

[a]Data taken with Separan AP-30, an identical polymer.

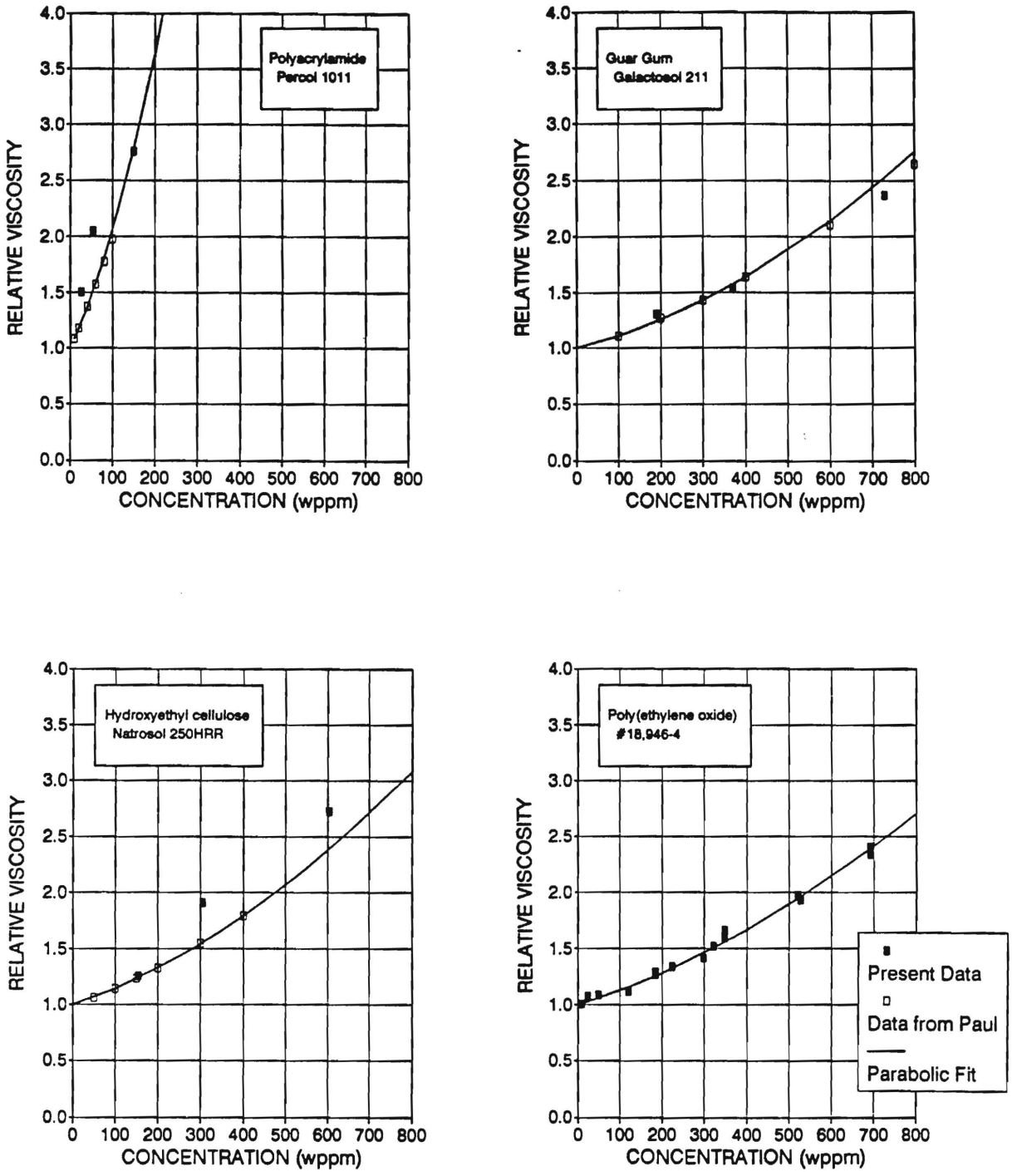

Figure 2.5: Solution Viscosity Ratios as a Function of Concentration for all Polymers used in the Present Investigation. (Curves shown were calculated from Equation 2.1 using the Parameters Listed in Table 2.1.)

2.3 Polymer Solution Surface Tensions

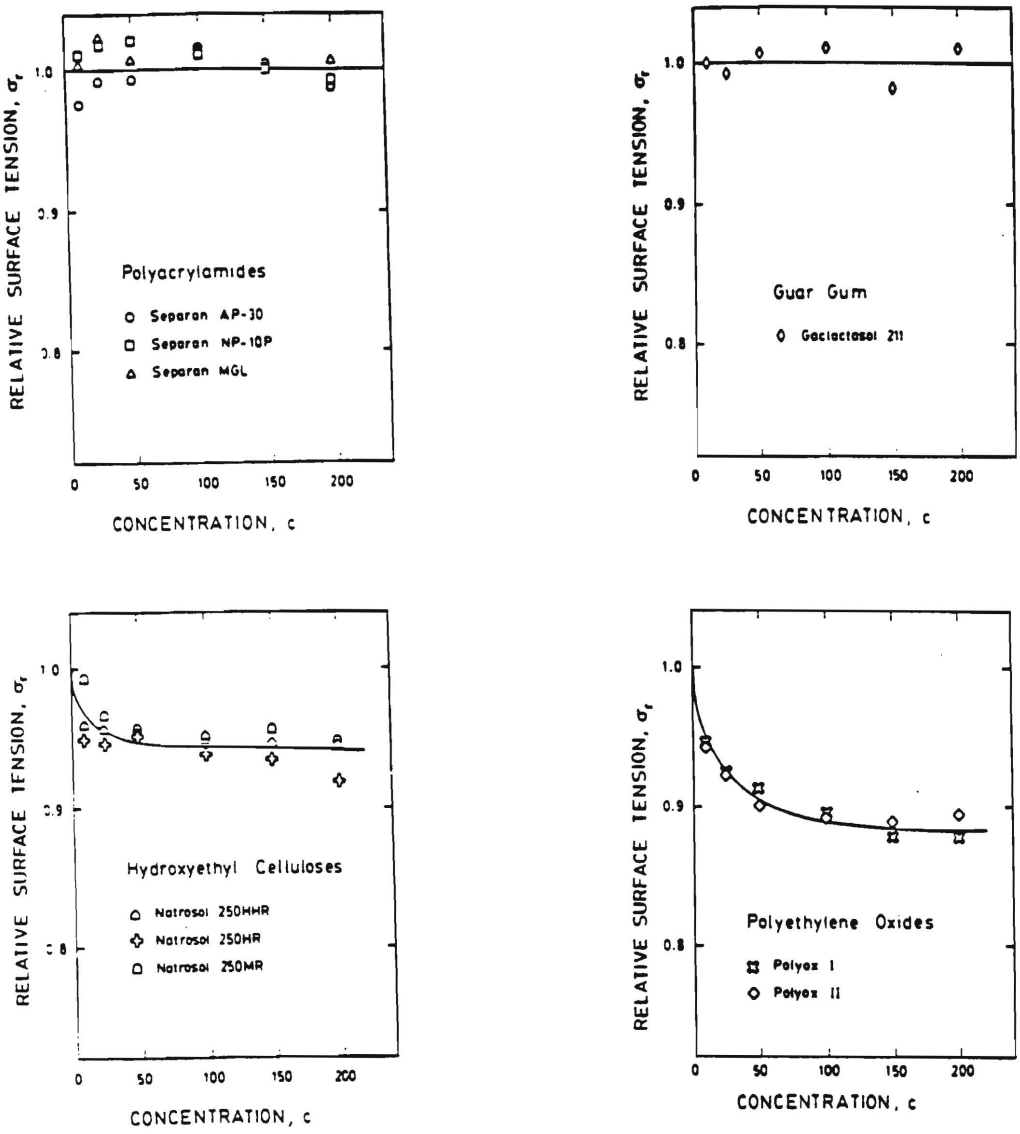

Figure 2.6: Surface tension measurements from Paul [20].

2.4 Age Effects in Poly(ethylene oxide) Solutions

The viscosity of dilute aqueous solutions of poly(ethylene oxide) has been observed to decrease with time [24]. This effect is attributed to fragmenting of the linear molecules, since viscosity is highly dependent on the longest molecules present. In the figure below the viscosity of an aqueous solution of PEO is shown as a function of wall shear rate, since PEO is a non- Newtonian fluid. (The viscosity values presented in this report were all measured at low wall shear rates—less than 200 sec^{-1})—where the viscosity is nearly independent of shear rate.) Over the course of four days the viscosity (measured at low shear rates) drops by almost 15%.

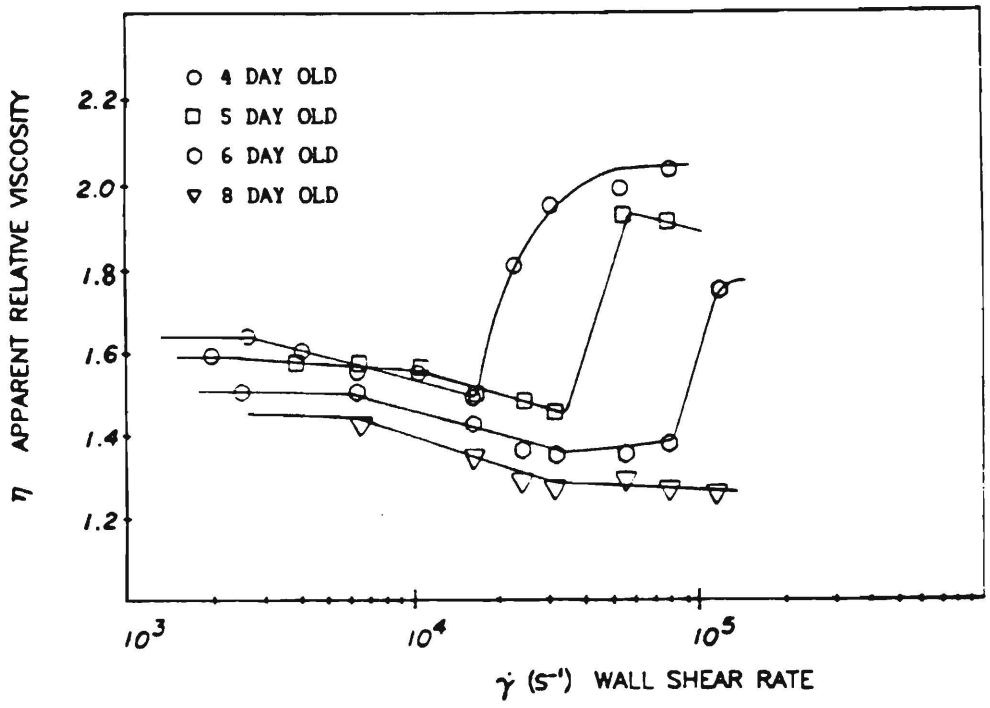

Figure 2.7: Effect of Age on the Relative Viscosity of a 500 wppm PEO Aqueous Solution

3 Experimental Apparatus and Procedures

3.1 Experimental Apparatus

The apparatus consists of three main systems: (1) the furnace and tipping mechanism, (2) the coolant tank and protective housing, and (3) the instrumentation. These systems are described in detail below. A schematic diagram of the experiment is given in Figure 3.2. Figure 3.3 contains a more detailed drawing of the tipping mechanism, and a photograph of this device is shown is Figure 3.4.

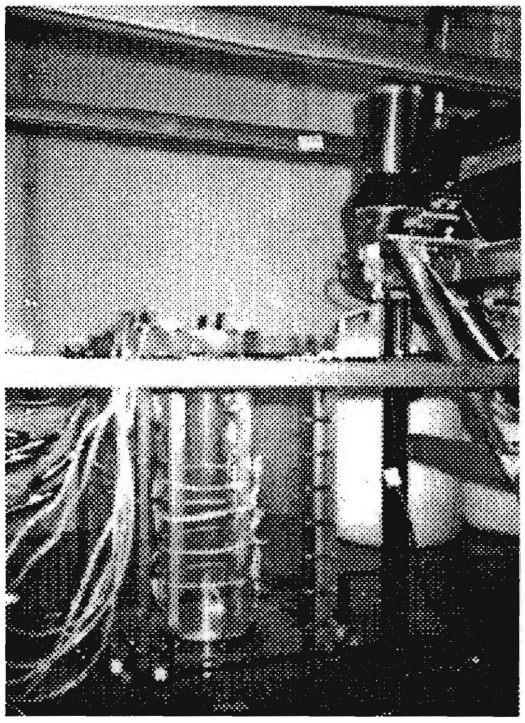

Figure 3.1: Photograph of the Experimental Apparatus

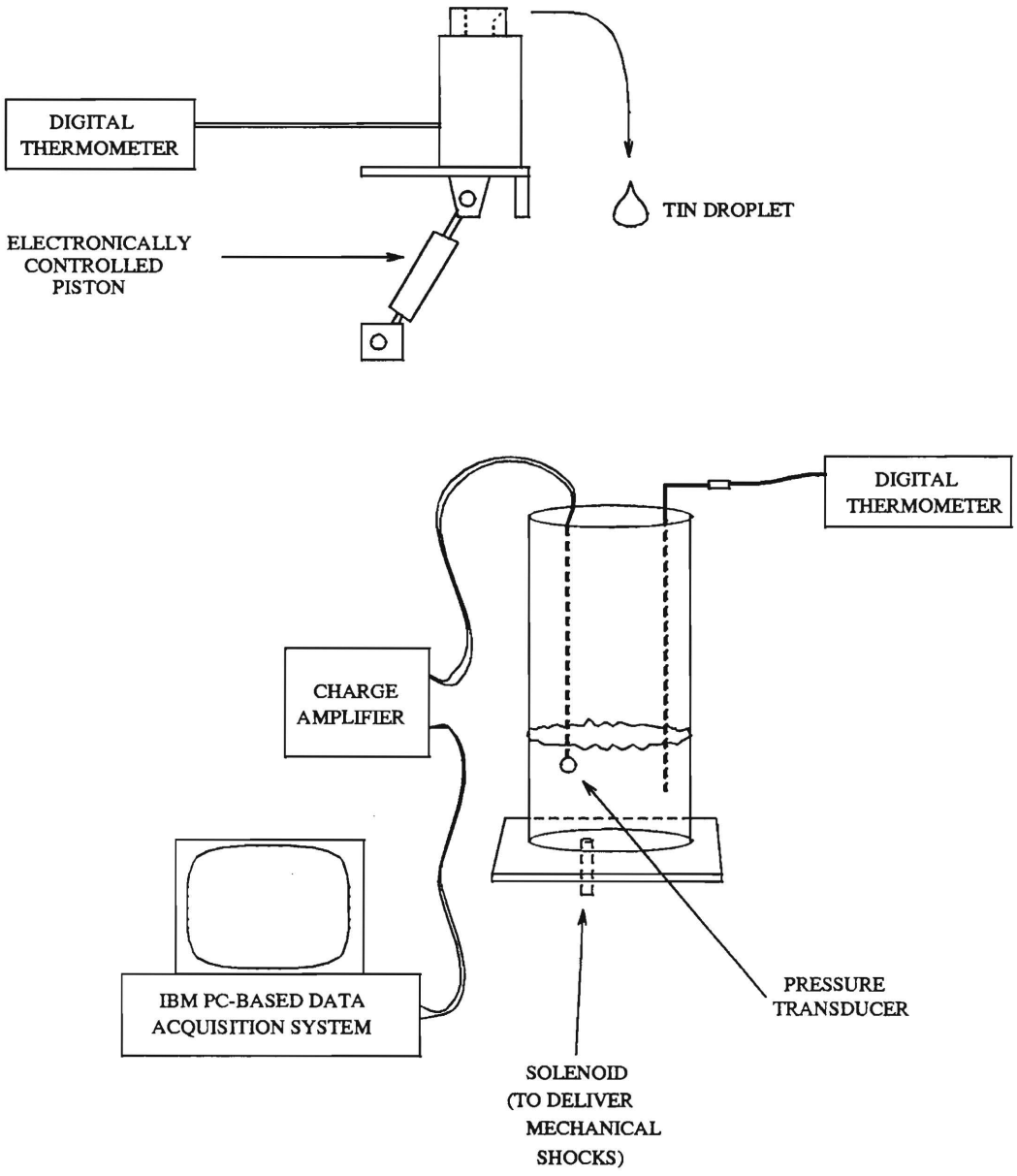

Figure 3.2: Schematic Diagram showing Experimental Arangement

1. **Furnace and Tipping Device**

Furnace and Crucible: Tin samples were melted in an electrically heated muffle furnace sold by Cole-Parmer (model L-02222-00). A temperature control box sold with the furnace regulated the temperature to $\pm 10°C$ using a thermocouple sensor in contact with the bottom of the crucible. The maximum operating temperature for the furnace was approximately 1200°C.

The furnace muffle was mounted on an iron base with a wooden handle to facilitate pouring. The base was attached to a metal plate with a hinge along the front side (refer to Figure 3.3), and samples were poured out by tipping the entire furnace forward. The distance from the hinged axis to the lip of the crucible cup was 26.0 cm.

The melt was held in a tall graphite crucible in the shape of a tall cup (open at the top) approximately 12.5 cm high and 3.5 cm inner diameter. The upper lip of the cup has a notch which serves as a spout so that the molten metal can be poured out easily. The crucible was covered while the samples were heated, but the cover could be removed easily to check the appearance of the melt and to insert additional temperature probes as needed.

Crucible Lubricant: A boron nitride coating (Boron Nitride Lubricoat from ZYP Coatings, Inc., Oak Ridge, TN) was painted onto the inner surface of the crucible to prevent the molten tin from sticking as it was poured. Without the coating, the graphite of the crucibles tended to pit and disintegrate after several heating cycles. This lubricant was extremely effective when the tin temperature was above approximately 800°C—the molten metal did

not wet the surface and flowed quickly and easily, similar to a drop of mercury at room temperature. However, at lower temperatures the coating was less effective: the tin had a tendency to spread out and stick on the spout and solidify. Because the coatings are water-based, small amounts of NO_x gases can be produced on the first heating if the coating is not completely dry. Freshly coated crucibles, therefore, were first heated without any sample inside to ensure that no contaminants were present when samples were introduced. Once dry, the coatings did not react at all with the molten tin in the temperature range used. Recoating was usually necessary after several dozen experiments to repair chips and small cracks.

Argon Cover Gas: To prevent oxidation of the samples, argon gas was used to expel the air from the crucibles before the tin was added and to cover the sample as it heated. Cylinders of purified argon were used. (On one occasion a cheaper grade of argon was used without any visible oxidation of the sample.) The gas flowed through a length of 1/4 inch stainless steel tubing which extended almost to the bottom of the crucible. The pressure was regulated at 20±2 psia, giving a flow rate of 0.24 liters per minute at 25°C. (The flow rate was monitored to ±5% with a Brooks rotameter tube.) No oxidation at all occured when the cover gas was used; in its absence the surface of the tin granules quickly whitened.

Tipping Mechanism: An electrically-controlled air piston provided reproducible tipping of the furnace. One end of the piston was held fixed to the tabletop, and the other was attached to the furnace baseplate 9 cm from the hinge on the front edge using a pin so

that it could swivel freely as the plate tipped. Air flow to the piston was controlled by a solenoid air valve connected to a regulated 40 psig air line. When the valve was opened the piston moved at a constant velocity, pushing the furnace from its initial upright position to a position 15° below the horizontal in approximately 12.4 seconds. (Thus, the lip of cup was moving with a velocity of approximately 4.2 cm/sec downward when the tin poured out.) The point at which the molten tin droplet ejected from the crucible spout varied slightly with the temperature of the molten tin: above 800°C the melt usually split into a cluster of droplets which poured from the spout in rapid succesion approximately 10° below the horizontal, at lower temperatures the melt did not flow as easily on the lubricant coating, and the droplets fell off the tip of the spout at the bottom of its swing. Usually, 1–4 individual drops of melt could be distinguished pouring from the crucible.

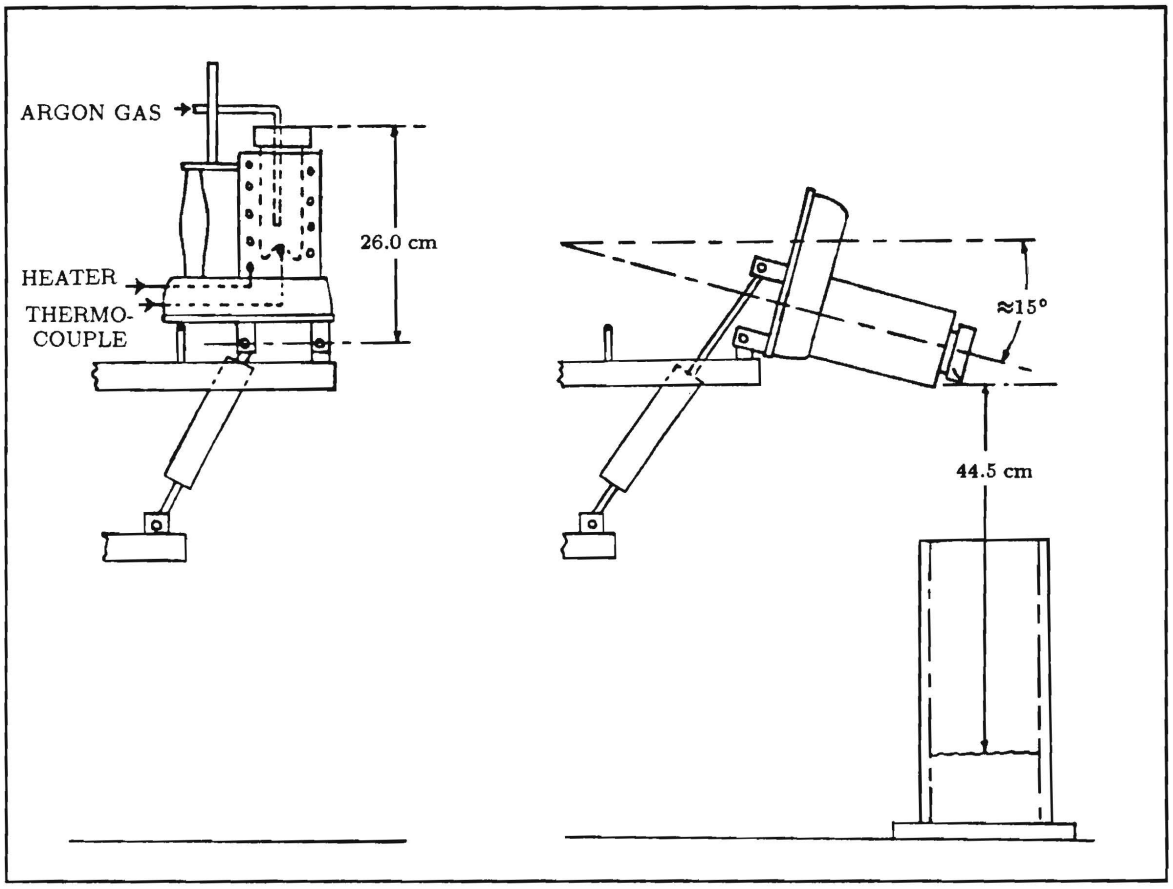

Figure 3.3: Schematic Diagram of the Furnace and Tipping Mechanism

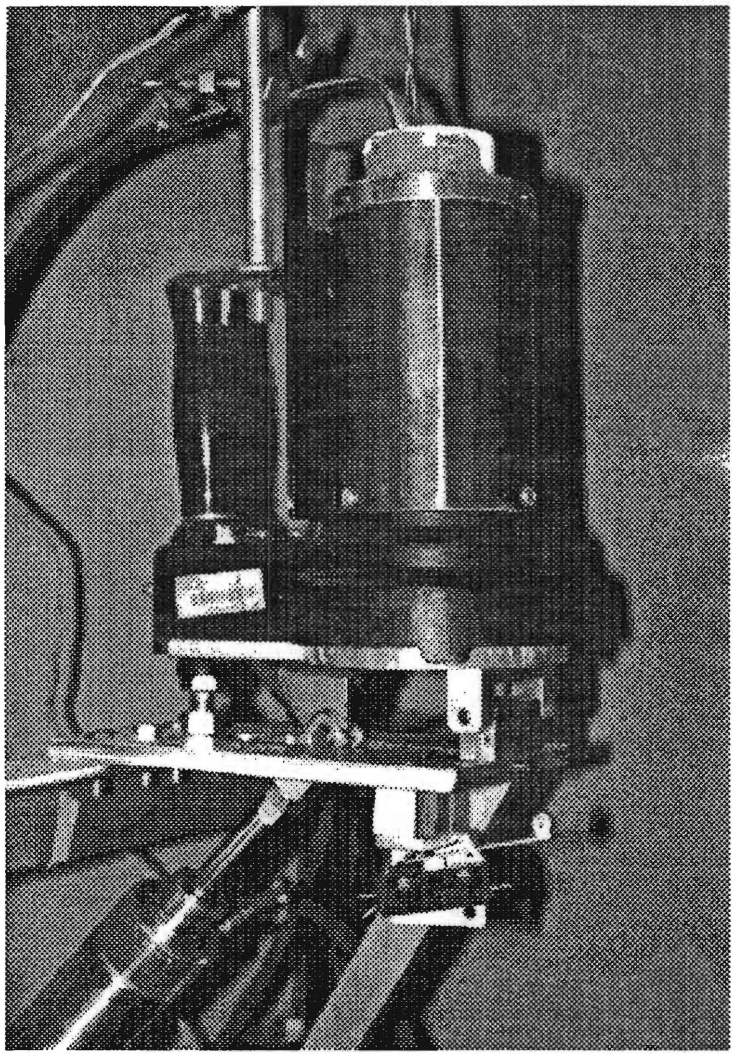

Figure 3.4: Photograph of the Tipping Mechanism and Furnace

2. **Coolant Vessel and Protective Housing**

Coolant Vessel: The vessel was made from a plexiglass cylinder 12.5 cm inner diameter, 34.0 cm tall, with walls 1.3 cm thick. The bottom was also made from plexiglass, and the vessel was sealed by fusing the two pieces together and securing the arrangement with four screws tapped throught the bottom slab into the cylinder walls. No damage to the vessel from the explosions was ever observed. With one liter of coolant solution in the vessel the liquid height was approximately 10.0 cm above the bottom and 44.5 cm below the crucible spout at its lowest position.

Protective Housing: A protective box 47.0 cm high and 30.5 cm on each side made from slabs of plexiglass 2.5 cm thick surrounded the vessel on three sides and the bottom. A solenoid with a spring-loaded metal pin was attached the the bottom plate so that it could deliver a sharp blow directly to the bottom of the vessel. (The pressure signal from this blow was used to ensure that the data acquisition system was working properly before each experiment and that the piezoelectric crystal pressure sensor had not been damaged.)

3. **Instrumentation**

Pressure Transducers: Piezoelectric crystal transducers purchased from Specialty Engineering Associates (Milpitas, CA) were used to measure the transient pressure waves in the liquid during the experiment. The transducers were made from circular disks of z-cut lithium niobate 0.64 cm in diameter and 0.064 cm in thickness with gold-over-chrome vapor-deposited electrical contacts. The

cable (approximately 115 cm in length) was a fine gage twisted pair with a grounded shield (Beldon #8640), and a conductive coating extended the shielding over the crystal as well. One side of the twisted pair was also grounded; the cable terminated in a standard BNC connector which could be plugged directly into the charge amplifier. The capacitance of the sensor (including cable) was 300±5 pF. The sensing element was covered in plastic and painted with polyurethane to waterproof the assembly. A thin layer of silicone rubber adhesive sealant was added to the sensing element and that portion of the cable which would be submerged in the liquid to assure waterproofing. The conversion factor from charge output to pressure was determined experimentally to be 61.25 kPa/pC (see Appendix B for the calibration procedure).

During the experiments, the cable was secured to a glass rod and then clamped to the top of the vessel so that the sensor did not move. For each experiment, the sensor was positioned approximately 1.5 cm from the wall of the vessel halfway between the liquid surface and the bottom.

Charge Amplifiers: A model 5004 charge amplifier from Kistler Instrument Corporation (Amherst, NY) was used to amplify the signals from the pressure transducer. (Piezoelectric sensors produce charge signals rather than voltage signals in response to an applied pressure.) The circuit diagram and frequency response characteristics for the amplifier are given in Appendix **??**. Twelve capacitor settings are provided to select the pressure range of interest, three resistor settings to choose a low frequency cut-off for measurements, and a ten-turn dial to adjust for the transducer sensitivity. Each of these settings was fixed for all of the data in this investi-

gation. The most sensitive scale was used, and the resistor was set to "Short" (giving a low frequency 3dB cut-off of 100 Hz). The sensitivity dial was locked on a convenient value. (More details about the effect of these settings are given in Appendix B.) High frequencies were cut-off using a 180 kHz 3dB filter. The amplifier and pressure transducer were calibrated as a single measurement unit to give a conversion factor of -24.01 kPa/Volt for abrupt pressure jumps. (Appendix A describes the calibration procedure used and the interpretation of its results.) The amplifier output is limited to ± 10 Volts (240.1 kPa), and an indicator light is provided which flashes when the output has saturated.

Data Acquisition System: Transient pressure signals from the charge amplifier output were digitized, stored, and analyzed using an EGAA Computerscope data acquisition system from RC Electronics (Goleta, CA). The system includes an analog-to-digital conversion board which plugs into a personal computer and software to control the board, display signals, and analyze data. Our system was installed on an AT- compatible with a monochrome VGA monitor (the sytem requires an XT- compatible with EGA monitor or better). The board provides 12 bit A/D conversion over a user-supplied voltage range, and the data samples are stored as two 8 bit bytes. The Computerscope software allows the system to function as a 16 channel digital oscilloscope with a maximum data acquisition rate of 1 MHz for a single channel, and a maximum data buffer of 32 kBytes.

For the experiments conducted in this investigation, the maximum voltage range of ± 10 Volts was used in the A/D conversion. (Thus, the voltage was sampled with an error of ± 5 mV.) Data acquisi-

tion was triggered when the pressure signal exceeded a very low threshold, 25 mV (0.60 kPa). (This level was still high enough that the pressure disturbance due to the entry of the melt into the coolant would not trigger the system.) In order to cover a long enough timespan, the period between data samples was set at 25 μsec. This is a potential problem, since the sampling frequency (40 kHz) was well below the amplifier's filter cut-off point, and the rise time of the explosion pressure shock waves was much less than 25 μsec. For this reason, the experiment was repeated several times to obtain a more accurate idea of what the peak pressure values were.

Thermocouple Temperature Sensors: K-type thermocouples enclosed in stainless steel sheaths were used to measure the melt temperature. The sheaths were not coated, but there was no evidence that the steel was reacting with the molten tin. A digital thermometer from Omega (Stamford, CT) converted the thermocouple signal into a temperature accurate to $\pm 1°C$ in the range of interest.

4. Materials

Tin Metal: High quality granulated tin from Fisher Scientific (catelog #T127-500) was used for all of the experiments. This is a fine grain form of tin (20 mesh) which melts quickly due to the small size of the grains. Iron and copper impurities were present at 0.001% levels, and lead was present at 0.008%.

Polymer Additives: Each of the polymer additives came in the form of a dry, fine powder. Each sample came in an air-tight container supplied by the manufacturer, and all were stored at room temperature for several months during the course of the experiment.

Deionized Water: Deionized water used to make all of the polymer solutions and to rinse the coolant vessel between experiments came from a Barnstead three cartridge water deionization unit from Cole-Parmer Instrument Company. Three fresh cartridges were installed at the beginning of the experimental series: Fisher catalog #09-034-104 (contains a resin for the removal of colloids and bacteria and activated charcoal for the removal of organics), #09-034 (a high capacity two bed anion/cation filter), and #09-034-3 (an ultrapure anion/cation mixed bed filter). No degassing of the water was performed, but it was stored in large Nalgene jugs for several days before mixing the polymer solutions. After mixing, the solutions were allowed to sit for an additional 24 hours, so that the amount of dissolved gases was probably very low.

5. Other Equipment

Capillary Viscometers: Kinematic viscosities were measured with a size 50 Cannon-Fenske capillary viscometer (Fisher model 13-617B). The viscometers were placed in a constant temperature viscometer bath at 25.00±0.02°C for most of these measurements (a few were performed at room temperature, approximately 23.5°C). To prevent errors due to solution aging effects, viscosities were

measured within two days of the day on which the batch of solution was used in the experiment.

Stirring Paddles Three-bladed stainless steel paddles $2\frac{1}{2}$ inch diameter (provided with Cole-Parmer mixer #L-04651-00) were used. An aluminum paddle of identical shape was also tested without any detrimental effect on the solutions.

3.2 Preparation of Polymer Solutions

Polymer solutions were prepared following the method described by Paul [20]. These solutions were made in 8 liter batches using deionized water stored for several days in large Nalgene containers. (The containers were closed to prevent dust or dirt from falling into the solutions, but no degassing was performed and no preservatives were added.) Eight liters of water measured out with a graduated cylinder were placed in a plastic bucket, and a stirring motor running at ≈300 rpm was used to create a vortex over 90% of the depth. The bottom of the vortex was kept above the stirring paddle to minimize the amount of air mixed into the water. (Since frothy bubbles could easily form in the slightly viscous solutions if the mixing was too vigorous, it was possible to judge whether large amounts of air were being mixed in.) The appropriate mass of dry polymer (typically 0.50–2.50 ± 0.01 grams) was slowly sifted into the vortex to prevent any clumping of the polymers.[3] After adding the polymer powder, the stirrer was turned down to ≈80 rpm for several hours (usually 6-8 hours). Solutions were open to the air during

[3]Data for solution viscosity *vs.* polymer concentration are tabulated in Section 2

this procedure.

Polymer solution properties typically change as the the solution becomes more homogeneous, so we aged our solutions for at least 24 hours before measuring their viscosities and using them in the experiment.[4] During the aging period the solutions were covered and stored at room temperature.

The viscosities and drag-reducing properties of high molecular weight polymers are highly dependent on the molecular weight of the *longest* polymer chains in solution, so degradation of the solutions can be a problem. Mechanical shear, chemical attact, biological attack, contamination, and simple aging all degrade aqueous polymer solutions. Section 2 contains more information for the polymers included in this study.

3.3 Experimental Procedure

Before each experiment 12.00±0.01 g of tin was measured out and 1.0 liter of coolant was placed in the vessel. The cover gas supply was turned on, and the furnace was allowed to heat up to several hundred degrees before the tin sample was placed in the crucible. Once the sampled was melted a thermocouple was positioned in the melt. All samples were initially heated to 1000°C. If 1000°C was the desire final temperature, the crucible cover was removed, and the furnace was tipped using the mechanism described above. If a lower tin temperature was desired for the experiment, the furnace was turned off and the sample was allowed to cool to the selected temperature (heating to 1000°C ensured that the sample was completely melted). Before tipping the furnace, the samples were checked for oxidation. Data acquisition was triggered automatically if an explosion occured. Qualitative observations about the appearance of the melt as it fell (whether widely separated clusters

[4]See Section 2 for discussion of aging effects in PEO solutions.

or a single mass could be seen), about the relative loudness of the explosion, and about the distribution of debris fragments (to ensure that the melt was falling into the center of the vessel each time, etc.). After the experiment, the fragmented debris was carefully filtered from the polymer solution in the vessel and stored in marked bottles. The vessel was rinsed several times with deionized water, and a new charge of solution was added for the next experiment. A complete series of ten experiments was performed with one of the solutions before conducting tests with a different polymer solution.

4 Results

Four series of experiments with different coolants were carried out. Within each series, several sets of experiments with different initial conditions were conducted. Each set included ten or more experiments at identical conditions:

- **Series 1:** Experiments with pure deionized water (at 25°C) as the coolant. Molten tin temperatures of 600, 700, 800, 900, and 1000°C used.

- **Series 2:** Experiments with aqueous solutions of four different polymer additives (all at 25°C). For each additive, solutions with viscosity ratios of approximately 1.25, 1.50, and 2.00 were used with molten tin at 1000°C.

- **Series 3:** Experiments with aqueous solutions of glycerol (η_r=1.68, 1.94, and 2.97) to determine whether the polymeric nature of the other additives was an important factor. The molten tin temperature was 1000°C.

- **Series 4:** Additional experiments with poly(ethylene oxide), one of the additives examined in Set 2. Solutions with viscosity ratios 1.25, 1.50, and 2.00 tested with molten tin at 600, 700, 800, and 900°C. Also, extremely dilute solutions with viscosity ratios 1.01, 1.02, 1.07, and 1.13 tested with molten tin at 1000°C.

The experimental data consisted of digitized pressure signals for each experiment, photographs of fragmented debris, and measurements of the distribution of particle sizes for the finely fragmented debris resulting from the vapor explosions. Photographs were taken of the debris from one representative experiment in each set and are included below. The corresponding transient pressure signals accompany the photographs. Additional pressure signals are given in Appendix D. The photographs show qualitatively the extent of fragmentation (fine fragmentation of the metal is characteristic of steam explosions), and they reveal the striking difference in the appearance of debris from experiments involving explosive interactions and those which had none. The pressure signals also allow the time scale and relative violence of the interactions to be compared quantitatively. Results for the complete group of experiments were summarized by plotting the maximum pressure measured in each series and by determining the observed frequency of explosions above several pressure reference values. (These reference values were related to the magnitude of the peak pressures measured in water.) A tabular summary of the peak pressure data for every experiment performed for this report is provided in Appendix C.

4.1 Series 1: Fragmentation in Pure Water

Series 1 contained five sets of experiments (pure water at 25°C with T_{tin} varying from 600 to 1000°C) with ten experiments in each set. These experiments in water served as the reference for all of the other solutions. Pressure signals for a representative experiment in pure water is shown in Figure 4.1; the tin temperature was 1000°C. This experiment produced "typical" results with respect to the magnitude of the pressure peaks recorded and the degree

of fragmentation. In 4.1a the complete record (800 msec of data collected every 25 μsec) is given, while 4.1b shows a more detailed view of the transient pressure during one of the explosive interactions. All of the pressure signals recorded in pure water included multiple explosions bursts similar to those visible in Figure 4.1a. Acquisition of these signals was triggered at approximately 60 msec; in frame a the initial "buffer period" is evident. Pressure deviations due to the entry of the melt into the coolant were undetectable even though the triggering threshold was extremely low.

Figure 4.2 contains pressure signals and photographs from one representative experiment for each of the five sets in series 1. (Note the changes of scale for the pressure and time axes in going from Figure 4.1 to Figure 4.2.) In the first four pictures (T_{tin}=1000, 900, 800, and 700°C) large amounts of finely fragmented debris are visible. Smaller amounts are visible in the fifth photograph. Larger chunks which did not interact with the coolant can be seen in every photograph. The metal was almost completely fragmented in all of the experiments with water (in agreement with the results of Dullforce [25]). In water, these larger pieces often had fairly sharp corners and were often in the form of thin, crumpled sheets of metal. (This is especially evident in the last two pictures of Figure 4.2.) Although the fragmented debris appears dark gray in the photographic reproductions, the surface of the metal is shiny and clean, and no oxidation was found.

Graphs of the maximum pressure recorded for each experiment in water are shown in Figure 4.3 (one graph for each set). For clarity, the peak pressure values were sorted in decreasing order so that the range of values could be seen clearly. The average of the ten peak values is indicated by a labelled line on each graph. Although there is some variation in the average peak pressure value for each set, the explosions were generally mild (compared to the results for the other coolant solutions given below).

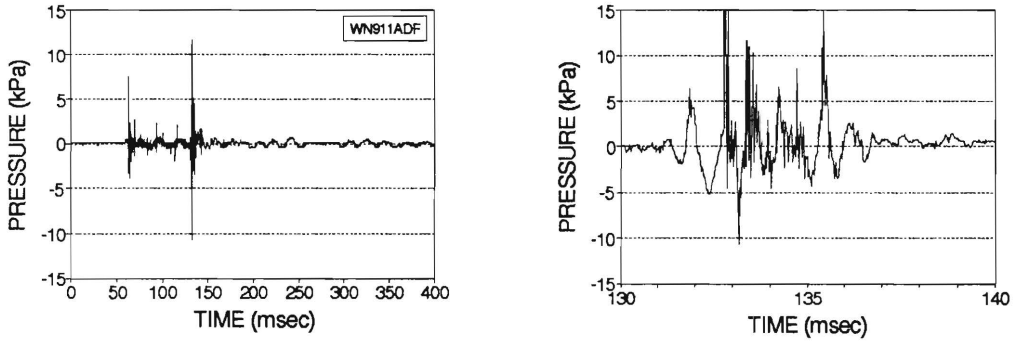

(a) (b)

Figure 4.1: A typical pressure signal from a spontaneous explosion in pure water with T_{tin}=1000°C. In frame (b) the time scale is expanded around the strongest pressure peak visible in frame (a).

T_{tin} = 700°C

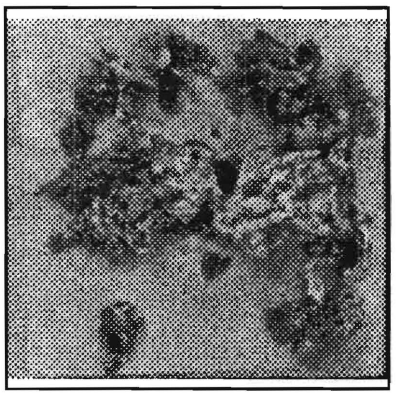

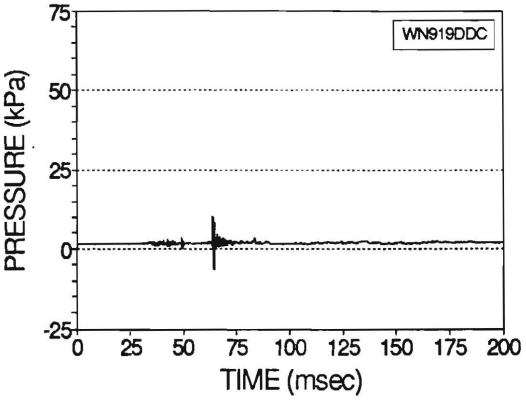

600°C

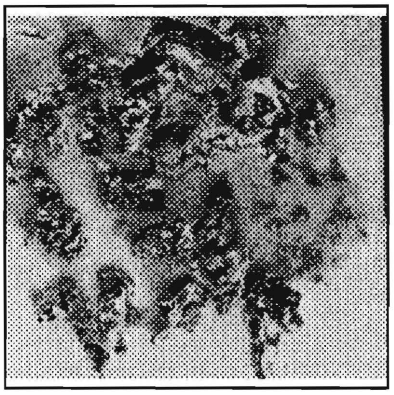

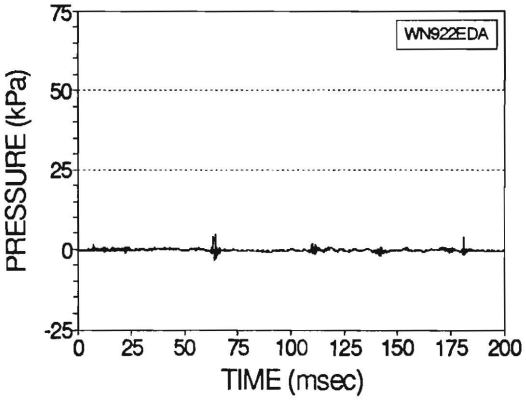

Figure 4.2: Fragmentation in Water (Continued)

T_{tin} = 1000°C

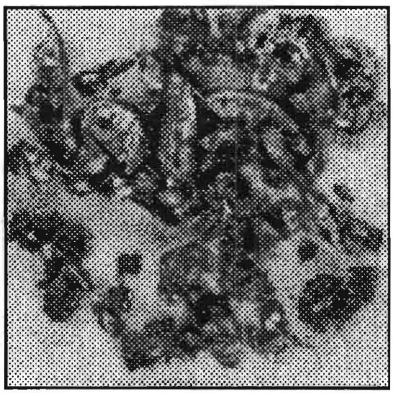

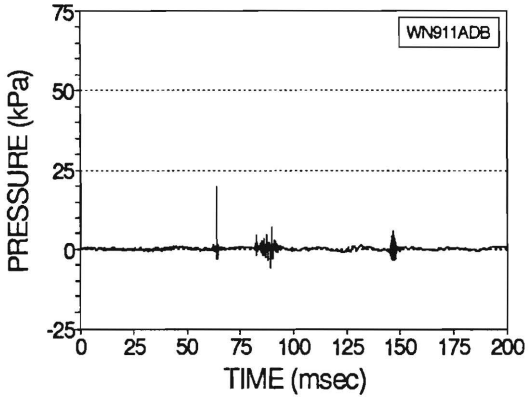

900°C

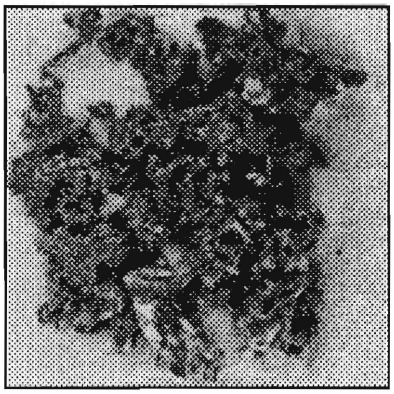

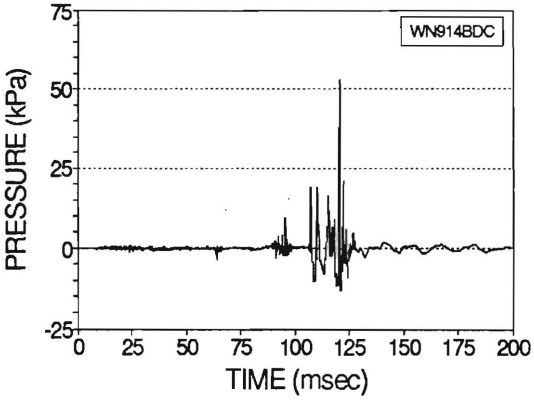

800°C

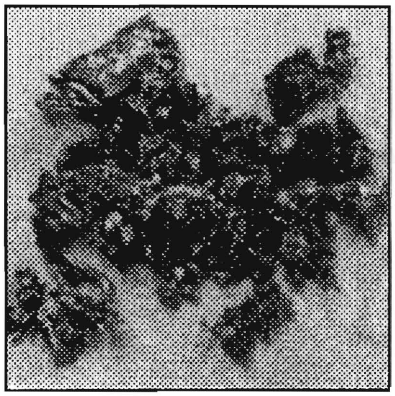

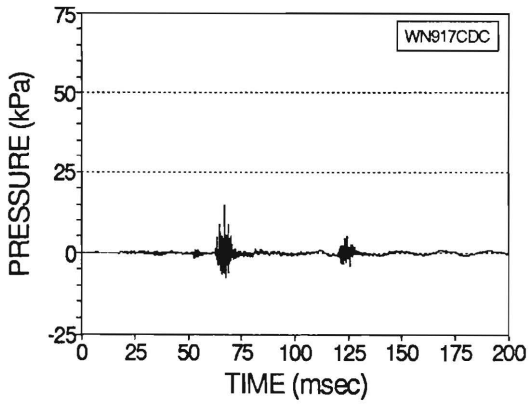

Figure 4.2: Examples of Fragmentation and Pressure Signals in Water

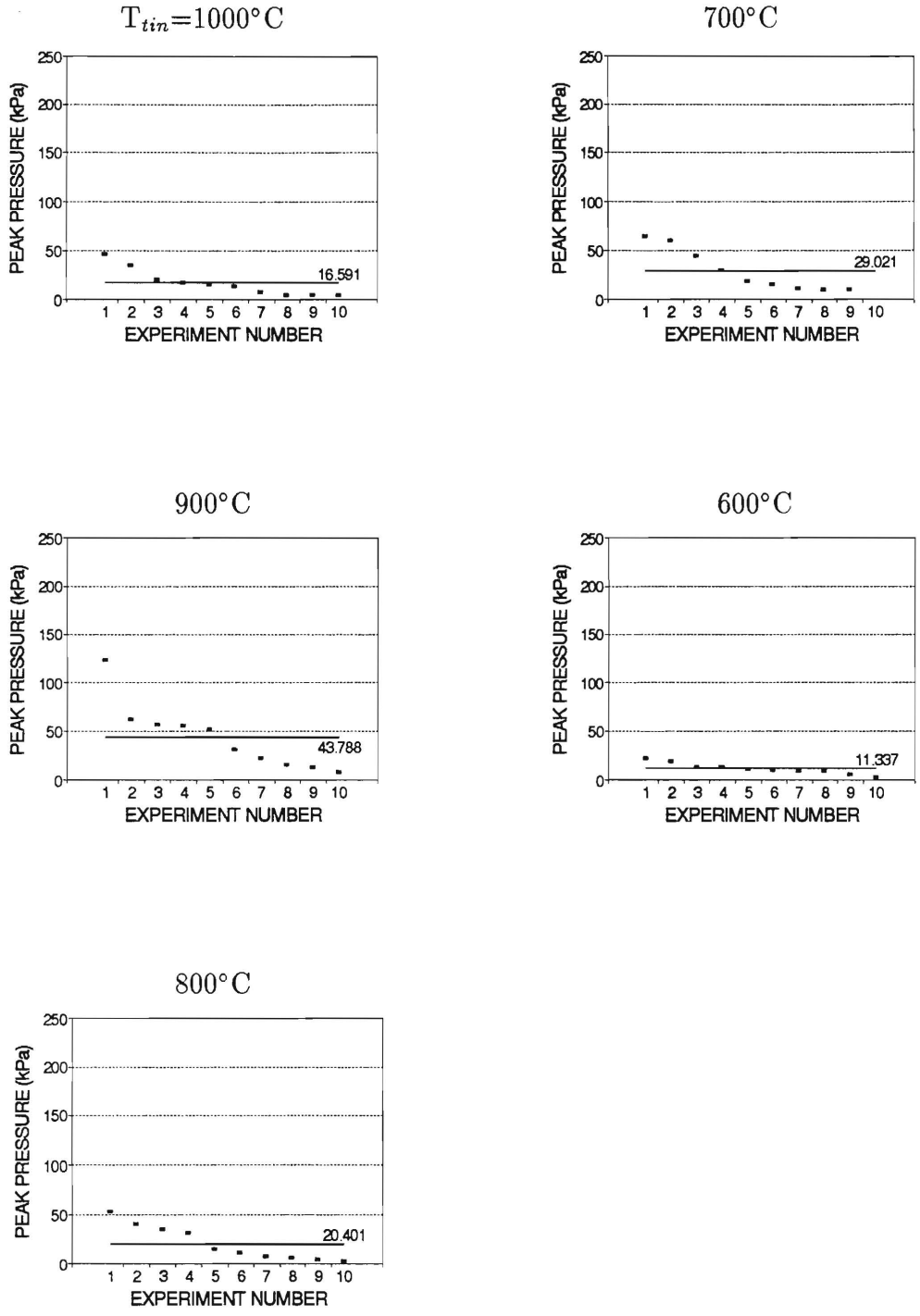

Figure 4.3: Maximum pressures recorded in pure water. (The melt temperature for each set is given above the graph. Labelled lines indicate the average peak pressure value.)

4.2 Series 2 and 3: Fragmentation in the Polymer and Glycerol Solutions

Series 2 contained 12 sets of experiments: four different polymer additives were tested, with three solutions ($\eta_r \approx$1.25, 1.50, and 2.00) for each. The melt temperature was 1000°C for all of the experiments in this series. Results for selected experiments are contained in Figures 4.6–4.7. The measured viscosity ratio for each solution, $\eta_r = \eta_{solution}/\eta_{water}$, is listed on the left. Series 3 contained 3 sets of experiments with aqueous solutions of glycerol (η_r=1.68, 1.94, and 2.97). Graphs of the peak pressures measured during this set of experiments are given in Figure 4.12.

Fragmented debris from explosions in the polymer and glycerol solutions had the same visual appearance as debris from pure water; there were no gross differences to the naked eye in the size of the finest particles or in their color. However, the unfragmented debris (that is, drops of tin which solidified without interacting violently with the coolant) was often noticeably different from the "crumpled thin sheets" retrieved from the experiments in water. As the reproduced photographs on the following pages reveal, the unexploded metal tended to form rounded drops (refer to Figures 4.6–4.7). As the solution viscosity ratio increased from 1.25 to 2.00 this tendency became more pronounced. Poly(ethylene oxide) solutions produced the most extreme examples: the smaller particles were nearly spherical (Figure 4.7). Large fragments which did not explode were usually red-hot as they fell through the coolant, and they sometimes burned the plexiglass bottom slightly. The color of the unexploded debris also varied from uniformly shiny fragments retrieved from pure water: occasionally, fragments acquired a tinge of color (slightly golden yellow or bluish purple). We believe this coloration resulted from the burning plexiglass, since the colored droplets were mostly rounded fragments found flattened on the bottom. Coloration of the unexploded de-

bris did not correlate with the violence of the explosion. Pressure signals recorded in the polymer solutions are also provided in Figures 4.6–4.7. Note that among the experiments with water selected for display in Figure 4.2 the results shown for T_{tin}=900°C (experiment #WN914BDC) were the most violent recorded in water.

Figures 4.10–4.12 contain peak pressure summaries for all of the experiments in series 2 and 3. For the purposes of comparison, the plot for pure water with T_{tin}=1000°C from Figure 4.3 is reproduced in each.

η_r =
1.31

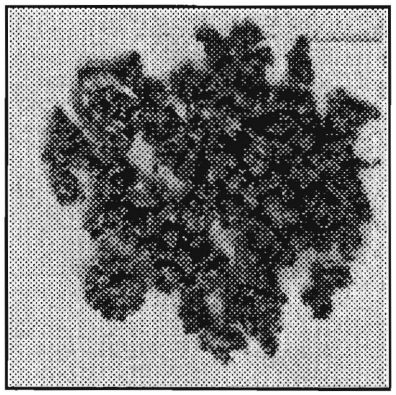

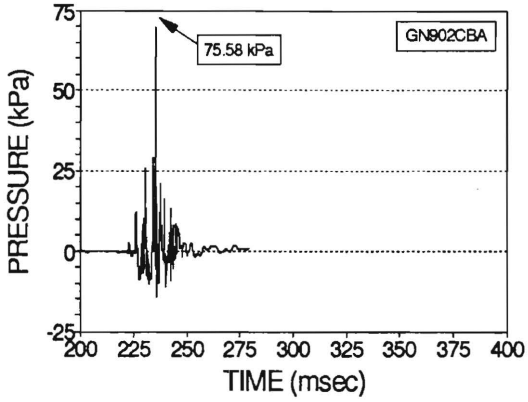

1.54

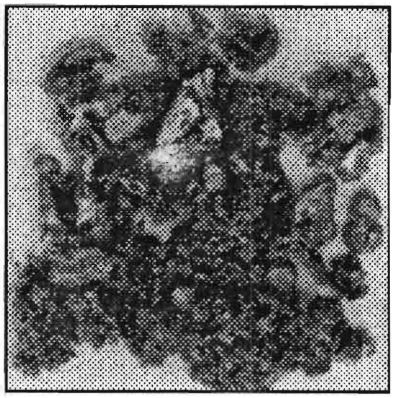

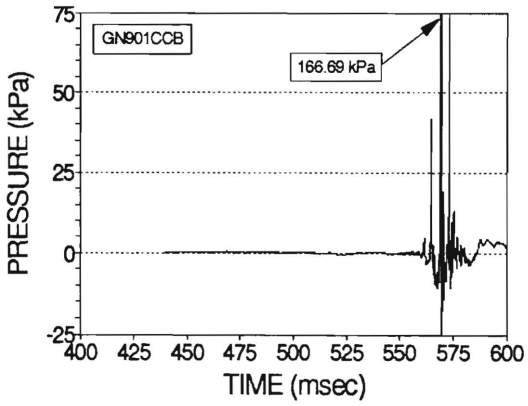

2.00

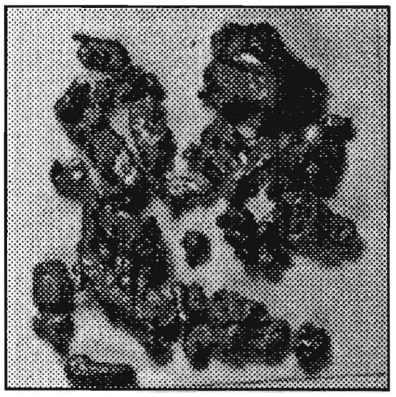

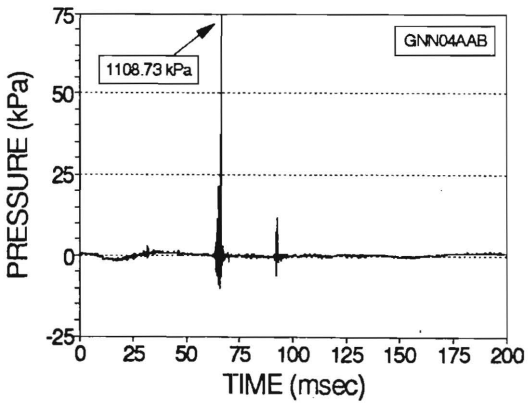

Figure 4.4: Examples of Fragmentation and Pressure Signals in Aqueous Solutions of Guar Gum (Galactosol 211). T_{tin}=1000°C.

η_r =
1.26

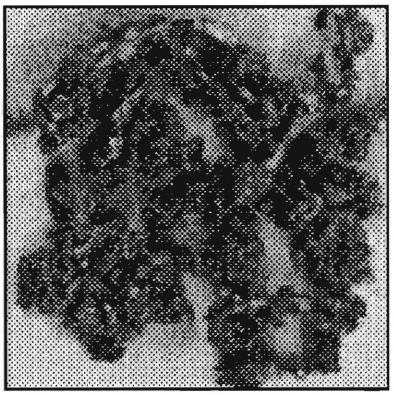

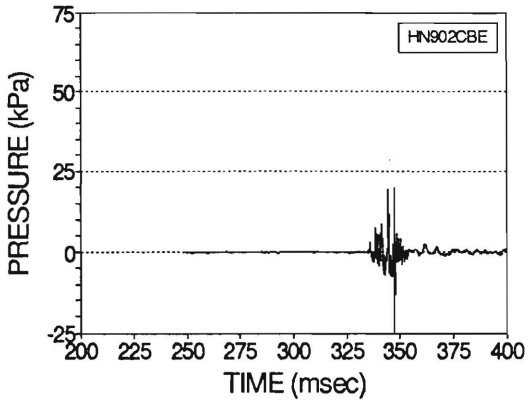

1.55

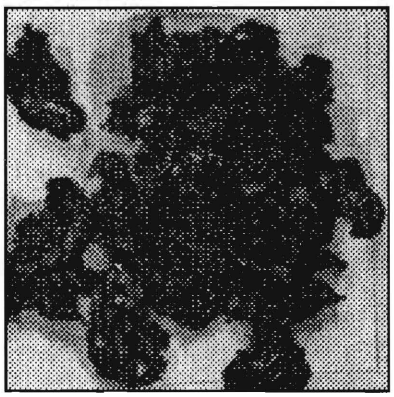

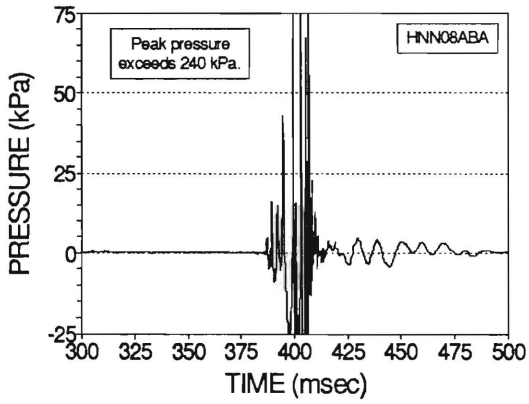

1.91

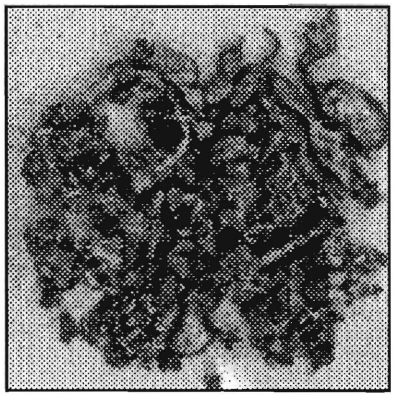

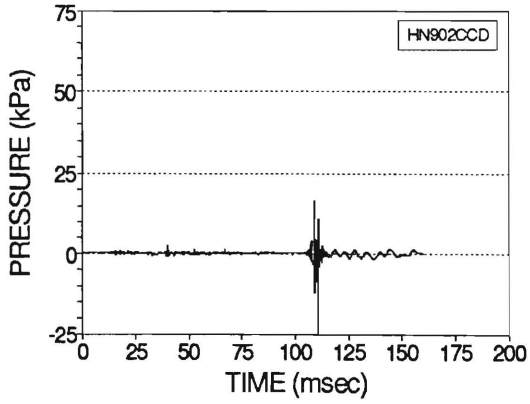

Figure 4.5: Examples of Fragmentation and Pressure Signals in Aqueous Solutions of Hydroxyethyl Cellulose (Natrosol 250HHR). T_{tin}=1000°C.

η_r = 1.25

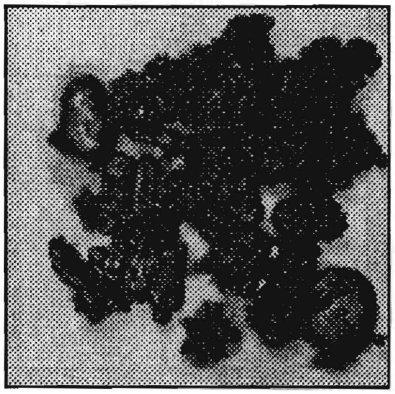

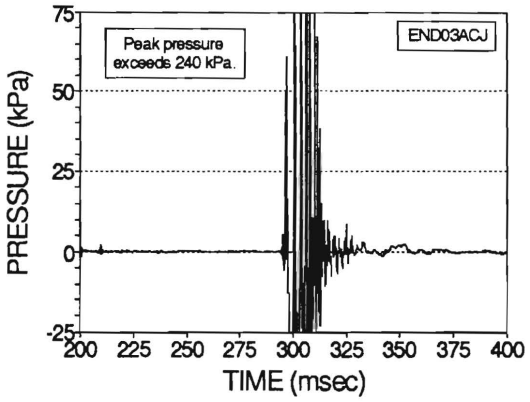

1.51

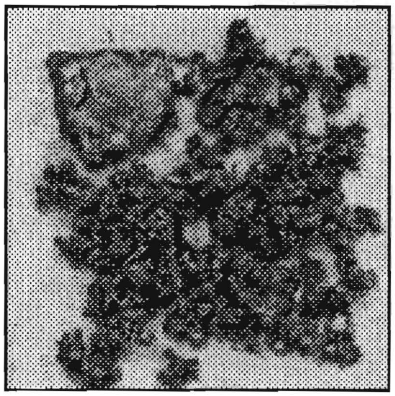

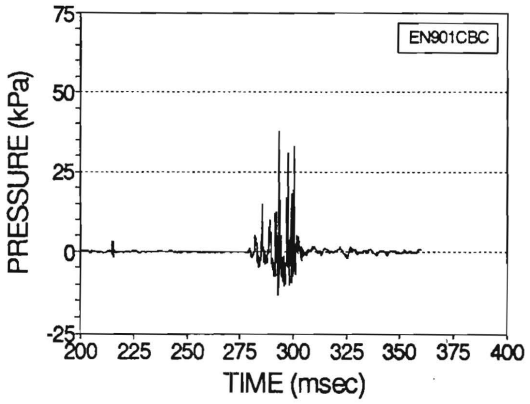

2.05

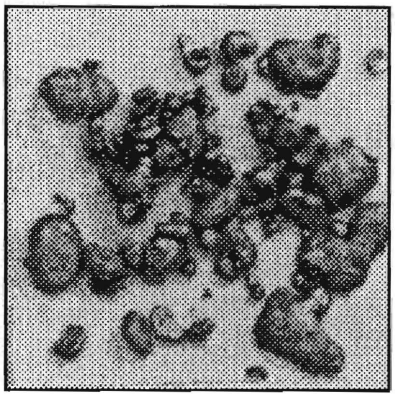

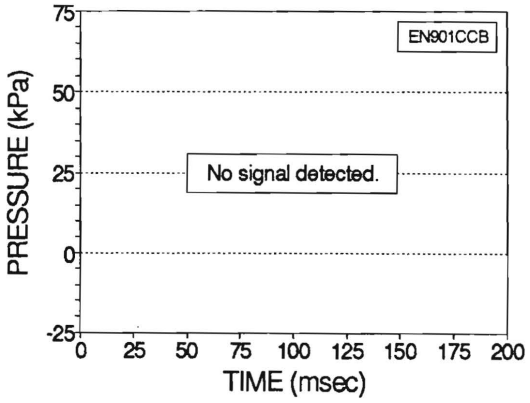

Figure 4.6: Examples of Fragmentation and Pressure Signals in Aqueous Solutions of Polyacrylamide (Percol 1011). T_{tin}=1000°C.

η_r =
1.29

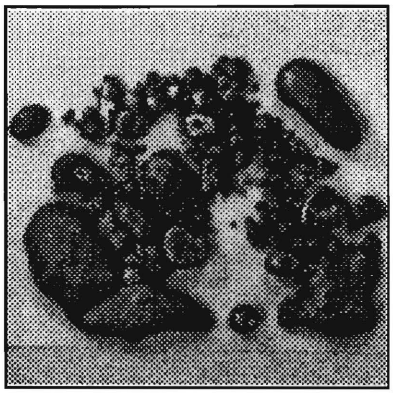

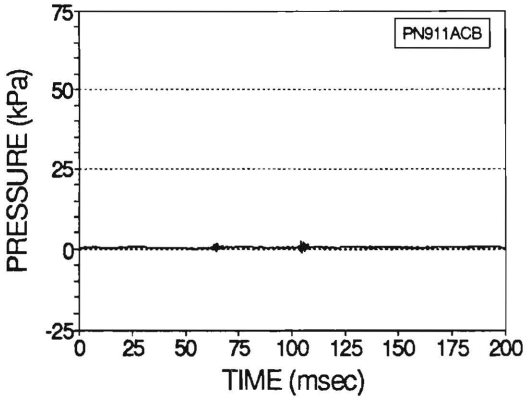

1.52

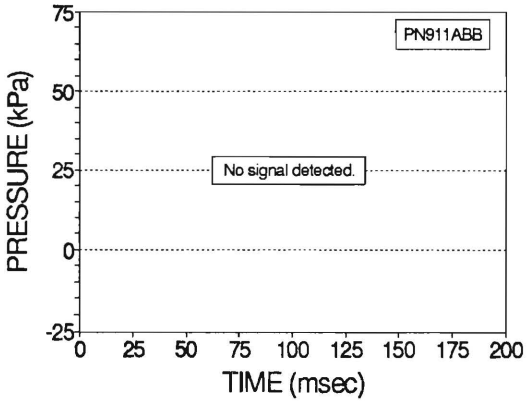

1.97

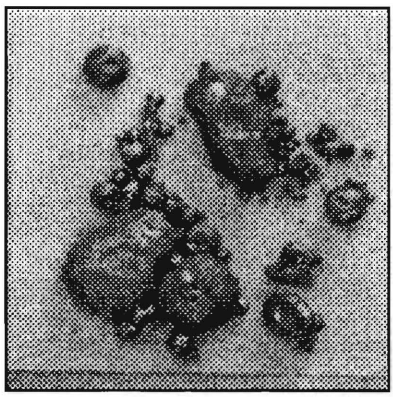

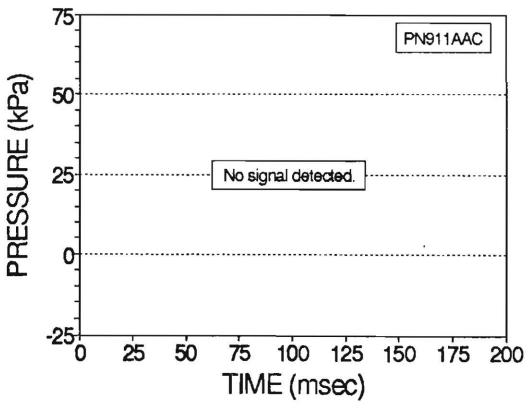

Figure 4.7: Examples of Fragmentation and Pressure Signals in Aqueous Solutions of Poly(ethylene oxide). T_{tin}=1000°C.

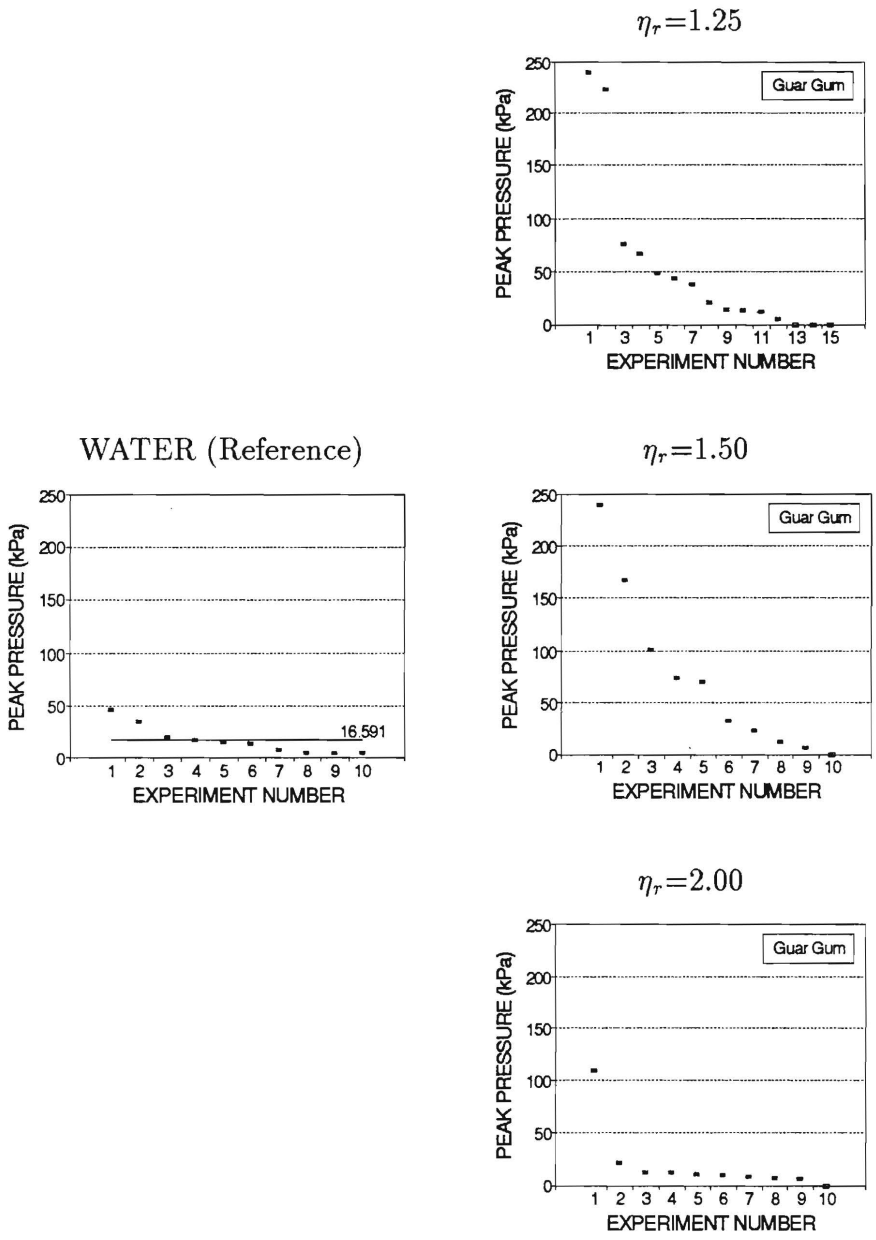

Figure 4.8: Maximum pressures recorded in aqueous solutions of guar gum, (Galactosol 211). The solution viscosity ratio, η_r, is listed above each plot. The melt temperature for all experiments was 1000°C. Experiments without any explosive interactions are marked with an open square, □.

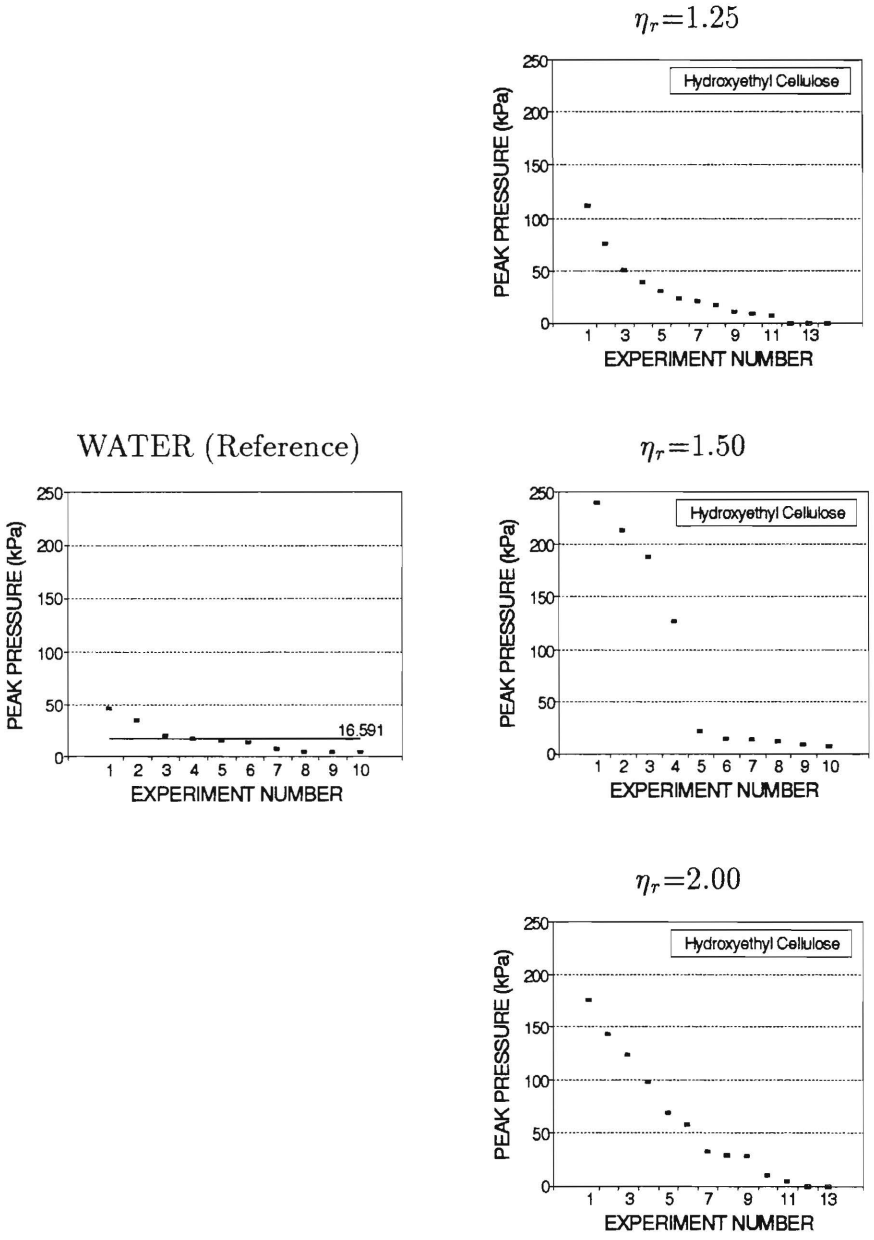

Figure 4.9: Maximum pressures recorded in aqueous solutions of hydroxyethyl cellulose, (Natrosol 211). The solution viscosity ratio, η_r, is listed above each plot. The melt temperature for all experiments was 1000°C. Experiments without any explosive interactions are marked with an open square, □.

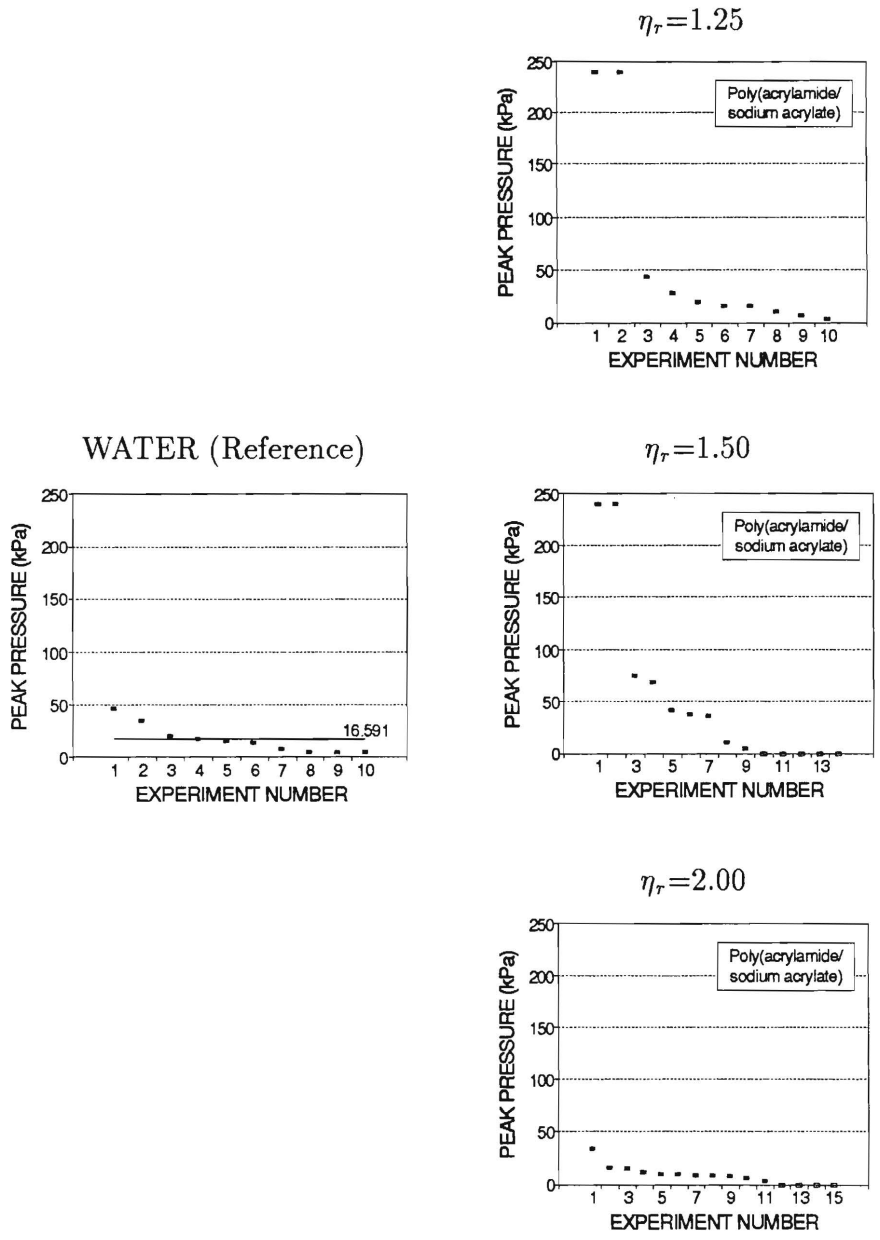

Figure 4.10: Maximum pressures recorded in aqueous solutions of poly(acrylamide/sodium acrylate) (Percol 1011). The solution viscosity ratio, η_r, is listed above each plot. The melt temperature for all experiments was 1000°C. Experiments without any explosive interactions are marked with an open square, □.

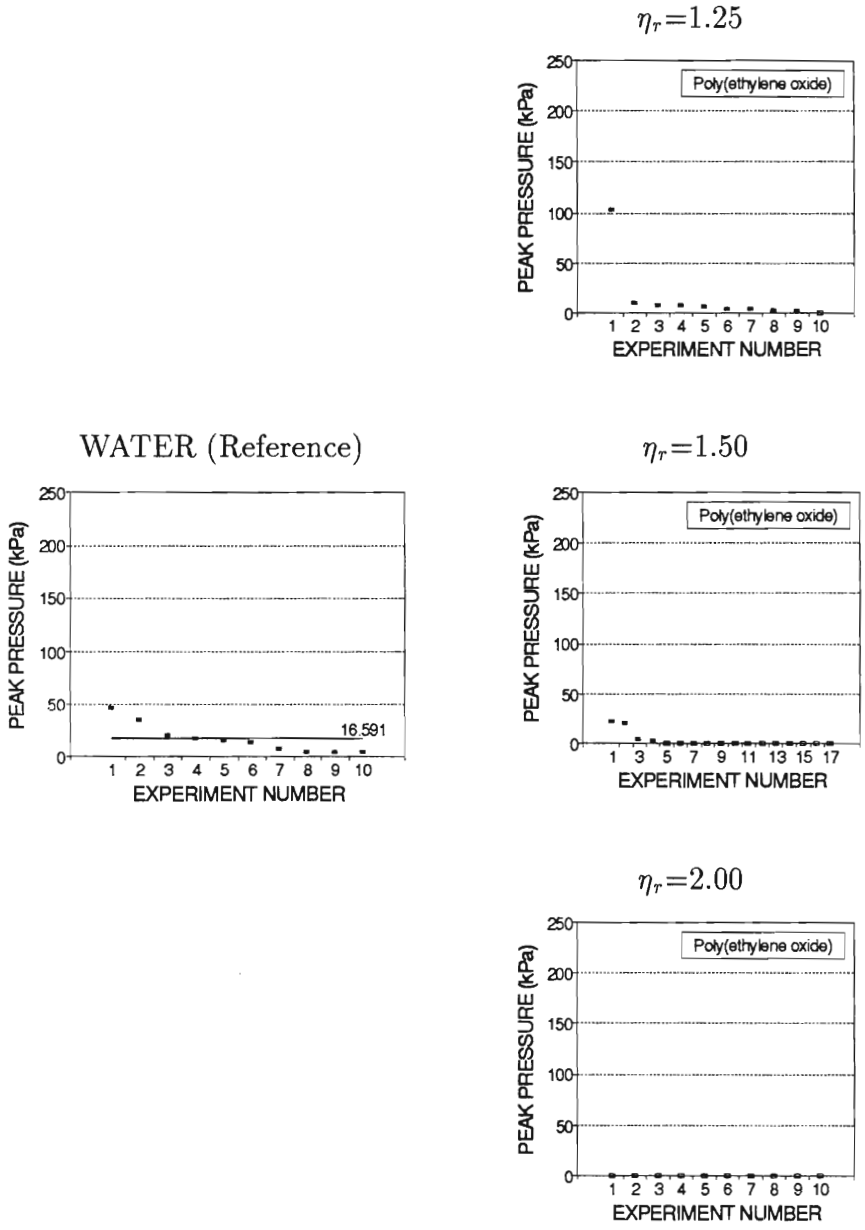

Figure 4.11: Maximum pressures recorded in aqueous solutions of poly(ethylene oxide). The solution viscosity ratio, η_r, is listed above each plot. The melt temperature for all experiments was 1000°C. Experiments without any explosive interactions are marked with an open square, □.

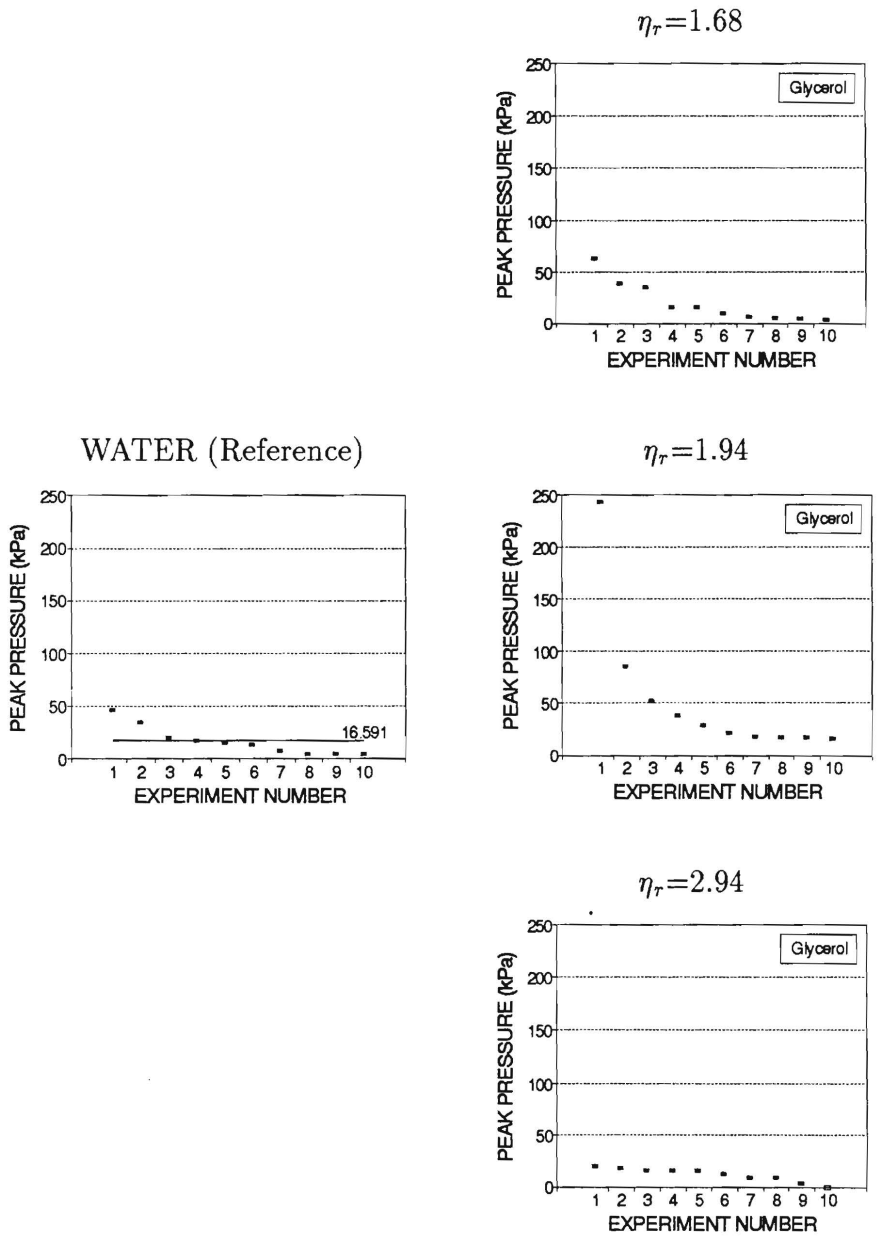

Figure 4.12: Maximum pressures recorded in aqueous solutions of glycerol. The solution viscosity ratio, η_r, is listed above each plot. The melt temperature for all experiments was 1000°C.

4.3 Series 4: Additional Fragmentation Experiments with Poly(ethylene oxide)

The experiments in series 4 were used to examine the effect of the molten tin temperature in experiments with poly(ethylene oxide) solution as the coolant and also to examine the behavior of poly(ethylene oxide) in very dilute solutions.

4.3.1 Effect of Melt Temperature

The results of the experiments with poly(ethylene oxied) in Series 2 showed that it suppressed spontaneous explosions when the tin temperature was 1000°C. The Series 1 experiments with water indicated that melt temperature did not affect the appearance or quantity of finely fragmented particles, nor did it alter the range of peak pressures recorded. This result held for poly(ethylene oxide) solutions as well; neither the appearance of the debris nor the range of peak pressures changed significantly as the melt temperature varied. Figure 4.13 contains photographs for selected experiments for the case with T_{tin}=900°C which can be compared with those in Figure 4.7. Figures 4.14–4.16 show the peak pressures measured for T_{tin}=1000, 900, 800, 700, and 600°C for poly(ethylene oxide) solutions with η_r=1.25, 1.50, and 2.00. Isolated strong explosions appeared in experiments at each temperature, but variation of the melt temperature did not affect the frequency of this phenomenon.

4.3.2 Experiments with Extremely Dilute Solutions

Extremely strong explosion signals (several times larger than any measured in water) occurred in the lower viscosity solutions of polyacrylamide, guar gum, and hydroxyethyl cellulose. As the solution viscosities increased, however, spontaneous explosions were suppressed. The poly(ethylene oxide) solutions examined in series 2 (viscosity ratios of 1.25 and larger) effectively suppressed spontaneous explosions, however. To test whether explosions with peak pressures larger than those in water also occurred in poly(ethylene oxide) solutions, several more dilute solutions were prepared with viscosity ratios ranging from 1.01 (polymer concentration 10 wppm) to 1.13 (100 wppm). This was indeed the case: explosions more violent than those observed in water appeared in poly(ethylene oxide) solutions whose viscosity was only slightly larger than water. The peak pressures measured in these solutions are displayed below in Figure 4.17.

η_r =
1.29

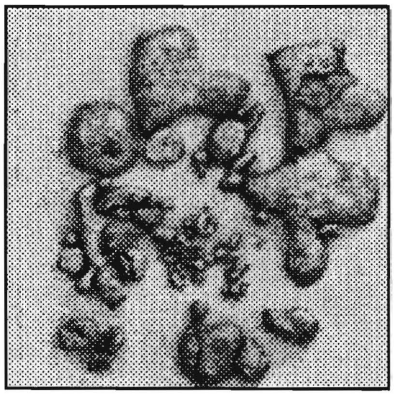

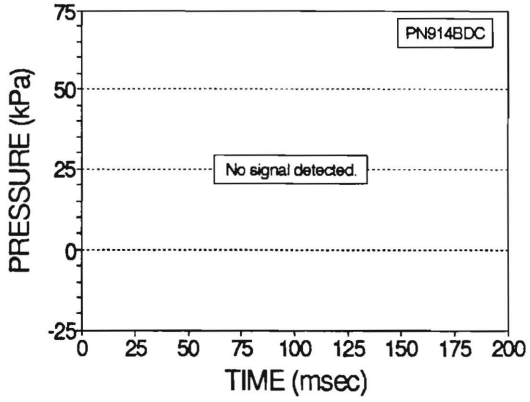

1.52

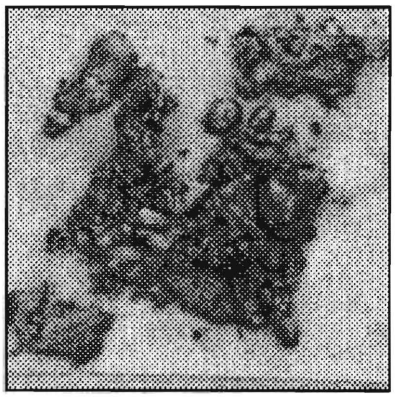

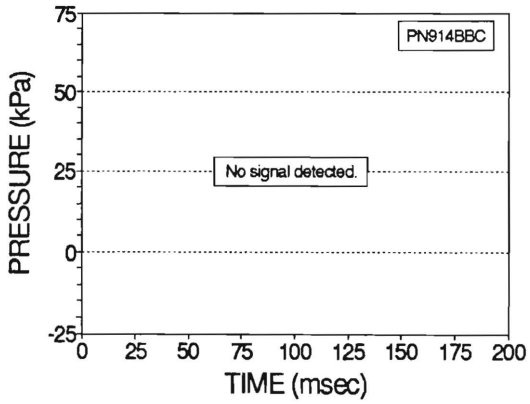

1.97

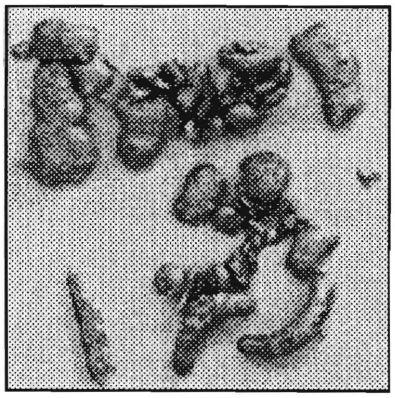

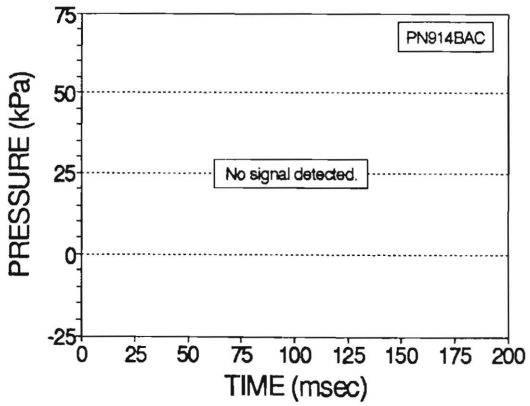

Figure 4.13: Examples of Fragmentation and Pressure Signals in Aqueous Solutions of Poly(ethylene oxide). T_{tin}=900°C.

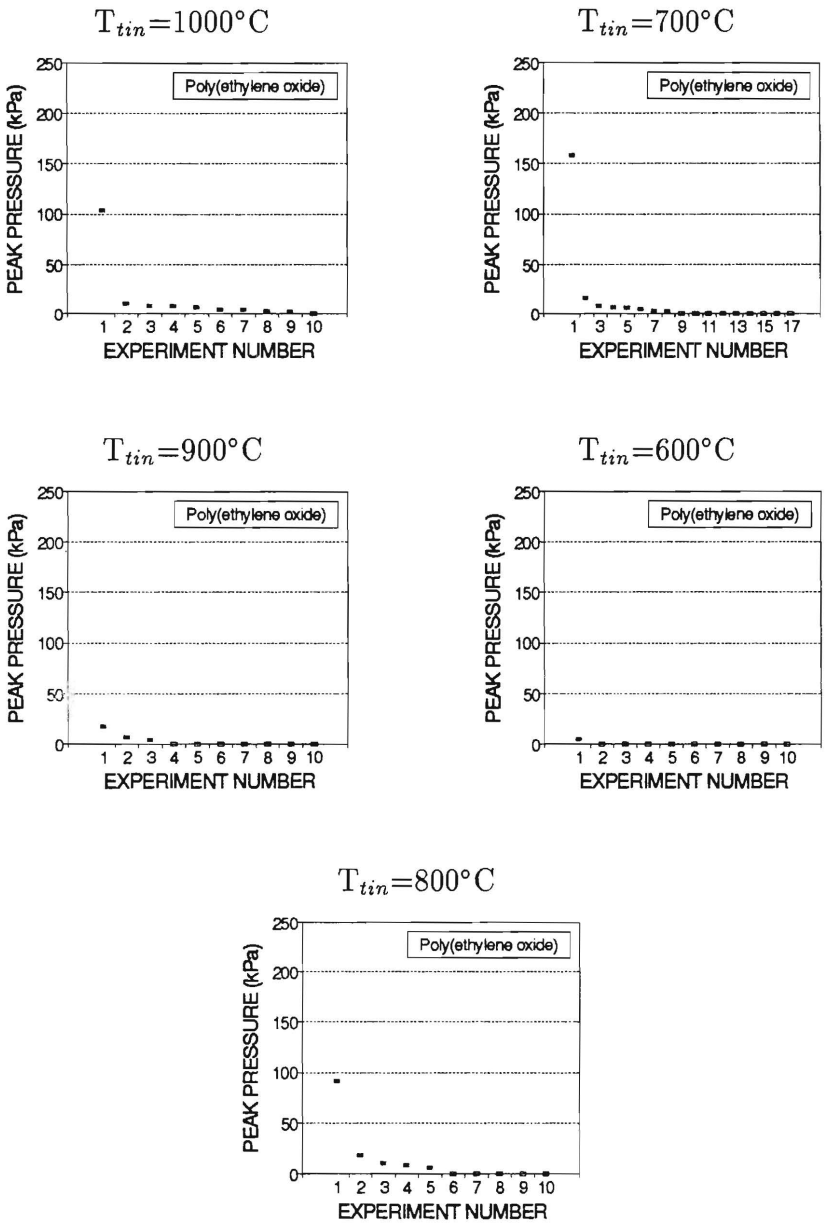

Figure 4.14: Maximum pressures recorded in aqueous solutions of poly(ethylene oxide) with $\eta_r \approx 1.25$. The melt temperature for each experiment is listed above each plot. Experiments without any explosive interactions are marked with an open square, □.

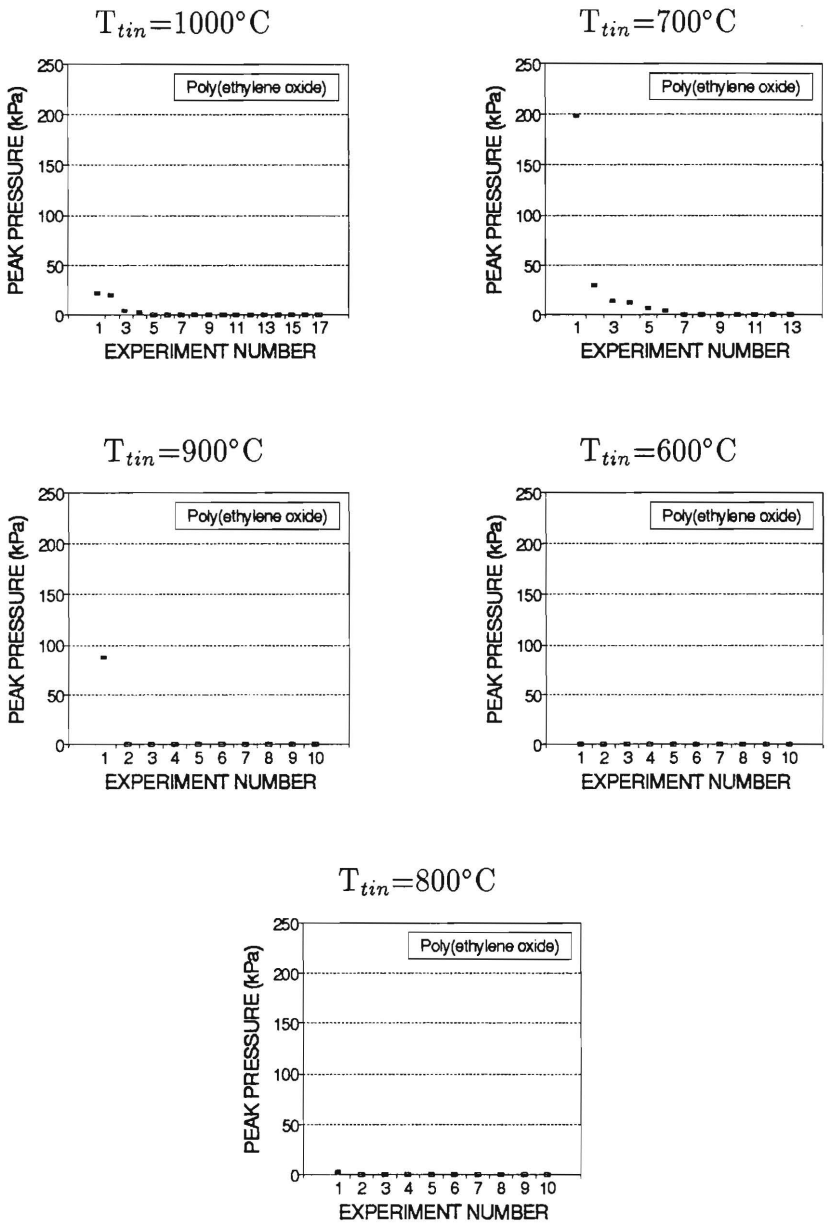

Figure 4.15: Maximum pressures recorded in aqueous solutions of poly(ethylene oxide) with $\eta_r \approx 1.50$. The melt temperature for each experiment is listed above each plot. Experiments without any explosive interactions are marked with an open square, □.

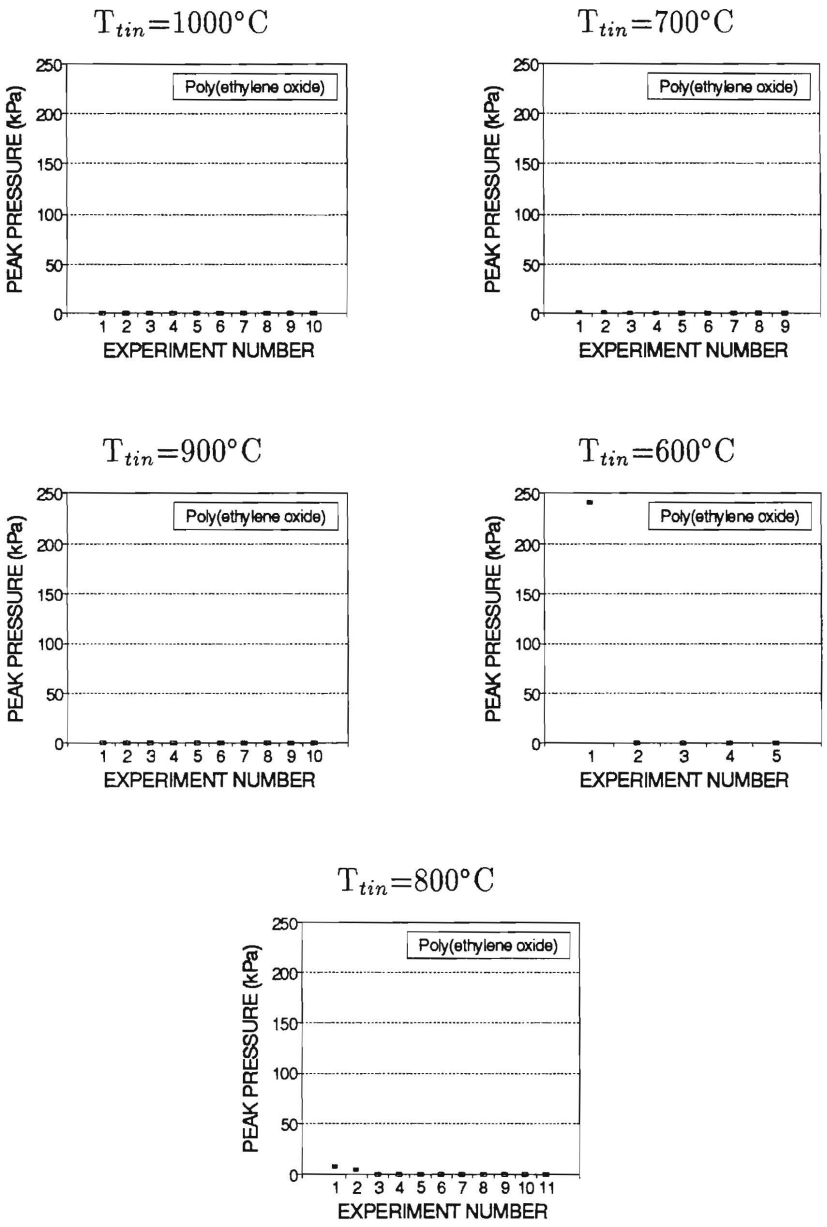

Figure 4.16: Maximum pressures recorded in aqueous solutions of poly(ethylene oxide) with $\eta_r \approx 2.00$. The melt temperature for each experiment is listed above each plot. Experiments without any explosive interactions are marked with an open square, □.

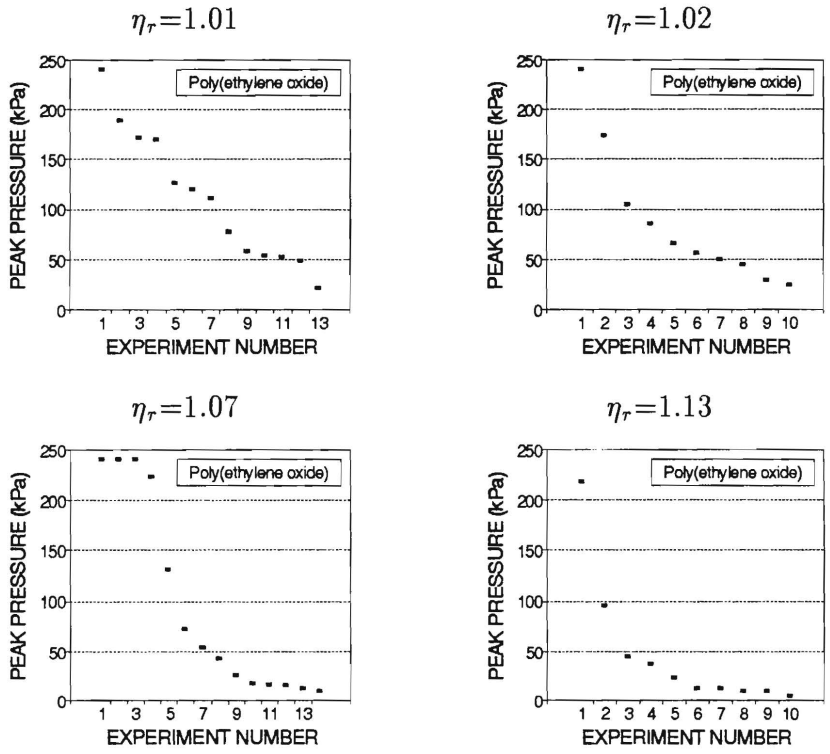

Figure 4.17: Maximum pressures recorded in aqueous solutions of poly(ethylene oxide) with viscosity ratios in the range from 1.01 to 1.13. T_{tin}=1000°C.

4.4 Frequency and Magnitude of Explosions

The relative effectiveness of each polymer additive was determined by calculating the fraction of experiments in each set whose peak pressure exceeded a given level and plotting these values against the solution viscosity ratio, η_r. Three different threshold values (0.6 kPa,20.0 kPa, and 75.0 kPa) were used with the data from the experiments with T_{tin}=1000°C to produce the graphs on the following page (Figure 4.18). On each graph three reference frequencies from the set of ten experiments with water and T_{tin}=1000° are indicated by open squares on the y-axis ($\eta_{r,water} \equiv 1$).

The smallest threshold used,0.6 kPa, was the triggering level for the data acquisition system. Since only steam explosions produced signals strong enough to trigger the system (while spashing or the entry of the melt into the liquid could not), the values in for the curves labelled "all explosions" are the measured frequencies for vapor explosions of any magnitude. When water was the coolant vapor explosions always occurred and produced detectable signals (the reference point at 100%). When poly(ethylene oxide) was added to the coolant water, detectable pressure signals were greatly reduced as the solution viscosity increased. None of the other additives reduced the total number of detectable interactions appreciably.

The next largest threshold value, 25.0 kPa, was approximately equal to the average value of the ten peak pressures for the experiments with pure water at T_{tin}=1000°C: 30% of the experiments with pure water had a maximum pressure larger than 20 kPa. Explosions of this magnitude occurred less frequently in poly(ethylene oxide) solutions when the solution viscosity ratio was above approximately 1.25. Peak pressures of this magnitude occurred *more* frequently for the other three polymers in solutions with $\eta_r \leq 1.50$, but as the solution viscosities increased the frequency of spontaneous explosions for each of these three polymers dropped below the level for water alone.

The most striking result was that weakly viscous solutions could produce

more powerful explosion signals than any recorded in pure water. Only one peak pressure in fifty experiments in water exceeded 75 kPa (Figure 4.3), so this value was used as the largest threshold in Figure 4.18. All four of the polymer additives increased the frequency of these powerful explosions to some degree, but hydroxyethyl cellulose and guar gum were the worst in this respect.

4.5 Particle Size Distribution Measurements

In general, the tin samples appeared to fragment most completely in pure water. In the various polymer solutions it was more common to find solidified drops of fairly large size which had not interacted violently with the coolant. In order to quantify this observation, particle size distributions were determined for the debris from selected experiments. Debris was collected after each experiment by rinsing out the plexiglass vessel with water into a clean beaker and then straining out the remaining coolant solution using a paper or by allowing the excess to evaporate by gently heating the collected debris in an oven. A set of standard measurement seives with mesh sizes ranging from 45 microns up to 20,000 microns were used with a vibration stand to sort the metal fragments. To assure good separation the samples were shaken violently for several minutes. The total mass of the sample was measured before and after the separation procedure to ensure that the major fraction of each tin sample had been collected and sifted without loss. Typically, from the 12 gram samples which were added to the furnace crucible, approximately 11.5–11.7 grams of explosions residue were retreived. Differences in the sample mass before and after the separation were negligible ($\ll 1\%$). For each series of ten experiments, two were selected for determination of the particle size distributions. One experiment with a peak pressure near the maximum for the series and one with a peak pressure near the average value were chosen for these tests.

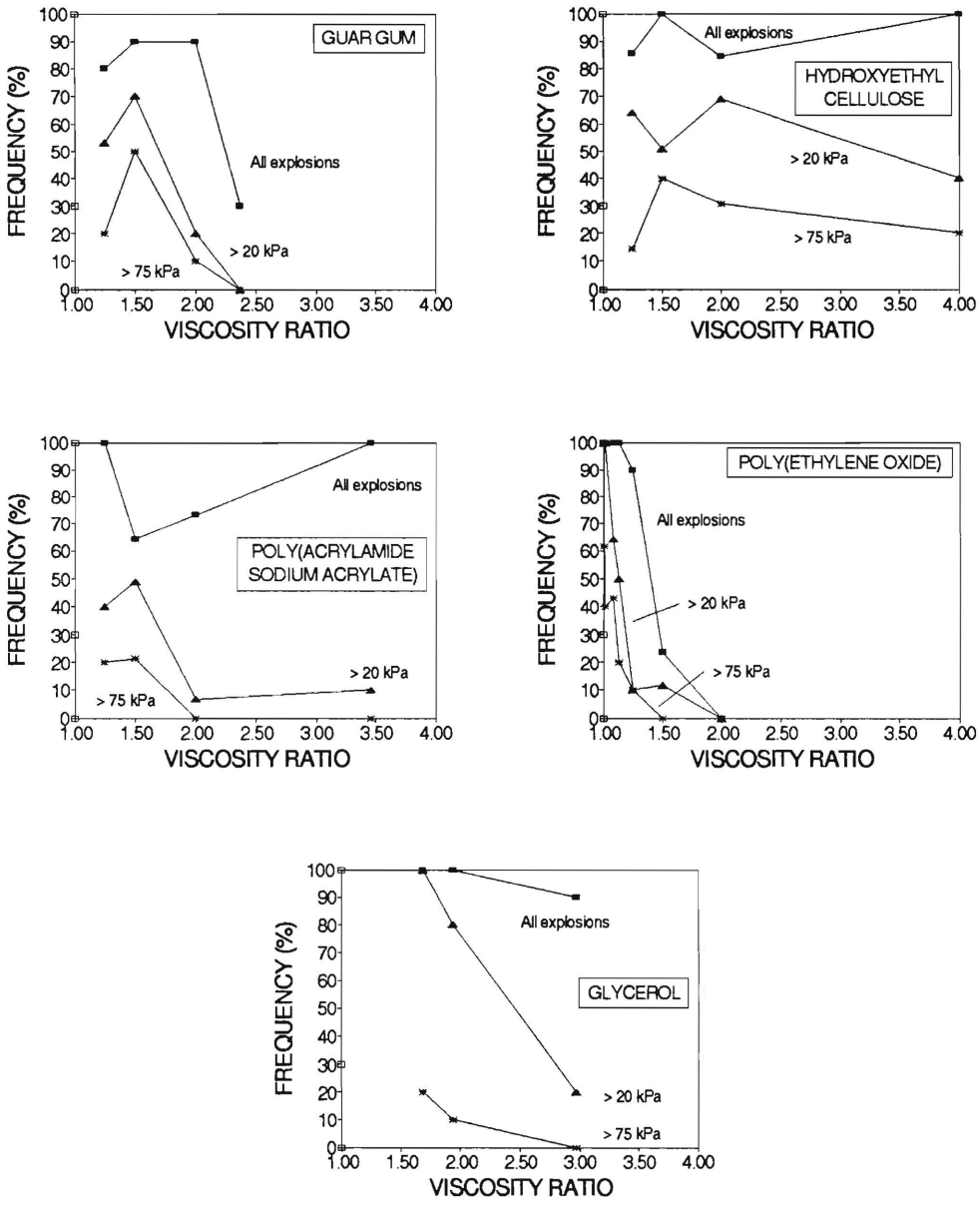

Figure 4.18: Observed frequencies for spontaneous vapor explosions which propduced peak pressures larger than 0.6, 20.0, and 75.0 kPa. The tin temperature was 1000°C for all of the experiments used to produce this figure.

Figure 4.19 includes results for a representative set of these test. For each of the four polymeric additives examined, the cumulative mass percentages are given for the fragmented debris from explosions in coolant solutions with viscosity ratio 1.25. The results from one of the experiments with water are provided for reference. In each case an experiment was selected whose peak pressure was near the middle of the series range. The peak pressures were:

water:	2.44 kPa
guar gum:	6.97 kPa
hydroxyethyl cellulose:	4.51 kPa
poly(ethylene oxide):	1.53 kPa
poly(acrylamide/sodium acrylate):	240 kPa

The cumulative percentages are shifted towards larger particles for the three experiments with polymeric additives which had relatively samll peak pressures. The solution made with the poly(acrylamide/sodium acrylate) additive had a peak pressure several times larger than any of the others shown; the cumulative mass curve is shifted correspondingly to the left, toward smaller particles. Particle mass distribution curves for all of the other measurements performed are given in Appendix E.

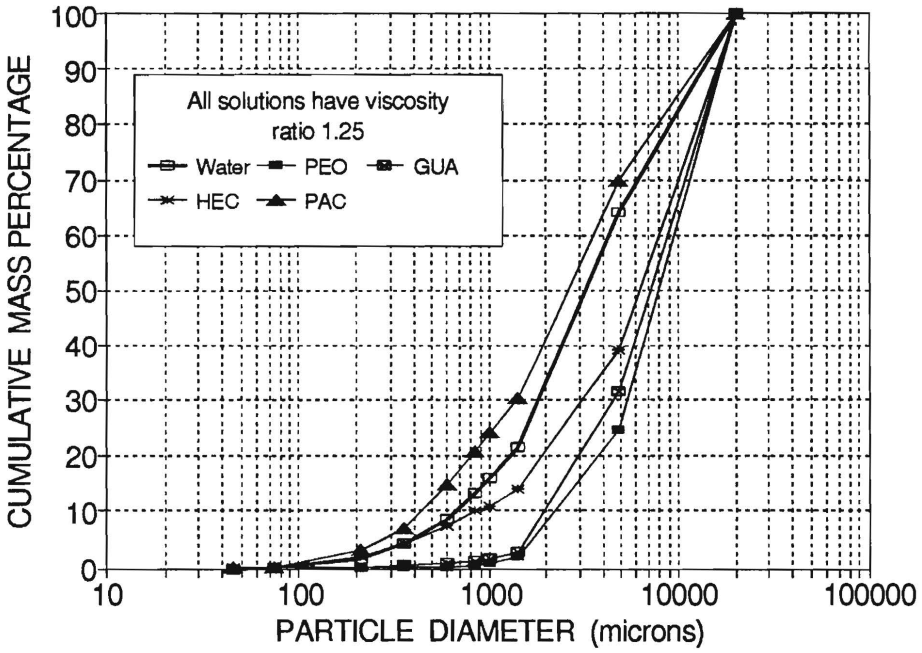

Figure 4.19: Particle size distributions for debris from explosions in coolants with viscosity ratio 1.25 prepared with the four polymeric additives. The abbreviations are: GUA=guar gum, PEO=poly(ethylene oxide), HEC=hydroxyethyl cellulose, and PAC=poly(acrylamide/sodium acrylate). The peak pressures for these experiments were 2.44 kPa (water), 6.97 kPa (GUA), 1.53 kPa (PEO), 4.51 kPa (HEC), and 240.00 kPa (PAC).

5 Discussion

Polymeric additives differ in their ability to suppress spontaneous steam explosions when used in dilute aqueous solutions with viscosity ratios in the range $1.00< \eta_r <4.00$. In general, fewer spontaneous explosions occurred as the solution viscosity increased. Strong explosions (with peak pressures many times larger than any observed in pure water) continued to occur as the solution viscosity was increased by the addition of polymeric additives, but their frequency diminished as the viscosity increased. Poly(ethylene oxide) was the most effective additive in this viscosity range; no explosions at all were detected for this additive when the viscosity ratio was 2.00 or larger (a concentration of approximately 525 wppm). The observed frequency of explosions in guar gum declined rapidly above η_r=2.50 (725 wppm). The threshold viscosity ratios for the other two polymeric additives examined, poly(acrylamide/sodium acrylate) and hydroxyethyl cellulose, were both above η_r=4.00 and have not been determined. In solutions of poly(acrylamide/sodium acrylate), however, peak pressures above 20 kPa were less frequent than in pure water when the solution viscosity ratio above 2.00. The frequency of explosions in hydroxyethyl cellulose solutions, however, did not change significantly in the examined viscosity range. These results are in agreement with Kim [16], Nelson and Guay [15], and Flory *et al.* [17], who all found that solutions several times more viscous than water suppressed both spontaneous and triggered explosions.

The threshold viscosity reported here for poly(ethylene oxide), η_r=2.00, is several times smaller than the thresholds reported elsewhere for other additives. Flory *et al.* noted that a five-fold increase of viscosity ($\eta_r \approx 5.0$) of carboxymethyl cellulose solution eliminated explosions, but they did not determine a threshold. Nelson and Guay reported a threshold of 0.025 Pa sec ($\eta_r \approx 25$) for a similar cellulose gum solution. Neither reported the height from which the tin was poured, however, so that the influence of the drop height

cannot be determined—the amount of entrained air which stabilizes film boiling depends strongly on drop height [10]. Consequently, the threshold for poly(ethylene oxide) reported here may be relatively low because the drop height was large (44.5 cm). Kim's reported threshold was much higher ($\eta_r \approx 240$) because an external trigger was applied to force explosions.

Different viscosity-temperature relations for the various polymers may explain these differences in the viscosity threshold for suppressing explosions. It is possible that aqueous solutions made with different additives which have the same viscosity at 25°C may have very different viscosities near the boiling point [15]. It is interesting that the most effective polymeric additive, poly(ethylene oxide), was the only additive with a negative solubility-temperature relation; the polymer comes out of solution within one or two degrees of the boiling point.

The observed increase in the likelihood of extremely violent explosions in solutions only slightly more viscous than water was not previously reported. McCracken [18] noted that stronger explosions appeared to occur in a more viscous coolant, but his evidence (degree of fragmentation) was indirect. He also did not observe any suppression of explosions as the viscosity increased. The increase in peak pressures for extremely dilute solutions reported in this investigation was a reproducible phenomenon. Complete sets of ten experiments with water and with the various polymer solutions were often interspersed without any variation of this trend.

Mechanistically, the increased frequency of strong explosions in the most dilute solutions is consistent with the impact of polymer additives on the transient boiling characteristics observed by Rouai [22], namely, the increase in both the critical heat flux and Leidenfrost temperature. Solutions made with glycerol, a non-polymeric additive, had similar behavior, however, indicating that transient boiling characteristics may not be the only source of this effect. Alternatively, increase in solution viscosity due to either polymeric or non-polymeric additives may have altered the behavior of air entrained

as the molten drops entered the coolant or the break-up of the drops themselves. Nevertheless, the competing factors of increased heat transfer and increased viscosity may explain the fundamentally different nature of the observed effect of the additives where they increase the severity of spontaneous explosions at very low concentrations and completely suppress them at higher concentrations. In summary, the data suggest that dilute solutions of polymeric additives, particularly poly(ethylene oxide), may be used to suppress vapor explosions, if and only if, it can be assured that the concentration can be maintained above a threshold value. At lower concentrations, more vigorous, albeit less frequent, explosions may result.

Appendix A:
Pressure Transducer Calibration

A Pressure Transducer Calibration

The pressure transducers are Z-cut lithium niobate disks 0.64 cm in diameter and 0.064 cm in thickness (Specialty Engineering Associates, Miltipas, CA). The dimensions are small enough so that equilibrium is established within the crystal in times which are short compared to the rise time of the pressure pulse (Huff 1975). Aluminum-over-chrome electrodes are vapor-deposited on opposite faces of the disk and connect to a 3 foot cable (Beldon 8640 with grounded shield).

A.1 Calibration Procedure and Results

The calibration was performed by placing the transducer in a water- filled piston (I.D. $\approx$ 4 inches) and pressurizing it in an electronically-controlled loading cell. The controller produces a voltage signal proportional to load. The piston was loaded in a square wave pattern, oscillating between 100 pounds and a larger load value which we varied to provide calibration points for pressure steps of 5 psi through 50 psi. The period was about 0.4 seconds, and the pressure rise time 3 msec.

Two transducers were connected to Kistler charge amplifiers with all settings the same as those used in the experiment. Voltage signals from the amplifiers and load cell were collected simultaneously with our EGAA system. The voltage-pressure relationship was linear for both sensors, and a least squares best fit line was calculated calculated for each (P is the pressure increase in psi):

$$\begin{aligned} \#1: \quad \text{Output Voltage} &= -0.288\ P + 0.07, \\ \#2: \quad &= -0.278\ P + 0.09. \end{aligned}$$

All pressure values contained in this report were calculated using a conversion factor obtained by averaging the slopes and ignoring the small offsets.

$$\boxed{\text{C} = \text{-3.53 psi/Volt}}$$

A.2 Comparison with Published Data

For comparison with published data, the conversion factor for voltage was converted to charge using the known value for the charge amplifier capacitors (10 pF) and voltage gain.

$$\text{C}' = +0.884 \text{ psi/pCoulomb}$$

Each electrical contact covers an entire face of the crystal, so the transducer active area was taken to be 0.32 cm^2. The transducer's hydrostatic piezoelectric constant (the charge generated per unit active area per unit pressure increase) is:

$$\boxed{\text{K}_{exp} = \frac{1}{AC'} = 3.5 \text{ pC/cm}^2 \text{ psi}}$$

Graham employed a projectile impact method to obtain the piezoelectric coefficients for a transducer identical to ours (Graham 1973) and used these to calculate the hydrostatic constant: $\text{K}_{hydrostatic} = 6.31 \times 10^{-12}$ C/N (Huff and Graham 1975). Converting units:

$$\boxed{\text{K}_{lit} = 4.3 \text{ pC/cm}^2 \text{ psi.}}$$

We attribute the 16% discrepancy between results to the slower rise time of our pressure pulse. Graham's impact loading occured practically instantaneously, but our piston loading occured over 3 msec and allowed charge to leak away before the pressure pulse had reached its maximum, so our value appears lower. The RC time constant of our measuring circuit was about 20 msec.

The pressure signals we measured had rise times on the order of microseconds, so Graham's reported value is probably more accurate. We used our own value for consistency, however, since other researchers in this field have used very similar gages calibrated with similar methods (e.g. Nelson *et al.* 1987).

References for Calibration

Huff,C.F. and Graham, R.A., Appl. Phys. Letters, v27, n4, pp. 163–164, 1975.

Graham, R.A., Phys. Rev. B, v6, p. 4779, 1972.

Graham, R.A., Solid State Commun., v12, p. 503, 1973.

Nelson, L.S., Duda, P.M., Leisher, W.B., Kim, H., and Corradini, M.L., High Press. High Temp., v19, n2, pp. 235–236, 1987.

Appendix B:
Charge Amplifier Characteristics

B Charge Amplifier Characteristics

This appendix contains technical information about the Kistler model 5004 dual-mode charge amplifier used to amplify the pressure transducer signals. The amplifier is "dual-mode" because signals from both charge-producing and voltage-producing pressure transducers may be amplified, depending on which input connector is selected. Figure B contains the relevant portion of the circuit diagram. The amplification circuit is a three stage device consisting of an inverting current integrator, a filter, and a non-inverting amplifier with variable gain.

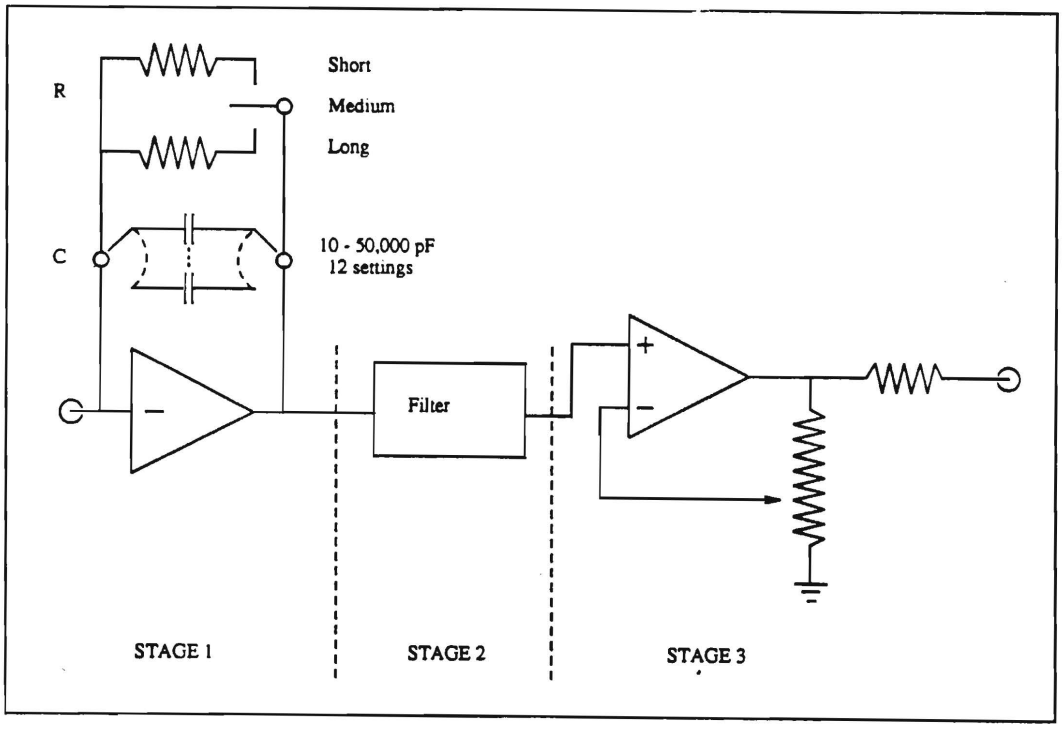

Figure B.1: Circuit Diagram for the Charge Amplifier

The first stage of the device is an inverting integrator. Signals from charge-producing transducers are connected directly to the inverting input of the op-amp; signals from voltage-producing sensors are connected across a precision capacitor to convert them into charge signals. Load changes on the pressure transducer generate small currents into the amplifier. The capacitor in the op-amp feedback loop "integrates" these signals so that the output of the first stage is V_1=-Q_{in}/C_{range}, where Q_{in} is the total integrated charge at due to the small currents. Twelve capacitor settings are available to adjust the value of C_{range}. These capacitors (and the op-amp itself) are highly insulating, so very little charge leaks off through them; resistor R in the feedback loop provides the only return to ground. Quasi-static measurements can be made by removing the resistor entirely ("Long" time integration), but the amplifier may drift into saturation if ground loops through the transducer are present. Resistor R allows such drift currents to leak off. With R in place, the elements in the feedback loop act as a high-pass filter with a 3dB point given by $1/RC_{range}$. Data in this report were collected with C_{range}=10 pF (the most sensitive range) and R=10^9 Ω (the "Short" time constant setting). The time constant for this combination is 0.01 seconds, that is, signals below 100 Hz were filtered out.

The second stage of the device is a low pass filter with a 3dB point of 180 kHz. The frequency response of the amplifier's final output is given in Figure B (the curve shown is for C_{range}=10 pF and assumes a capacitive transducer load of approximately 300 pF). The output from the filter is $V_2=\mathcal{R}V_1$, where the frequency response factor $\mathcal{R}$ is given by:

$$\mathcal{R} = \frac{1}{1 + \frac{1}{v(f)}\left(\frac{C_{range}+C_{load}}{C_{range}}\right)}$$

The value of v(f) is approximately 50,000 times the percentage shown on the frequency response graph for frequency f in Figure B.

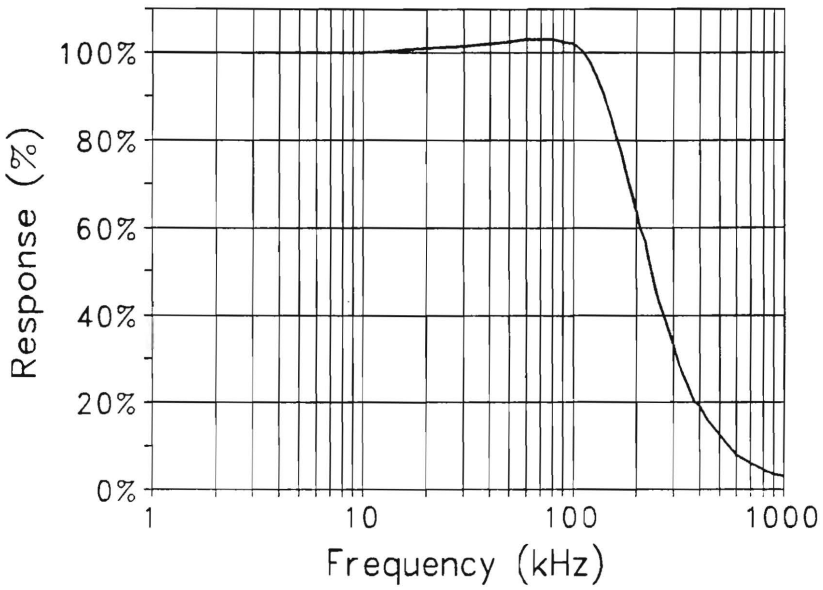

Figure B.2: Frequency Response of the Charge Amplifier

The third stage of the circuit is a adjustment setting for the transducer sensitivity. It is a non-inverting amplifier whose gain is given by $G_3 \approx 10/(\text{Dial Setting})$. The dial setting was 4.00 for all of the measurements in this report. The final voltage output for the charge amplifier is the product:

$$V_{out} = -\frac{Q_{in}\mathcal{R}G_3}{C_{range}}$$

This factor was used to calculate the lithium niobate pressure transducer's hydrostatic constant (which relates the charge produced by a step increase in pressure) once the voltage output had been measured during the calibration procedure (Appendix A). The condition $\mathcal{R} \approx 1$ was used for all calculations of peak pressures in this report.

Appendix C:
Summary of Peak Pressure Data

C Summary of Peak Pressure Data

NOTES

Viscosity Ratios: All values were measured except for those in parentheses. These were calculated from the concentration using the relations in Appendix 2.

Voltage Minima: Negative voltage corresponds to an increase in pressure.

NS=No Signal. (No pressure signal above the trigger treshold of 0.60 kPa.)

Time: Time value in the data file at which the minimum occured.

Table C.1: Peak Pressure Summary for Deionized Water

#	Name	T_{tin}	Peak Voltage (V)	Peak Pressure (kPa)	File Time (msec)
1	WN911ADA	1000°C	-0.1681	4.038	64.025
2	WN911ADB		-0.8317	19.981	64.000
3	WN911ADC		-0.7000	16.817	150.000
4	WN911ADD		1.8237	43.812	125.625
5	WN911ADE		-0.1744	4.190	69.025
6	WN911ADF		-1.4294	34.339	132.800
7	WN911ADG		3.0019	72.117	131.200
8	WN911ADH		-0.1673	4.019	70.025
9	WN911ADI		-0.3153	7.575	63.925
10	WN911ADJ		-0.5583	13.412	150.025
1	WN914BDA	900°C	-0.3625	8.709	103.850
2	WN914BDB		-0.6335	15.219	118.175
3	WN914BDC		-2.1733	52.211	120.800
4	WN914BDD		-5.1359	123.383	81.150
5	WN914BDE		-2.2875	54.954	112.500
6	WN914BDF		-2.3274	55.913	90.725
7	WN914BDG		-2.5805	61.993	327.400
8	WN914BDH		-0.5227	12.557	77.600
9	WN914BDI		-1.2884	30.952	67.650
10	WN914BDJ		-0.9153	21.989	113.075
1	WN917CDA	800°C	-1.6659	40.021	111.475
2	WN917CDB		-1.4224	34.171	106.925
3	WN917CDC		-0.6100	14.654	67.375
4	WN917CDD		-0.1166	2.801	66.600
5	WN917CDE		-0.4383	10.530	164.200
6	WN917CDF		-2.1880	52.564	618.075
7	WN917CDG		-1.2994	31.216	72.275
8	WN917CDH		-0.3137	7.536	70.400
9	WN917CDI		-0.1846	4.435	65.350
10	WN917CDJ		-0.2532	6.083	64.700

(Table continued on following page.)

Water (Continued)

#	Name	T_{tin}	Peak Voltage (V)	Peak Pressure (kPa)	File Time (msec)
1	WN919DDA	700°C	-0.7574	18.196	65.475
2	WN919DDB		-0.4598	11.046	70.825
3	WN919DDC		-0.4222	10.143	63.800
4	WN919DDD		No data		
5	WN919DDE		-0.6192	14.875	106.175
6	WN919DDF		-0.4247	10.203	166.650
7	WN919DDG		-1.8426	44.266	116.725
8	WN919DDH		-2.6818	64.427	172.450
9	WN919DDI		-1.1892	28.569	66.425
10	WN919DDJ		-2.4753	59.466	539.250
1	WN922EDA	600°C	-0.2039	4.898	64.600
2	WN922EDB		-0.1194	2.868	63.500
3	WN922EDC		-0.5279	12.682	89.675
4	WN922EDD		-0.3632	8.725	203.825
5	WN922EDE		-0.9159	22.003	98.125
6	WN922EDF		-0.7926	19.041	65.000
7	WN922EDG		-0.4285	10.294	73.075
8	WN922EDH		-0.4422	10.623	64.675
9	WN922EDI		-0.3876	9.312	123.700
10	WN922EDJ		-0.5379	12.922	296.500

Table C.2: Peak Pressure Summary for Galactosol 211
(Melt Temperature: 1000°C)

#	Name	Batch	Viscosity Ratio (25°C)	Peak Voltage (V)	Peak Pressure (kPa)	File Time (msec)
1	GNN04ACA	11/01/91-1	1.262	-0.522	12.540	94.600
2	GNN04ACB			-0.234	5.622	63.725
3	GNN04ACC			-10.000	240.237	500.175
4	GNN04ACD			-0.550	13.213	192.000
5	GNN04ACE			-1.602	38.486	94.975
6	GNN04ACF			-0.874	20.997	106.025
7	GNN04ACG			-0.591	14.198	184.225
8	GNN04ACH			-2.002	48.095	67.300
9	GNN04ACI			-2.754	66.161	163.400
10	GNN04ACJ			-1.812	43.531	103.650
11	GN902CBA	8/29/91-2	1.31	-3.146	75.583	242.320
12	GN902CBB			NS	0.000	
13	GN902CBC			NS	0.000	
14	GN902CBD			-9.278	222.882	134.340
15	GN902CBE			NS	0.000	
1	GNN04ABA	11/01/91-2	1.531	-2.935	70.510	423.600
2	GNN04ABB			-3.066	73.657	193.600
3	GNN04ABC			NS	0.000	
4	GNN04ABD			-10.000	240.237	593.900
5	GNN04ABE			-0.269	6.462	168.100
6	GNN04ABF			-1.353	32.504	82.600
7	GNN04ABG			-0.500	12.012	64.000
8	GNN04ABH			-0.967	23.231	65.575
9	GN901CCA	8/29/91-3	1.54	-4.187	100.580	50.680
10	GN901CCB			-6.939	166.691	569.340
1	GNN04AAA	11/01/91-3	2.00	-0.513	12.324	64.600
2	GNN04AAB			-4.526	108.731	66.450
3	GNN04AAC			-0.425	10.210	65.175
4	GNN04AAD			-0.898	21.573	186.950
5	GNN04AAE			-0.337	8.096	293.475

(Table continued on following page.)

Galactosol (Continued)

#	Name	Batch	Viscosity Ratio (25°C)	Peak Voltage (V)	Peak Pressure (kPa)	File Time (msec)
6	GNN04AAF	11/01/91-3	2.00	-0.244	5.862	63.850
7	GNN04AAG			-0.278	6.679	70.300
8	GNN04AAH			-0.527	12.660	97.425
9	GNN04AAI			-0.400	9.609	64.175
10	GNN04AAJ			NS	0.000	
1	GN830CDA	8/24/91-2	2.37	-0.300	7.207	N/A
2	GN830CDB			NS	0.000	
3	GN830CDC			NS	0.000	

Table C.3: Peak Pressure Summary for Natrosol 250HHR
(Melt Temperature: 1000°C)

#	Name	Batch	Viscosity Ratio (25°C)	Peak Voltage (V)	Peak Pressure (kPa)	File Time (msec)
1	HNN08ACA	11/06/91-1	1.23	-4.644	111.566	109.800
2	HNN08ACB			-0.439	10.546	128.050
3	HNN08ACC			-1.616	38.822	88.625
4	HNN08ACD			-0.854	20.516	171.925
5	HNN08ACE			-1.294	31.087	102.400
6	HNN08ACF			-3.145	75.555	168.950
7	HNN08ACG			-0.732	17.585	202.325
8	HNN08ACH			-0.293	7.039	105.900
9	HNN08ACI			-0.356	8.552	69.925
10	HNN08ACJ			-2.134	51.267	69.850
11	HN902CBA	8/27/91-3	1.26	NS	0.000	
12	HN902CBB			-0.966	23.207	51.060
13	HN902CBC			No data		
14	HN902CBD			NS	0.000	
15	HN902CBE			-1.118	3.895	55.660
1	HNN08ABA	11/06/91-2	1.55	-10.000	240.237	399.525
2	HNN08ABB			-0.576	13.838	68.975
3	HNN08ABC			-0.898	21.573	111.350
4	HNN08ABD			-0.479	11.507	64.550
5	HNN08ABE			-5.308	127.518	84.800
6	HNN08ABF			-0.293	7.039	187.200
7	HNN08ABG			-7.852	188.634	377.925
8	HNN08ABH			-0.557	13.381	361.325
9	HNN08ABI			-0.356	8.552	126.350
10	HNN08ABJ			-8.882	213.378	71.700
1	HNN08AAA	11/06/91-3	1.96	5.981	143.686	75.650
2	HNN08AAB			2.397	57.585	92.375
3	HNN08AAC			5.142	123.530	228.475
4	HNN08AAD			1.357	32.600	107.575
5	HNN08AAE			4.063	97.608	121.275

(Table continued on following page.)

Natrosol (Continued)

#	Name	Batch	Viscosity Ratio (25°C)	Peak Voltage (V)	Peak Pressure (kPa)	File Time (msec)
6	HNN08AAF	11/06/91-3	1.96	7.329	176.070	596.200
7	HNN08AAG			1.211	29.093	86.125
8	HNN08AAH			0.151	3.628	150.350
9	HNN08AAI			0.415	9.970	432.125
10	HNN08AAJ			1.191	28.612	67.400
11	HN902CCA	9/01/91-1	1.91	No data		
12	HN902CCB			No data		
13	HN902CCC			NS	0.000	
14	HN902CCD			2.8307	68.004	110.160
15	HN902CCE			NS	0.000	
1	HN901CDA	8/30/91-1	2.72	N/A		
2	HN901CDB			NS	0.000	
3	HN901CDC			NS	0.000	
4	HN901CDD			NS	0.000	
5	HN901CDE			NS	0.000	
1	HN117ADA	1/10/92-1	4.09	0.742	17.826	64.075
2	HN117ADB			0.229	5.501	62.950
3	HN117ADC			0.137	3.291	64.000
4	HN117ADD			0.347	8.336	64.025
5	HN117ADE			10.000	240.237	68.300

Table C.4: Peak Pressure Summary for Percol 1011
(Melt Temperature: 1000°C)

#	Name	Batch	Viscosity Ratio (25°C)	Peak Voltage (V)	Peak Pressure (kPa)	File Time (msec)
1	ENN08ACA	11/07/91-1	1.03	-10.000	240.237	N/A
2	ENN08ACB			-6.074	145.920	220.750
3	ENN08ACC			-0.845	20.300	121.225
4	ENN08ACD			-8.540	205.162	125.900
5	ENN08ACE			-10.000	240.237	731.800
6	ENN08ACF			-5.830	140.058	535.500
7	ENN08ACG			-0.186	4.468	80.275
8	ENN08ACH			-3.472	83.410	233.625
9	ENN08ACI			-10.000	240.237	198.525
10	ENN08ACJ			-10.000	240.237	294.700
1	ENN08ABA	11/07/91-2	1.13	-0.742	17.826	203.900
2	ENN08ABB			-9.326	224.045	217.800
3	ENN08ABC			-2.437	58.546	121.650
4	ENN08ABD			-5.610	134.773	168.400
5	ENN08ABE			-3.154	75.771	96.900
6	ENN08ABF			-1.152	27.675	191.850
7	ENN08ABG			-1.572	37.765	69.250
8	ENN08ABH			-4.722	113.440	343.100
9	ENN08ABI			-1.851	44.468	252.225
10	ENN08ABJ			-1.465	35.195	65.000
1	END03ACA	11/29/91-1	1.25	-0.308	7.399	140.475
2	END03ACB			-0.127	3.051	142.650
3	END03ACC			-1.812	43.531	175.800
4	END03ACD			-0.840	20.180	130.575
5	END03ACE			-10.000	240.237	N/A
6	END03ACF	11/29/91-1	1.25	-0.425	10.210	63.850
7	END03ACG			-0.693	16.648	142.300
8	END03ACH			-1.182	28.396	164.200
9	END03ACI			-0.688	16.528	120.100
10	END03ACJ			-10.000	240.237	300.925

(Table continued on following page.)

Percol (Continued)

#	Name	Batch	Viscosity Ratio (25°C)	Peak Voltage (V)	Peak Pressure (kPa)	File Time (msec)
1	ENN08AAA	11/07/91-3	1.38	-6.592	158.364	156.825
2	ENN08AAB			-1.123	26.979	130.900
3	ENN08AAC			-0.947	22.750	227.875
4	ENN08AAD			-0.293	7.039	65.075
5	ENN08AAE			1.338	32.144	282.750
6	ENN08AAF			-1.343	32.264	123.650
7	ENN08AAG			-0.186	4.468	63.825
8	ENN08AAH			-1.553	37.309	354.300
9	ENN08AAI			-6.265	150.508	592.500
10	ENN08AAJ			-4.697	112.839	713.000
1	END03ABA	11/28/91-1	1.55	-3.135	75.314	253.950
2	END03ABB			-1.738	41.753	115.950
3	END03ABC			-2.837	68.155	338.575
4	END03ABD			-0.430	10.330	150.925
5	END03ABE			-1.509	36.252	265.675
6	END03ABF			-10.000	240.237	N/A
7	END03ABG			NS	0.000	
8	END03ABH			NS	0.000	
9	END03ABI			-0.190	4.565	169.975
10	END03ABJ			-10.000	240.237	N/A
11	EN901CBA	8/28/91-4	1.51	NS	0.000	
12	EN901CBB			NS	0.000	
13	EN901CBC			-1.574	37.818	293.880
14	EN901CBD			No data		
15	EN901CBE			NS	0.000	
1	END03AAA	11/28/91-2	2.15	-0.469	11.267	98.675
2	END03AAB			-0.352	8.456	101.625
3	END03AAC			0.396	9.513	88.125
4	END03AAD			-1.387	33.321	361.875
5	ENDO3AAE			-0.352	8.456	303.825

(Table continued on following page.)

Percol (Continued)

#	Name	Batch	Viscosity Ratio (25°C)	Peak Voltage (V)	Peak Pressure (kPa)	File Time (msec)
6	END03AAF	11/28/91-2	2.15	-0.249	5.982	118.550
7	END03AAG			-0.132	3.171	155.475
8	END03AAH			-0.410	9.850	352.700
9	END03AAI			-0.664	15.952	159.425
10	END03AAJ			-0.645	15.495	64.500
11	EN901CCA	8/29/91-1	2.05	-0.322	7.733	67.300
12	EN901CCB			NS	0.000	
13	EN901CCC			NS	0.000	
14	EN901CCD			NS	0.000	
15	EN901CCE			NS	0.000	
1	EN117ADA	1/10/92-2	3.46	0.181	4.348	255.275
2	EN117ADB			0.166	3.988	68.825
3	EN117ADC			0.586	14.078	85.950
4	EN117ADD			0.791	19.003	413.500
5	EN117ADE			0.488	11.724	412.125
6	EN117ADF	1/10/92-2	3.46	0.518	12.444	64.250
7	EN117ADG			0.605	14.534	64.575
8	EN117ADH			0.259	6.222	79.275
9	EN117ADI			0.166	3.988	54.450
10	EN117ADJ			0.166	3.988	64.025

Table C.5: Peak Pressure Summary for Poly(ethylene oxide)

#	Name	T_{tin}	Batch	Viscosity Ratio (25°C)	Peak Voltage (V)	Peak Pressure (kPa)	File Time (msec)
1	LOA916A	1000°C	9/12/91-1	1.01	-0.898	21.573	697.575
2	LOA916B		(10 wppm)		-2.016	48.437	120.275
3	LOA916C				No data		
4	LOA916D				-7.130	171.282	103.600
5	PN114ADA		1/7/92-1	1.01	-4.604	110.605	153.050
6	PN114ADB		(10 wppm)		-3.218	77.308	79.950
7	PN114ADC				-4.976	119.542	151.975
8	PN114ADD				-2.432	58.426	64.575
9	PN114ADE				-2.188	52.564	73.475
10	PN114ADF				-5.254	126.220	72.375
11	PN114ADG				-7.041	169.151	705.950
12	PN114ADH				-2.246	53.957	72.050
13	PN114ADI				-10.000	240.237	388.625
14	PN114ADJ				-7.847	188.514	103.525
1	PN114AEA	1000°C	1/6/92-3	1.02	-1.021	24.528	106.075
2	PN114AEB		(25 wppm)		-2.764	66.401	203.350
3	PN114AEC				-3.569	85.741	108.950
4	PN114AED				-10.000	240.237	478.400
5	PN114AEE				-2.056	49.393	326.450
6	PN114AEF				-2.358	56.648	241.100
7	PN114AEG				-7.212	173.259	87.950
8	PN114AEH				-1.875	45.044	172.850
9	PN114AEI				-1.250	30.030	114.800
10	PN114AEJ				-4.346	104.407	214.175
1	LOC916A	1000°C	9/12/91-3	1.09	-1.076	25.842	167.750
2	LOC916B		(50 wppm)		-0.708	17.009	655.175
3	LOC916C				-10.000	240.237	777.175
4	LOC916D				-0.522	12.545	91.575
5	PN114AFA		1/6/92-2	1.07	-10.000	240.237	287.650
6	PN114AFB		(50 wppm)		-9.287	223.108	358.700

(Table continued on following page.)

Poly(ethylene oxide) (Continued)

#	Name	T_{tin}	Batch	Viscosity Ratio (25°C)	Peak Voltage (V)	Peak Pressure (kPa)	File Time (msec)
7	PN114AFC	1000°C	1/6/92-2	1.07	-2.256	54.197	235.025
8	PN114AFD		(50 wppm)		-0.410	9.850	119.550
9	PN114AFE				-1.797	43.171	85.600
10	PN114AFF				-0.620	14.895	157.400
11	PN114AFG				-0.684	16.432	64.000
12	PN114AFH				-5.469	131.386	260.700
13	PN114AFI				-10.000	240.237	77.600
14	PN114AFJ				-3.022	72.600	277.775
1	PN114AGA	1000°C	1/6/92-1	1.13	-3.999	96.071	387.650
2	PN114AGB		(100 wppm)		-1.553	37.309	411.375
3	PN114AGC				-0.518	12.444	94.700
4	PN114AGD				-9.106	218.760	72.825
5	PN114AGE				-0.200	4.805	307.475
6	PN114AGF				-0.402	9.658	244.425
7	PN114AGG				-1.855	44.564	247.325
8	PN114AGH				-0.391	9.393	207.075
9	PN114AGI				-0.513	12.324	324.725
10	PN114AGJ				-0.966	23.207	115.000
1	PN911ACA	1000°C	9/8/91-1	1.29	-0.058	1.401	58.725
2	PN911ACB				-0.130	3.111	64.100
3	PN911ACC				-0.166	3.986	64.025
4	PN911ACD				-0.319	7.668	140.850
5	PN911ACE				NS	0.000	
6	PNN01ACA		10/28/91-1	1.27	-0.308	7.399	63.975
7	PNN01ACB				-4.302	103.350	75.300
8	PNN01ACC				-0.439	10.546	66.925
9	PNN01ACD				-0.156	3.748	68.425
10	PNN01ACE				-0.298	7.159	93.000

(Table continued on following page.)

Poly(ethylene oxide) (Continued)

#	Name	T_{tin}	Batch	Viscosity Ratio (25°C)	Peak Voltage (V)	Peak Pressure (kPa)	File Time (msec)
1	PN901CBA	1000°C	8/28/91-1	1.60	NS	0.000	
2	PN901CBB				NS	0.000	
3	PN901CBC				NS	0.000	
4	PN829CCA		8/27/91-2	1.58	NS	0.000	
5	PN829CCB				NS	0.000	
6	PN911ABA		9/5/91-5	1.52	NS	0.000	
7	PN911ABB				NS	0.000	
8	PN911ABC				NS	0.000	
9	PN911ABD				NS	0.000	
10	PN911ABE				NS	0.000	
11	PNN01ABA		10/28/91-2	1.49	NS	0.000	
12	PNN01ABB				NS	0.000	
13	PNN01ABC				NS	0.000	
14	PNN01ABD				-0.103	2.474	64.225
15	PNN01ABE				-0.835	20.060	64.000
16	PNN01ABF				-0.137	3.291	62.150
17	PNN01ABG				-0.918	22.054	229.450
1	PN911AAA	1000°C	9/5/91-6	1.97	NS	0.000	
2	PN911AAB				NS	0.000	
3	PN911AAC				NS	0.000	
4	PN911AAD				NS	0.000	
5	PN911AAE				NS	0.000	
6	PNN01AAA		10/28/91-3	1.97	NS	0.000	
7	PNN01AAB				NS	0.000	
8	PNN01AAC				NS	0.000	
9	PNN01AAD				NS	0.000	
10	PNN01AAE				NS	0.000	
1	PN914BCA	900°C	9/8/91-1	1.29	NS	0.000	
2	PN914BCB				NS	0.000	
3	PN914BCC				-0.287	6.904	123.175

(Table continued on following page.)

Poly(ethylene oxide) (Continued)

#	Name	T_{tin}	Batch	Viscosity Ratio (25°C)	Peak Voltage (V)	Peak Pressure (kPa)	File Time (msec)
4	PN914BCD	900°C	9/8/91-1	1.29	NS	0.000	
5	PN914BCE				NS	0.000	
6	PNN01BCA		10/29/91-1	1.27	NS	0.000	
7	PNN01BCB				NS	0.000	
8	PNN01BCC				NS	0.000	
9	PNN01BCD				-0.723	17.369	64.000
10	PNN01BCE				-0.146	3.507	64.225
1	PN914BBA	900°C	9/5/91-5	1.52	NS	0.000	
2	PN914BBB				NS	0.000	
3	PN914BBC				NS	0.000	
4	PN914BBD		9/8/91-2	1.42	NS	0.000	
5	PN914BBE				NS	0.000	
6	PNN01BBA		10/29/91-2	1.52	NS	0.000	
7	PNN01BBB				-3.613	86.798	70.650
8	PNN01BBC				NS	0.000	
9	PNN01BBD				NS	0.000	
10	PNN01BBE				NS	0.000	
1	PN914BAA	900°C	9/5/91-6	1.97	NS	0.000	
2	PN914BAB				NS	0.000	
3	PN914BAC				NS	0.000	
4	PN914BAD		9/8/91-3	1.93	NS	0.000	
5	PN914BAE				NS	0.000	
6	PNN01BAA		10/29/91-3	2.04	NS	0.000	
7	PNN01BAB				NS	0.000	
8	PNN01BAC				NS	0.000	
9	PNN01BAD				NS	0.000	
10	PNN01BAE				NS	0.000	
1	PN917CCA	800°C	9/5/91-4	1.34	NS	0.000	
2	PN917CCB				NS	0.000	
3	PN917CCC				NS	0.000	

(Table continued on following page.)

Poly(ethylene oxide) (Continued)

#	Name	T_{tin}	Batch	Viscosity Ratio (25°C)	Peak Voltage (V)	Peak Pressure (kPa)	File Time (msec)
4	PN917CCD				-0.234	5.631	64.275
5	PN917CCE				-0.452	10.849	109.175
6	PNN07CCA		11/06/91-4	(1.25)	-3.789	91.026	735.175
7	PNN07CCB				-0.747	17.946	67.075
8	PNN07CCC				NS	0.000	
9	PNN07CCD				NS	0.000	
10	PNN07CCE				-0.361	8.673	64.600
1	PN917CBF	800°C	9/9/91-2	(1.5)	NS	0.000	
2	PN917CBG				NS	0.000	
3	PN917CBH				NS	0.000	
4	PN917CBI				NS	0.000	
5	PN917CBJ				-0.128	3.068	57.875
6	PN024CAA		10/23/91-1	1.58	NS	0.000	
7	PN024CAB				NS	0.000	
8	PN024CAC				NS	0.000	
9	PN024CAD				NS	0.000	
10	PN024CAE				NS	0.000	
1	PN917CAF	800°C	9/9/91-3	(2.0)	NS	0.000	
2	PN917CAG				NS	0.000	
3	PN917CAH				NS	0.000	
4	PN917CAI				NS	0.000	
5	PN917CAJ				-0.314	7.543	76.125
6	PN917CAK				NS	0.000	
7	PN024CBA		10/23/91-2	2.097	-0.210	5.045	62.550
8	PN024CBB				NS	0.000	
9	PN024CBC				NS	0.000	
10	PN024CBD				NS	0.000	
11	PN024CBE				NS	0.000	

(Table continued on following page.)

Poly(ethylene oxide) (Continued)

#	Name	T_{tin}	Batch	Viscosity Ratio (25°C)	Peak Voltage (V)	Peak Pressure (kPa)	File Time (msec)
1	PNN06DCA	700°C	11/04/91-4	1.26	-0.059	1.417	64.350
2	PNN06DCB				-0.674	16.192	64.625
3	PNN06DCC				-0.293	7.039	64.700
4	PNN06DCD				NS	0.000	
5	PNN06DCE				NS	0.000	
6	PNN06DCF				-0.098	2.354	64.100
7	PNN06DCG				-0.186	4.468	67.550
8	PNN06DCH				-0.244	5.862	64.900
9	PNN06DCI				NS	0.000	
10	PNN06DCJ				-0.337	8.096	101.600
11	PN919DCA	700°C	9/9/91-1	1.27	-6.561	157.624	84.650
12	PN919DCB				NS	0.000	
13	PN919DCC				NS	0.000	
14	PN919DCD				NS	0.000	
15	PN919DCE				NS	0.000	
16	PN919DBA				NS	0.000	
17	PN919DBB				NS	0.000	
1	PNN06DBA	700°C	11/04/91-5	1.54	-0.498	11.964	65.300
2	PNN06DBB				-0.605	14.534	178.325
3	PNN06DBC				-0.161	3.868	64.875
4	PNN06DBD				NS	0.000	
5	PNN06DBE				NS	0.000	
6	PNN06DBF				NS	0.000	
7	PNN06DBG				NS	0.000	
8	PNN06DBH				-0.278	6.679	233.225
9	PNN06DBI				NS	0.000	
10	PNN06DBJ				-1.226	29.453	64.350
11	PN919DBC	700°C	9/10/91-2	(1.5)	NS	0.000	
12	PN919DBD				-8.256	198.328	76.500
13	PN919DBE				NS	0.000	

(Table continued on following page.)

Poly(ethylene oxide) (Continued)

#	Name	T_{tin}	Batch	Viscosity Ratio (25°C)	Peak Voltage (V)	Peak Pressure (kPa)	File Time (msec)
1	PNN06DAA	700°C	11/04/91-6	2.02	NS	0.000	
2	PNN06DAB				-0.132	3.171	64.675
3	PNN06DAC				NS	0.000	
4	PNN06DAD				NS	0.000	
5	PNN06DAE				-0.122	2.931	63.900
6	PNN06DAF				-0.161	3.868	64.525
7	PNN06DAG				NS	0.000	
8	PNN06DAH				NS	0.000	
9	PNN06DAI				NS	0.000	
10	PNN06DAJ				-0.122	2.931	64.650
11	PN919DAA	700°C	9/9/91-3	(2.0)	NS	0.000	
12	PN919DAB				NS	0.000	
13	PN919DAC				NS	0.000	
14	PN919DAD				-0.606	14.551	69.650
15	PN919DAE				NS	0.000	
1	PN922ECA	600°C	9/9/91-1	1.27	NS	0.000	
2	PN922ECB				NS	0.000	
3	PN922ECC		9/10/91-1	(1.25)	NS	0.000	
4	PN922ECD				NS	0.000	
5	PN922ECE				NS	0.000	
6	PNN06ECA		11/05/91-1	(1.25)	NS	0.000	
7	PNN06ECB				-0.200	4.805	N/A
8	PNN06ECC				NS	0.000	
9	PNN06ECD				NS	0.000	
10	PNN06ECE				NS	0.000	
1	PN922EBA	600°C	9/10/91-2	(1.5)	NS	0.000	
2	PN922EBB				NS	0.000	
3	PN922EBC				NS	0.000	
4	PN922EBD				NS	0.000	
5	PN922EBE				NS	0.000	

(Table continued on following page.)

Poly(ethylene oxide) (Continued)

#	Name	T_{tin}	Batch	Viscosity Ratio (25°C)	Peak Voltage (V)	Peak Pressure (kPa)	File Time (msec)
6	PNN06EBA	600°C	11/05/91-2	(1.5)	NS	0.000	
7	PNN06EBB				NS	0.000	
8	PNN06EBC				NS	0.000	
9	PNN06EBD				NS	0.000	
10	PNN06EBE				NS	0.000	
1	PN922EAA	600°C	9/10/91-3	(2.0)	NS	0.000	
2	PN922EAB				NS	0.000	
3	PN922EAC				-9.999	240.213	73.000
4	PN922EAD				NS	0.000	
5	PN922EAE				NS	0.000	
1	PN922EAA	600°C	11/04/91-4	2.45	NS	0.000	
2	PN922EAB				NS	0.000	
3	PN922EAC				NS	0.000	
4	PN922EAD				NS	0.000	
5	PN922EAE				NS	0.000	

Table C.6: Peak Pressure Summary for Glycerol
(Melt Temperature: 1000°C)

#	Name	Batch	Viscosity Ratio (25°C)	Peak Voltage (V)	Peak Pressure (kPa)	File Time (msec)
1	YN115AAA	1/11/92-3	1.68	2.598	63.232	126.350
2	YN115AAB			10.000	35.300	239.750
3	YN115AAC			1.563	5.517	188.950
4	YN115AAD			1.870	6.601	205.125
5	YN115AAE			4.653	16.425	149.250
6	YN115AAF			4.648	16.407	263.225
7	YN115AAG			0.854	3.015	91.525
8	YN115AAH			1.138	4.017	85.600
9	YN115AAI			2.827	9.979	150.250
10	YN115AAJ			1.616	39.331	162.820
1	YN115ABA	1/11/92-1	1.94	0.894	21.759	149.925
2	YN115ABB			0.684	16.648	141.600
3	YN115ABC			0.708	17.232	66.350
4	YN115ABD			1.563	38.041	134.750
5	YN115ABE			10.000	243.386	252.675
6	YN115ABF			0.713	17.353	106.650
7	YN115ABG			0.747	18.181	98.625
8	YN115ABH			2.153	52.401	137.550
9	YN115ABI			1.191	28.987	403.000
10	YN115ABJ			3.486	84.845	186.750
1	YN115ACA	1/11/92-2	2.97	0.518	12.607	106.550
2	YN115ACB			0.142	3.456	123.575
3	YN115ACC			0.625	15.212	122.350
4	YN115ACD			0.347	8.446	98.200
5	YN115ACE			0.830	20.201	67.025
6	YN115ACF			NS	0.000	
7	YN115ACG			0.635	15.455	88.150
8	YN115ACH			0.601	14.628	99.850
9	YN115ACI			0.356	8.665	121.500
10	YN115ACJ			0.752	18.303	415.650

Appendix D:
Selected Transient Pressure Signals

D Selected Transient Pressure Signals

NOTES

This appendix contains graphs of the digitized transient pressure signals for selected experiments. The experiments chosen were the same as those used for the particle size distribution tests (presented in the following appendix). In general, two experiments were selected from each of the series of ten experiments performed using a given coolant additive, tin temperature, and viscosity. The two experiments were selected so that the peak pressure for the first was near the average of the ten values for that series and the peak pressure for the second was the maximum obtained for the series. The peak pressure for each experiment is given in the upper right hand corner of each graph. Identical scales were used for each of the graphs. The vertical scale is measured in volts; negative voltage corresponds to an increase in pressure.

Water, T_{tin}=1000°C

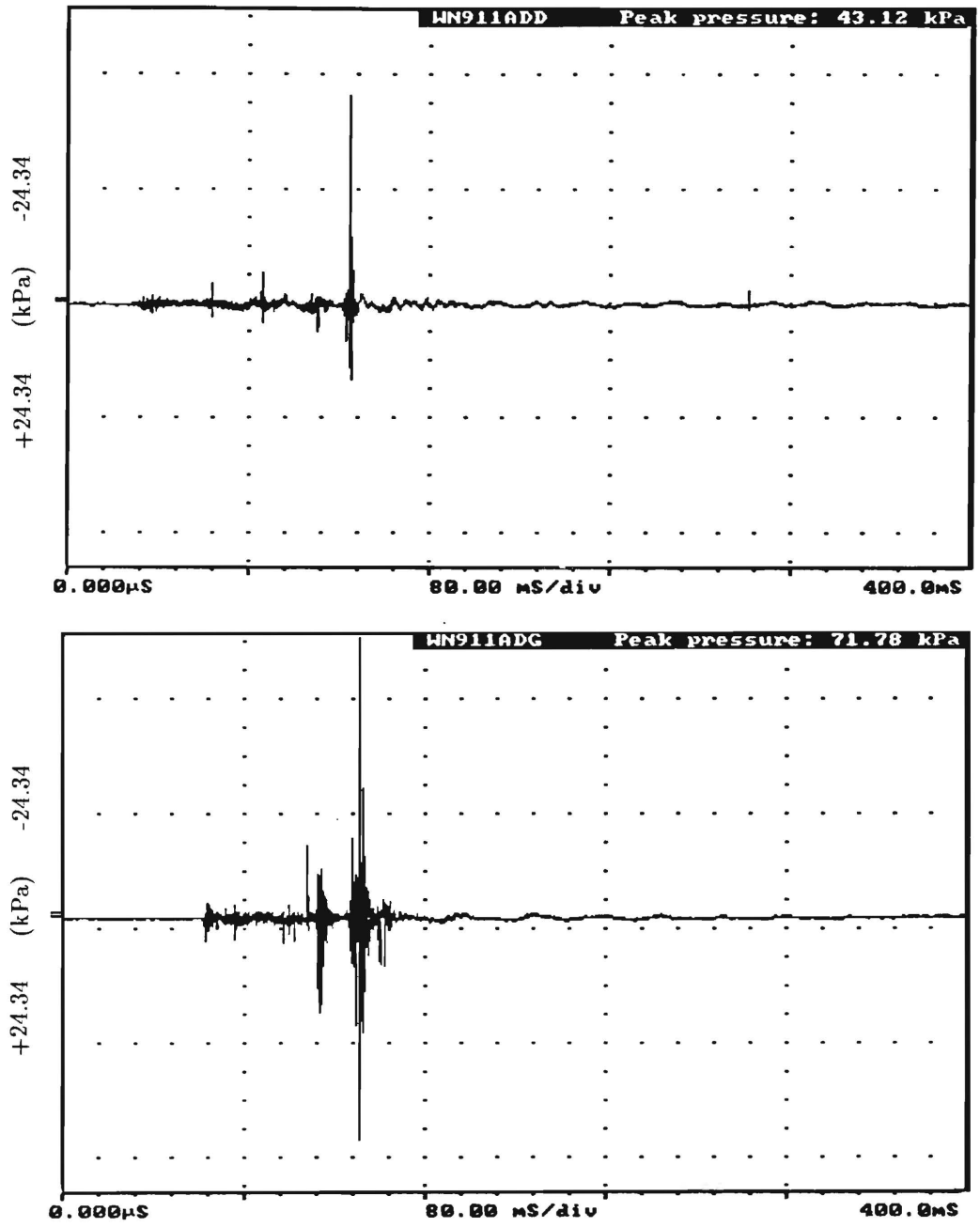

Figure D.1: Transient pressure signals for two experiments using pure water and T_{tin}=1000°C. The vertical scale for each graph is 1 volt/division (24.34 kPa/division). Values of the peak pressures are indicated on each graph.

Water, T_{tin}=900°C

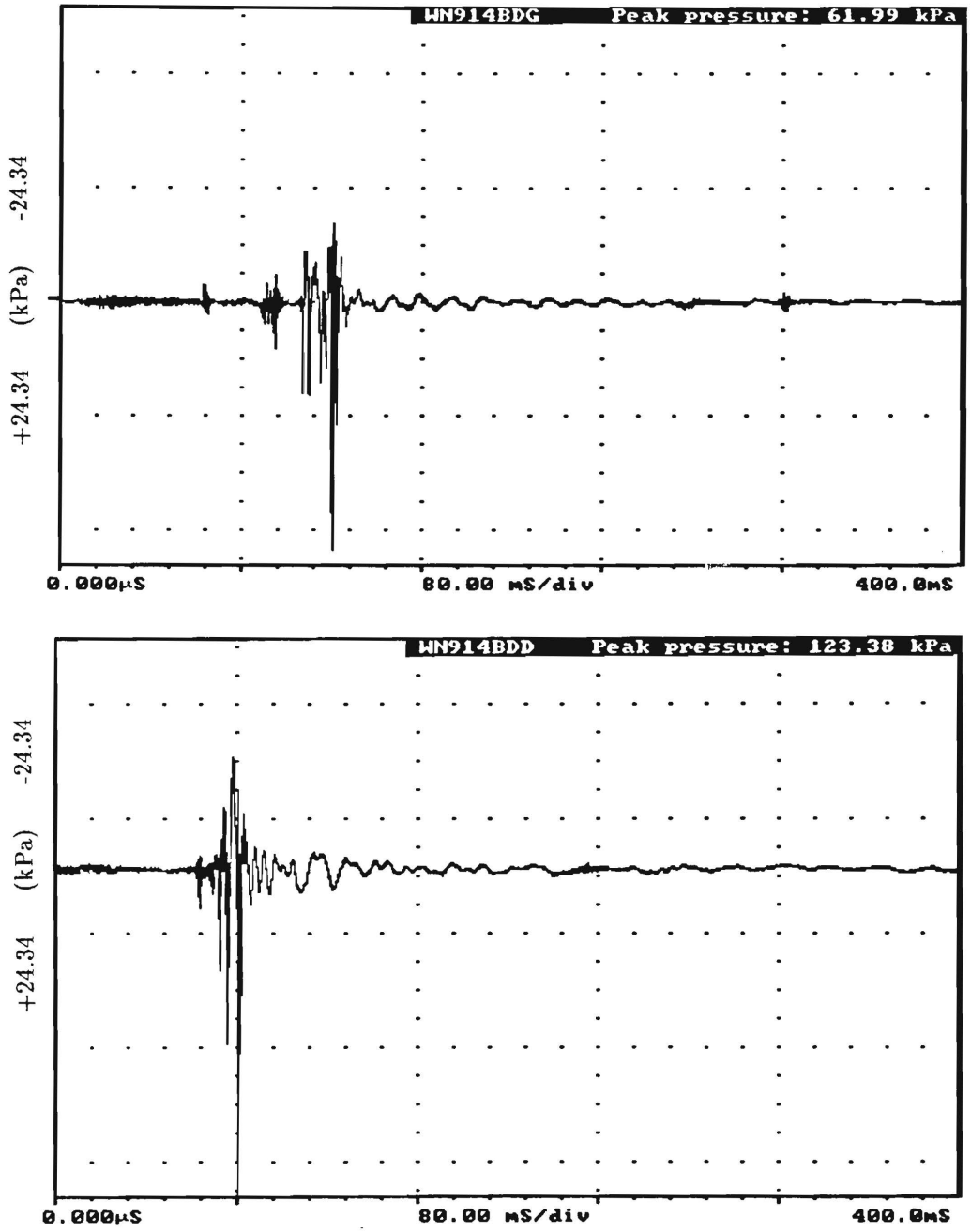

Figure D.2: Transient pressure signals for two experiments using pure water and T_{tin}=900°C. The vertical scale for each graph is 1 volt/division (24.34 kPa/division). Values of the peak pressures are indicated on each graph.

Water, T_{tin}=800°C

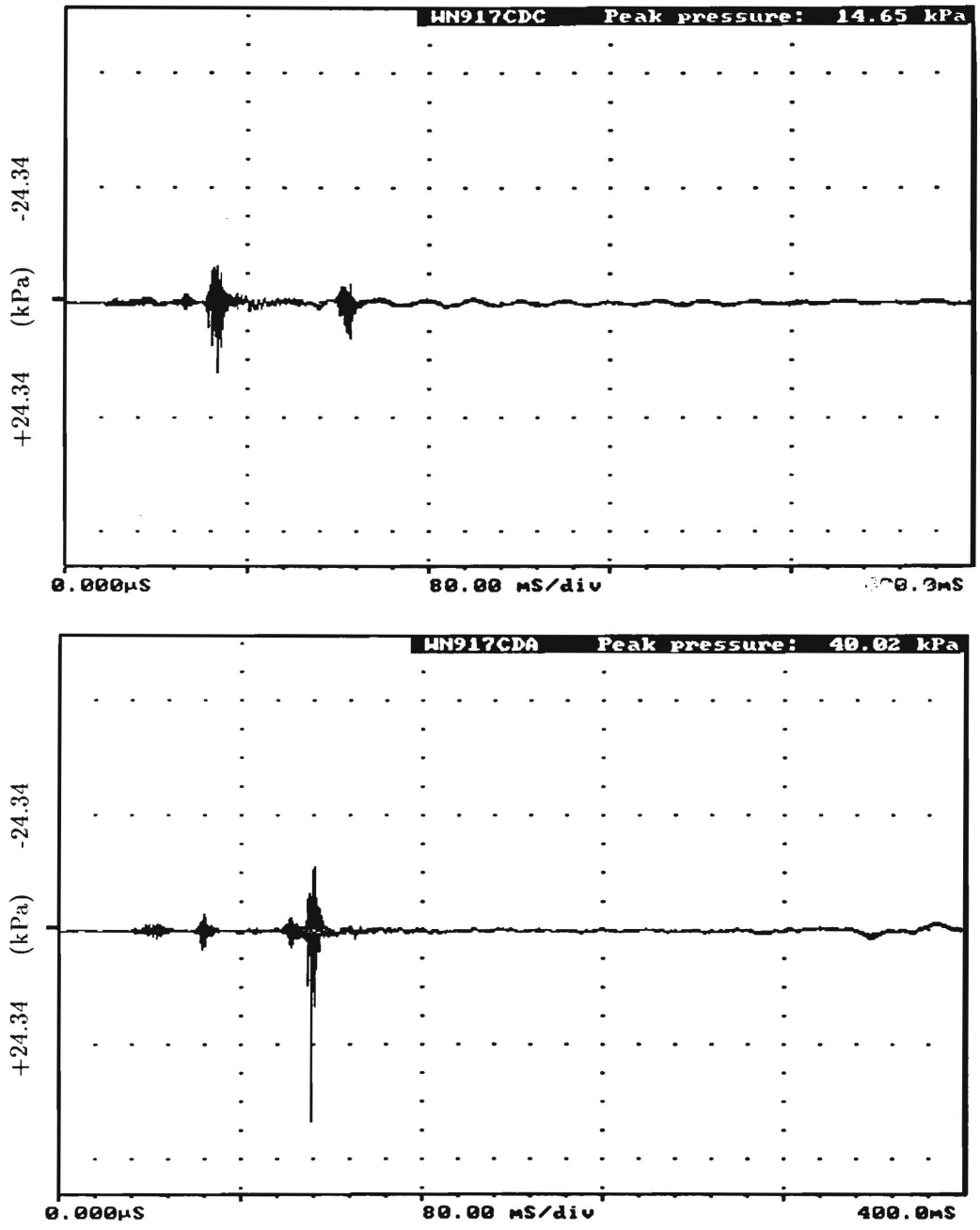

Figure D.3: Transient pressure signals for two experiments using pure water and T_{tin}=800°C. The vertical scale for each graph is 1 volt/division (24.34 kPa/division). Values of the peak pressures are indicated on each graph.

Water, T_{tin}=700°C

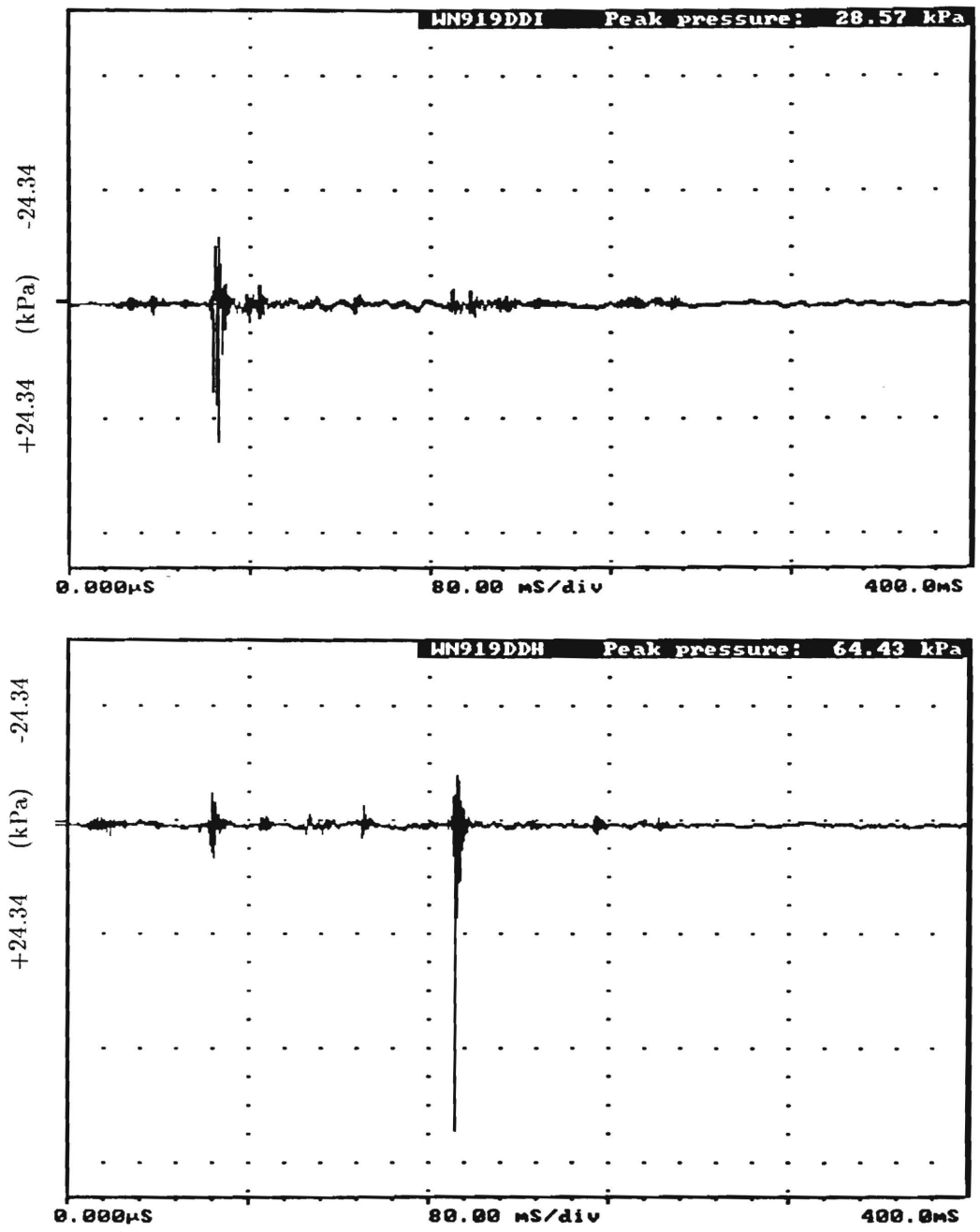

Figure D.4: Transient pressure signals for two experiments using pure water and T_{tin}=700°C. The vertical scale for each graph is 1 volt/division (24.34 kPa/division). Values of the peak pressures are indicated on each graph.

Water, T_{tin}=600°C

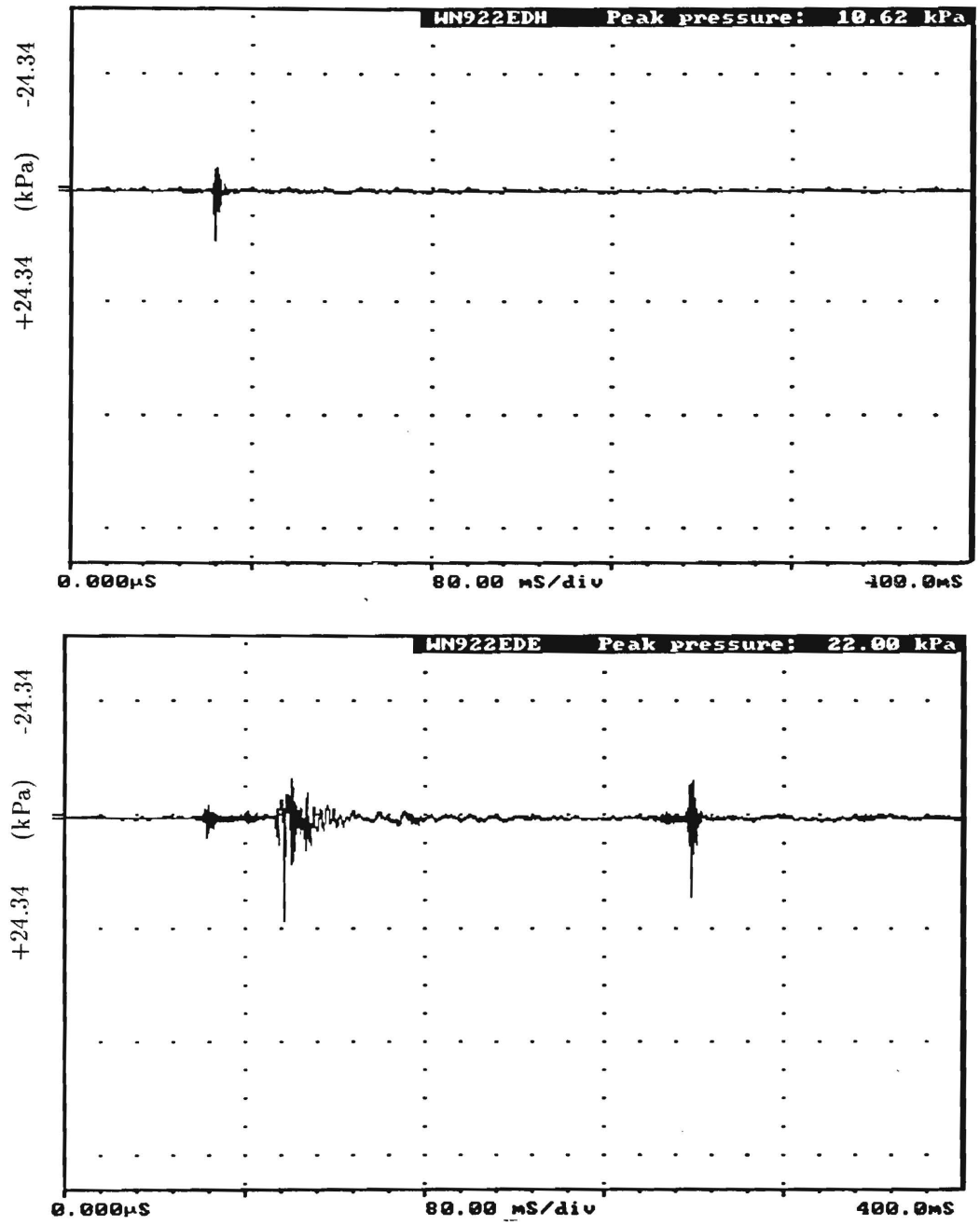

Figure D.5: Transient pressure signals for two experiments using pure water and T_{tin}=600°C. The vertical scale for each graph is 1 volt/division (24.34 kPa/division). Values of the peak pressures are indicated on each graph.

Guar gum, T_{tin}=1000°C, η_r=1.25

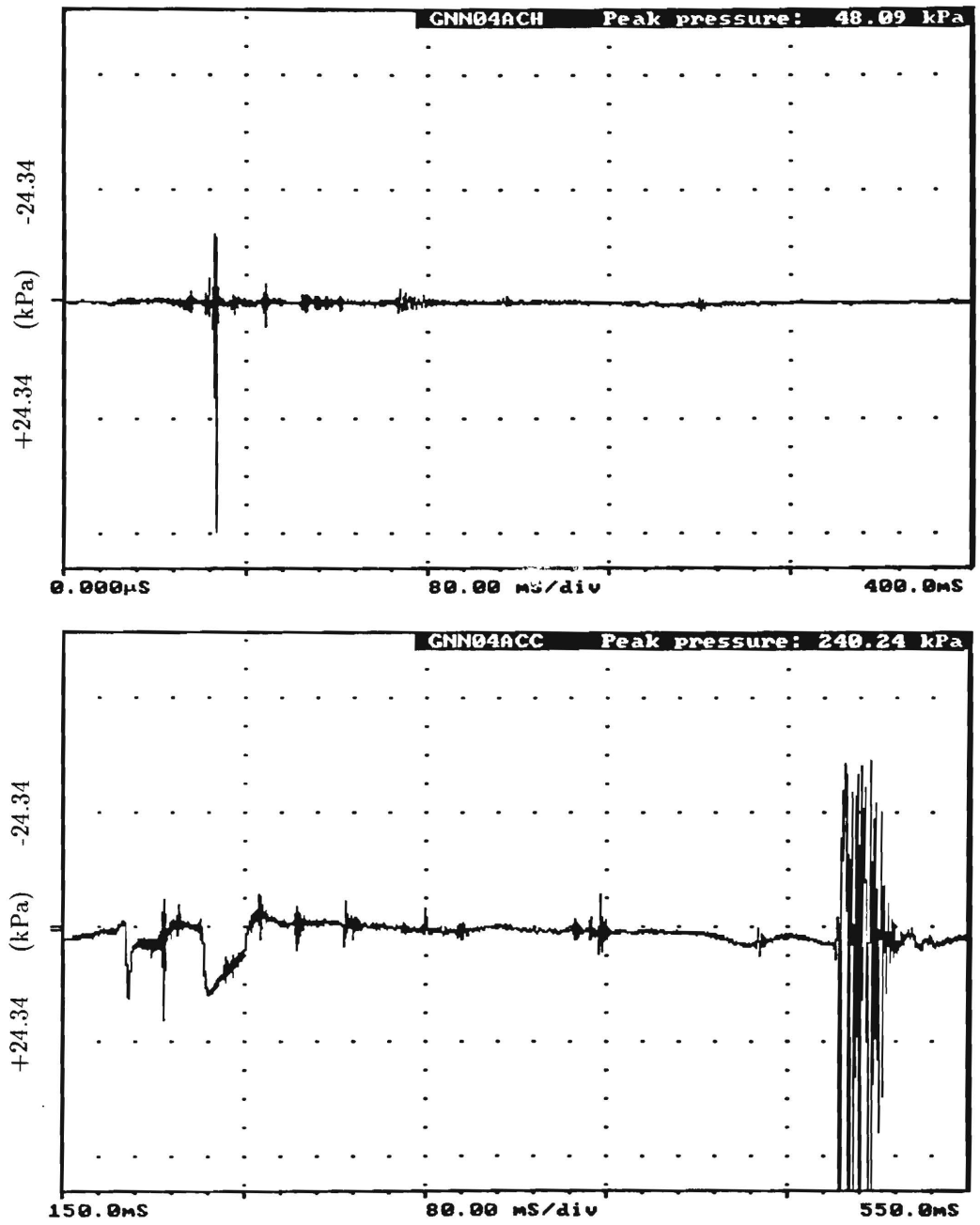

Figure D.6: Transient pressure signals for two experiments using guar gum with η_r=1.25 and T_{tin}=1000°C. The vertical scale for each graph is 1 volt/division (24.34 kPa/division). Values of the peak pressures are indicated on each graph.

Guar gum, T_{tin}=1000°C, η_r=1.54

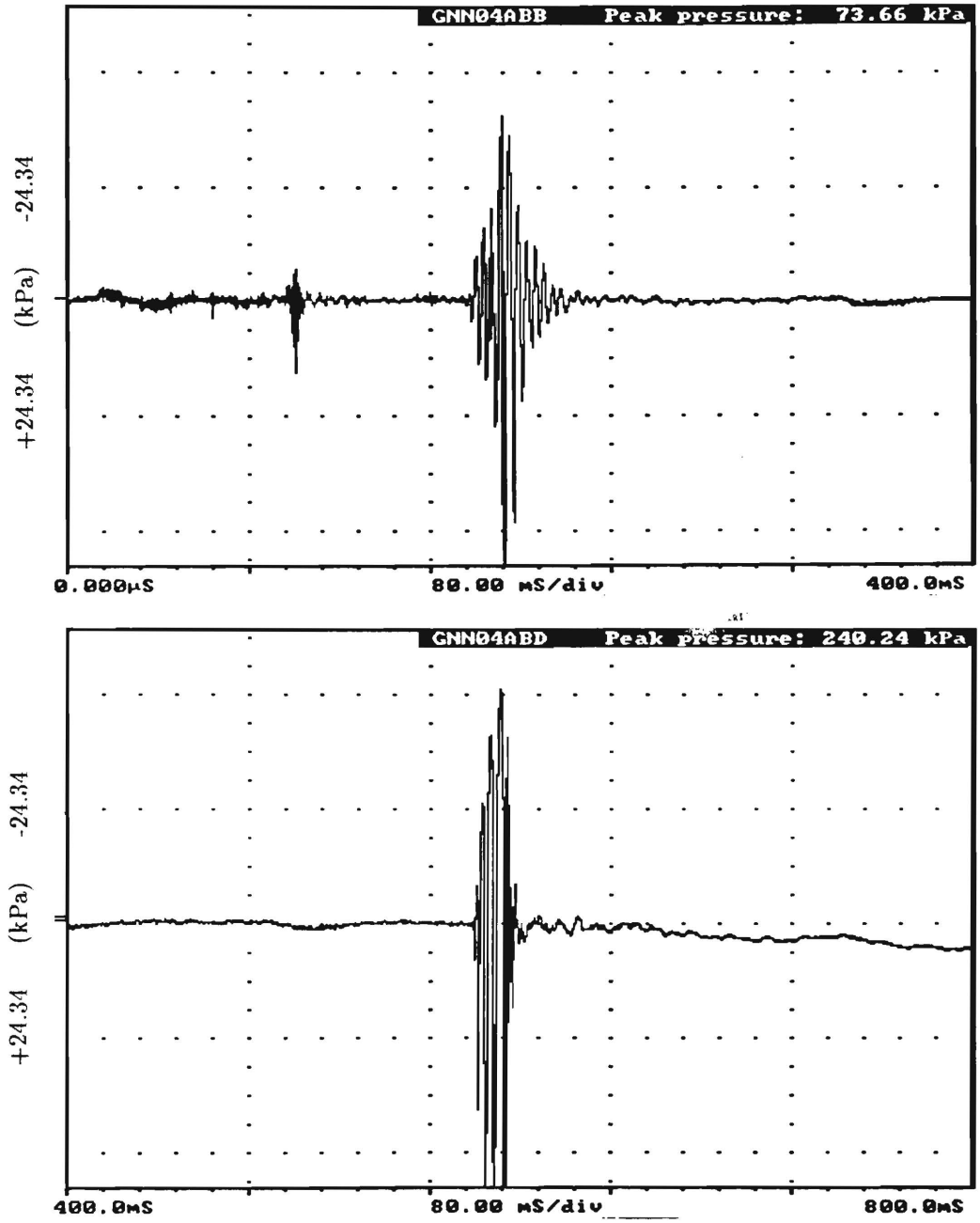

Figure D.7: Transient pressure signals for two experiments using guar gum with η_r=1.54 and T_{tin}=1000°C. The vertical scale for each graph is 1 volt/division (24.34 kPa/division). Values of the peak pressures are indicated on each graph.

Guar gum, T_{tin}=1000°C, η_r=2.00

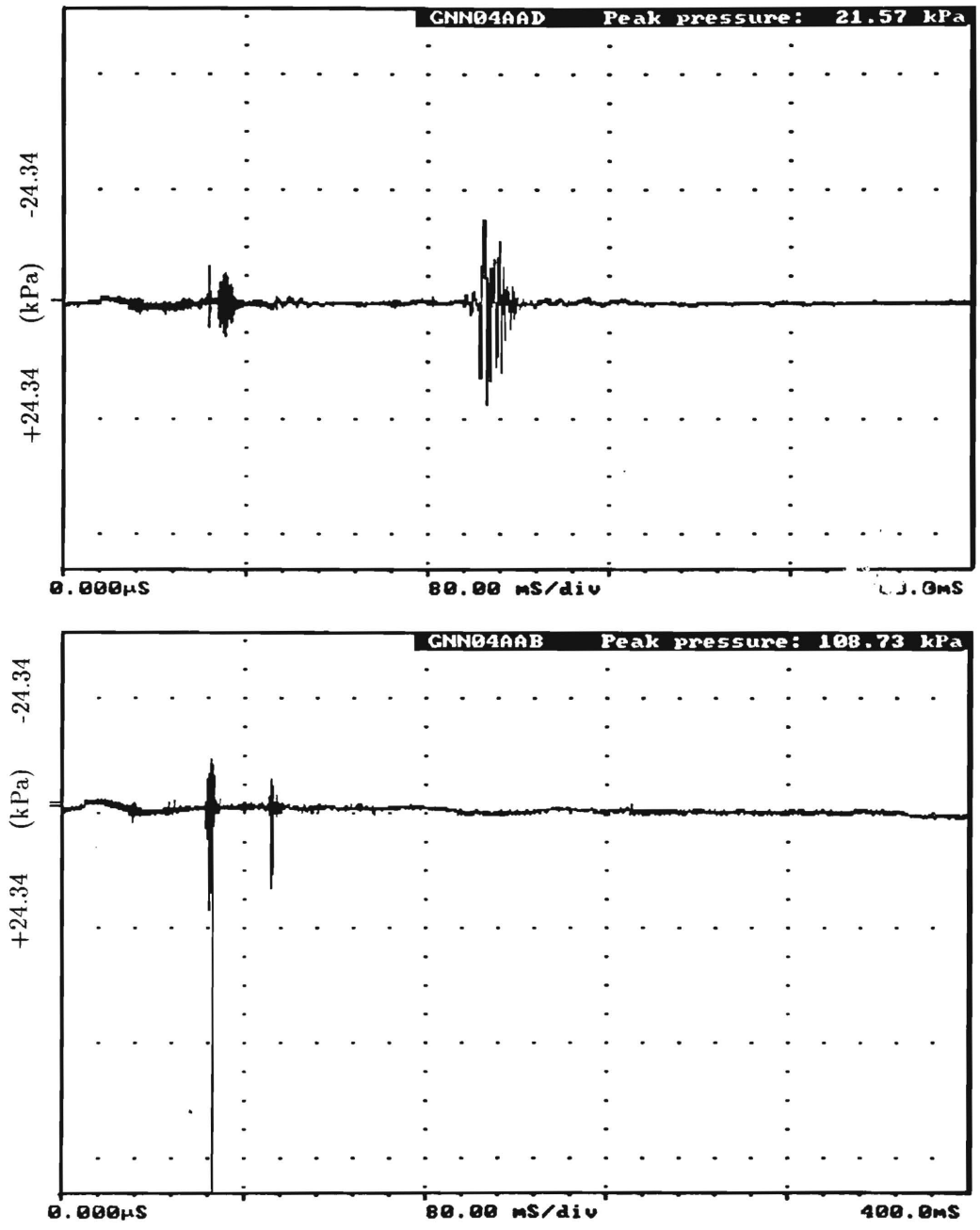

Figure D.8: Transient pressure signals for two experiments using guar gum with η_r=2.00 and T_{tin}=1000°C. The vertical scale for each graph is 1 volt/division (24.34 kPa/division). Values of the peak pressures are indicated on each graph.

Hydroxyethyl cellulose, T_{tin}=1000°C, η_r=1.23

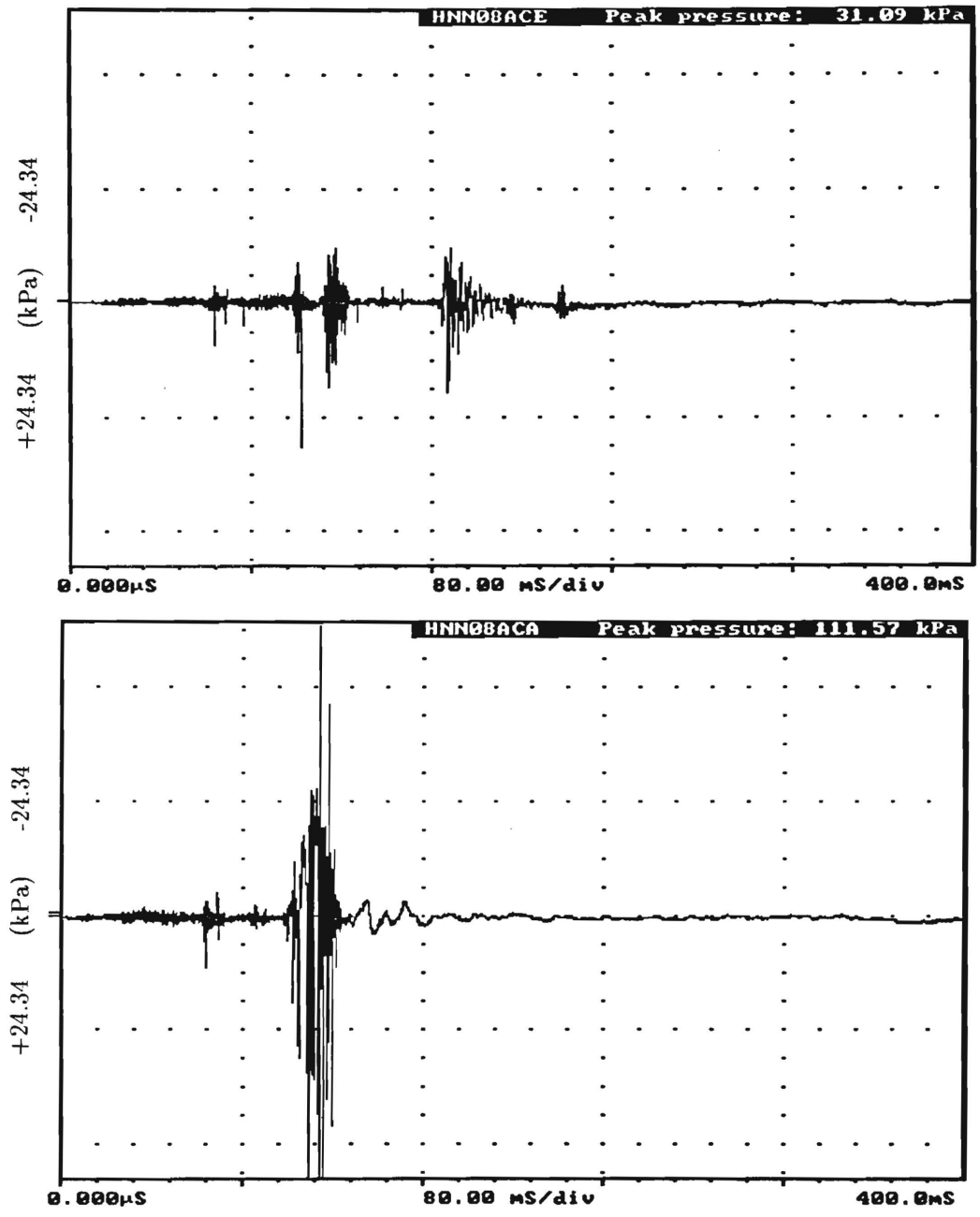

Figure D.9: Transient pressure signals for two experiments using hydroxyethyl cellulose with η_r=1.23 and T_{tin}=1000°C. The vertical scale for each graph is 1 volt/division (24.34 kPa/division). Values of the peak pressures are indicated on each graph.

Hydroxyethyl cellulose, T_{tin}=1000°C, η_r=1.55

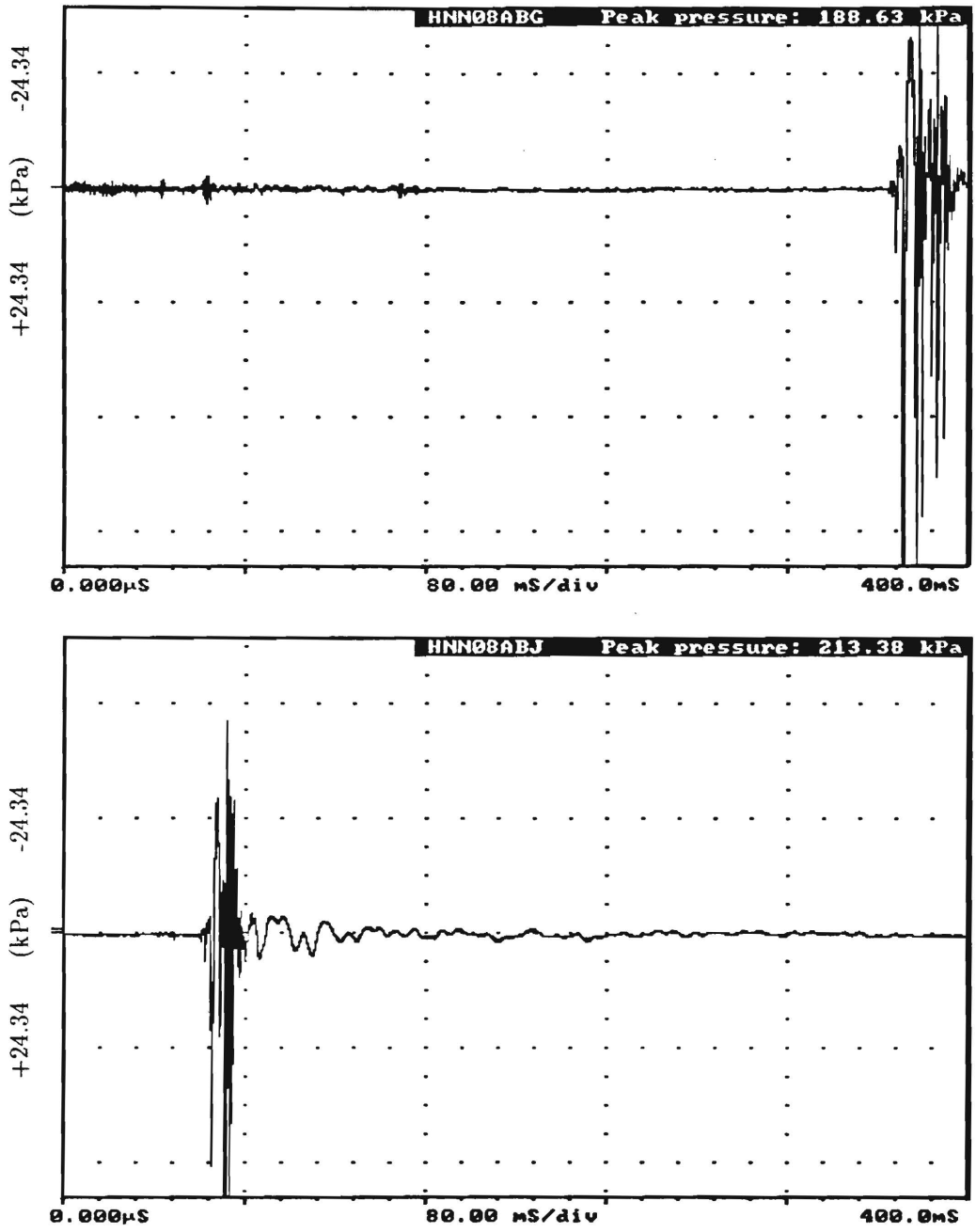

Figure D.10: Transient pressure signals for two experiments using hydroxyethyl cellulose with η_r=1.55 and T_{tin}=1000°C. The vertical scale for each graph is 1 volt/division (24.34 kPa/division). Values of the peak pressures are indicated on each graph.

Hydroxyethyl cellulose, T_{tin}=1000°C, η_r=1.96

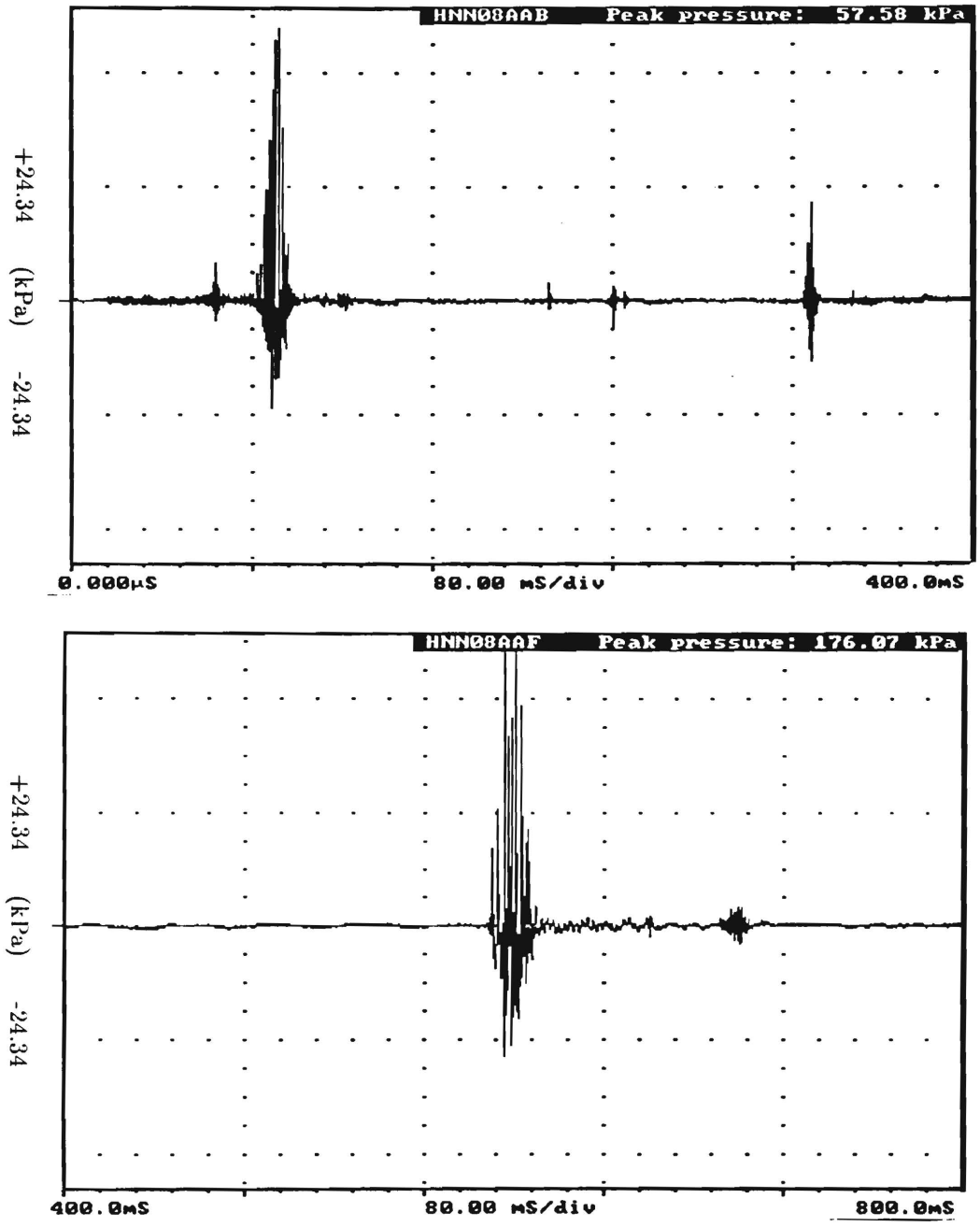

Figure D.11: Transient pressure signals for two experiments using hydroxyethyl cellulose with η_r=1.96 and T_{tin}=1000°C. The vertical scale for each graph is 1 volt/division (24.34 kPa/division). Values of the peak pressures are indicated on each graph.

Poly(acrylamide/sodium acrylate), T_{tin}=1000°C, η_r=1.25

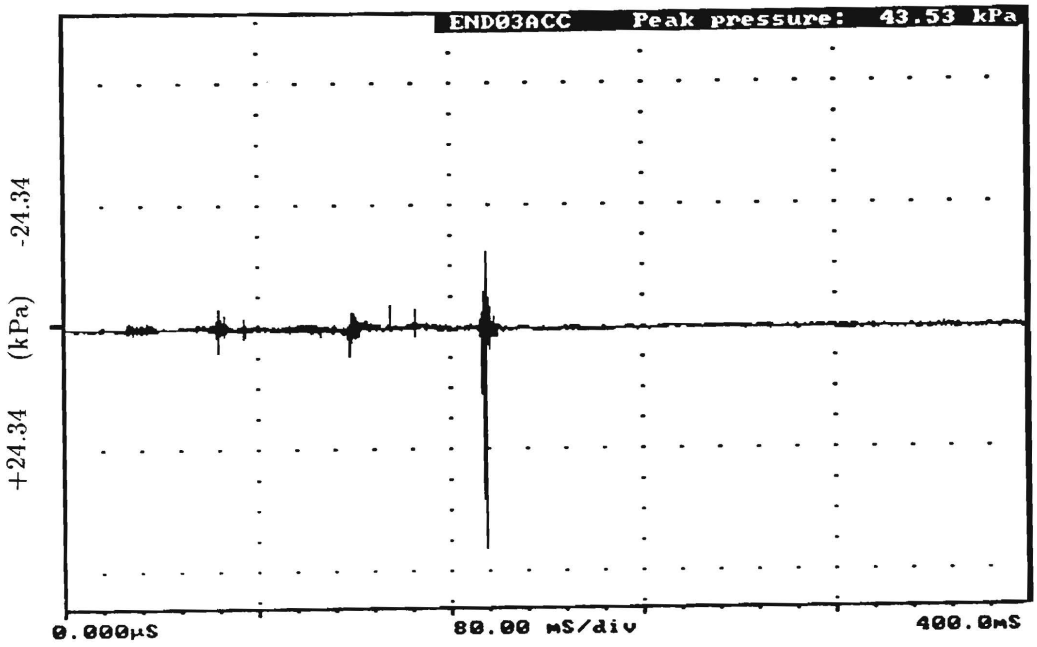

Figure D.12: Transient pressure signals for two experiments using poly(acrylamide/sodium acrylate)with η_r=1.25 and T_{tin}=1000°C. The vertical scale for each graph is 1 volt/division (24.34 kPa/division). Values of the peak pressures are indicated on each graph.

Poly(acrylamide/sodium acrylate), T_{tin}=1000°C, η_r=1.55

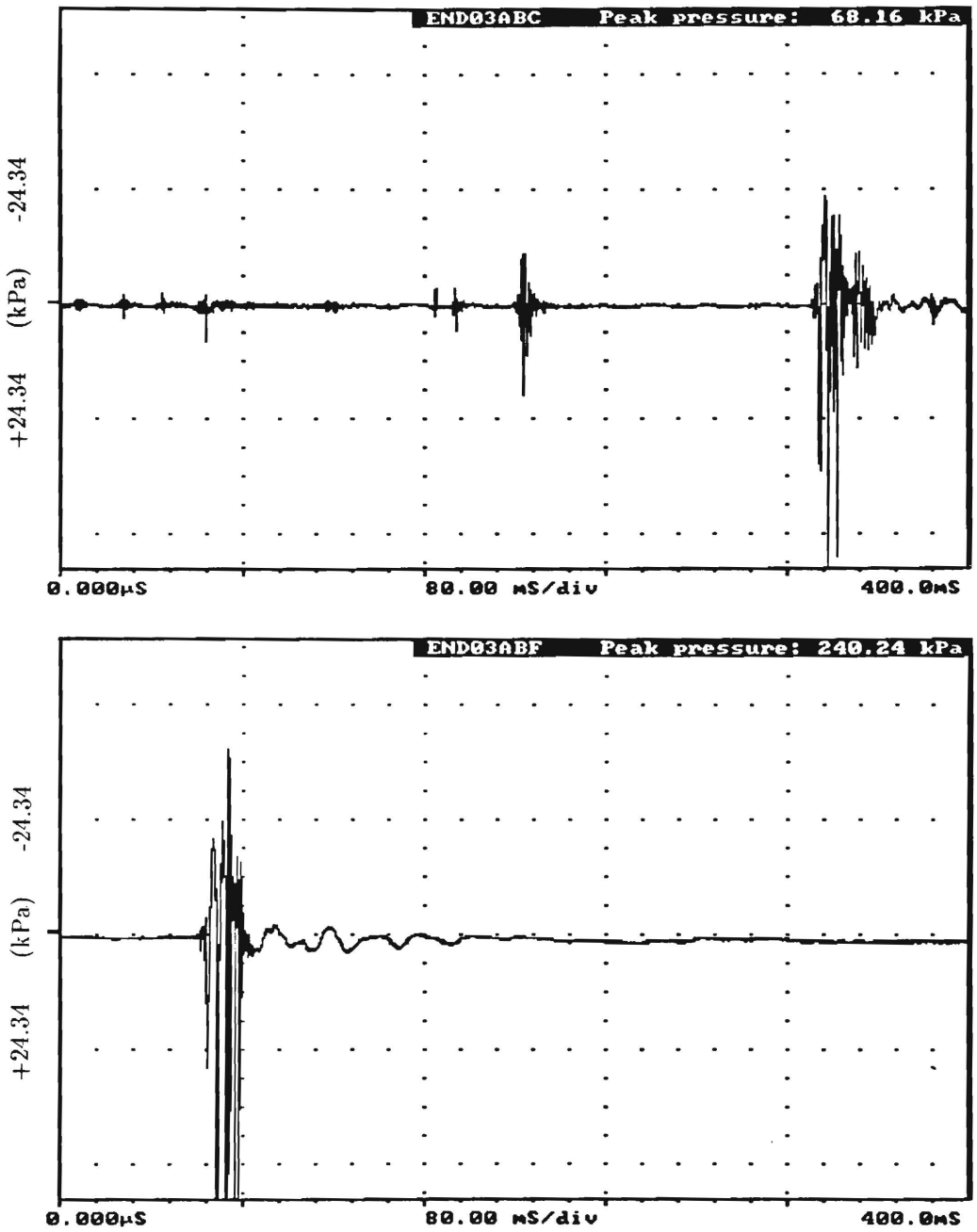

Figure D.13: Transient pressure signals for two experiments using poly(acrylamide/sodium acrylate)with η_r=1.55 and T_{tin}=1000°C. The vertical scale for each graph is 1 volt/division (24.34 kPa/division). Values of the peak pressures are indicated on each graph.

Poly(acrylamide/sodium acrylate), T_{tin}=1000°C, η_r=2.15

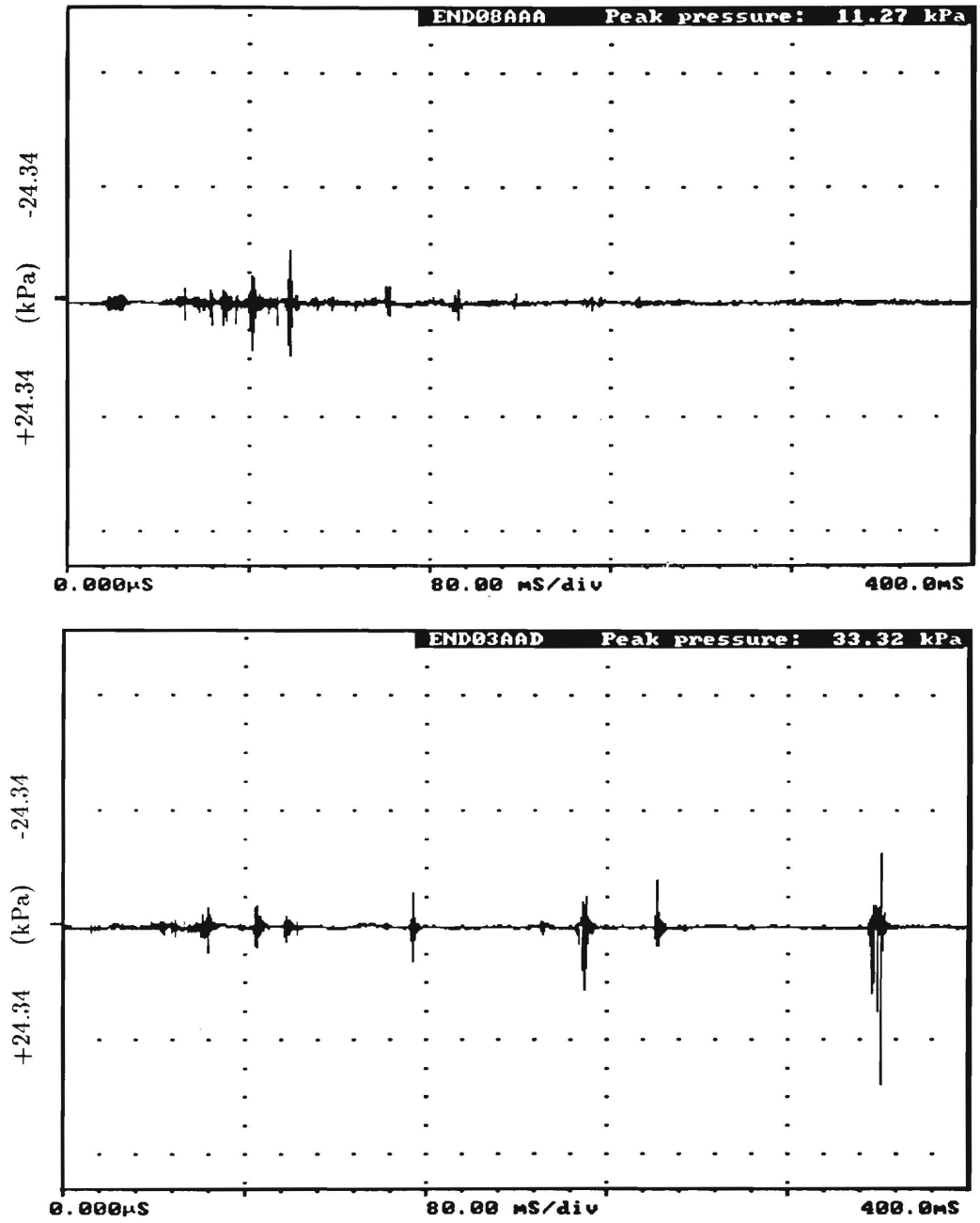

Figure D.14: Transient pressure signals for two experiments using poly(acrylamide/sodium acrylate)with η_r=2.15 and T_{tin}=1000°C. The vertical scale for each graph is 1 volt/division (24.34 kPa/division). Values of the peak pressures are indicated on each graph.

Poly(acrylamide/sodium acrylate), T_{tin}=1000°C, η_r=3.46

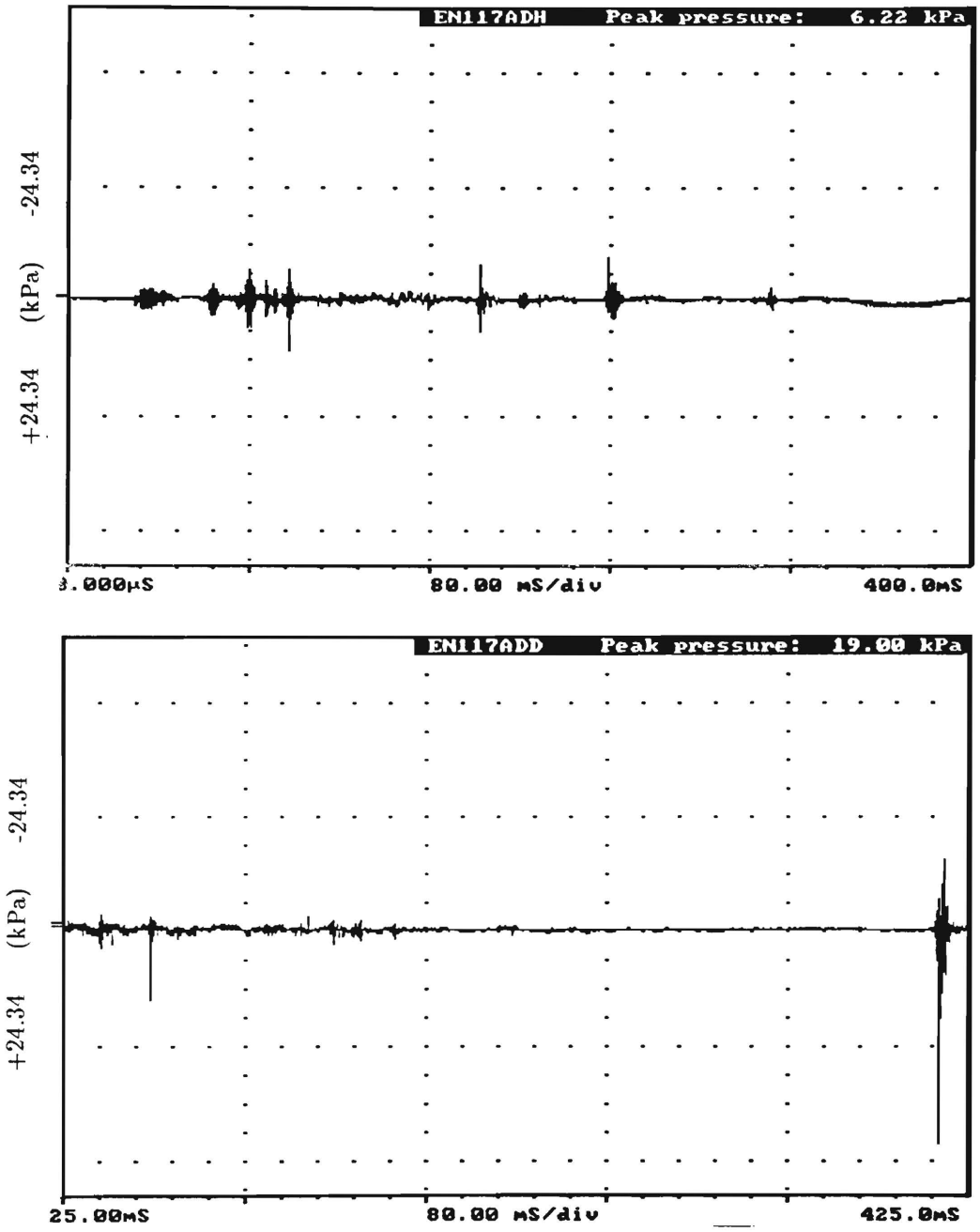

Figure D.15: Transient pressure signals for two experiments using poly(acrylamide/sodium acrylate)with η_r=3.46 and T_{tin}=1000°C. The vertical scale for each graph is 1 volt/division (24.34 kPa/division). Values of the peak pressures are indicated on each graph.

Poly(ethylene oxide), T_{tin}=1000°C, η_r=1.01

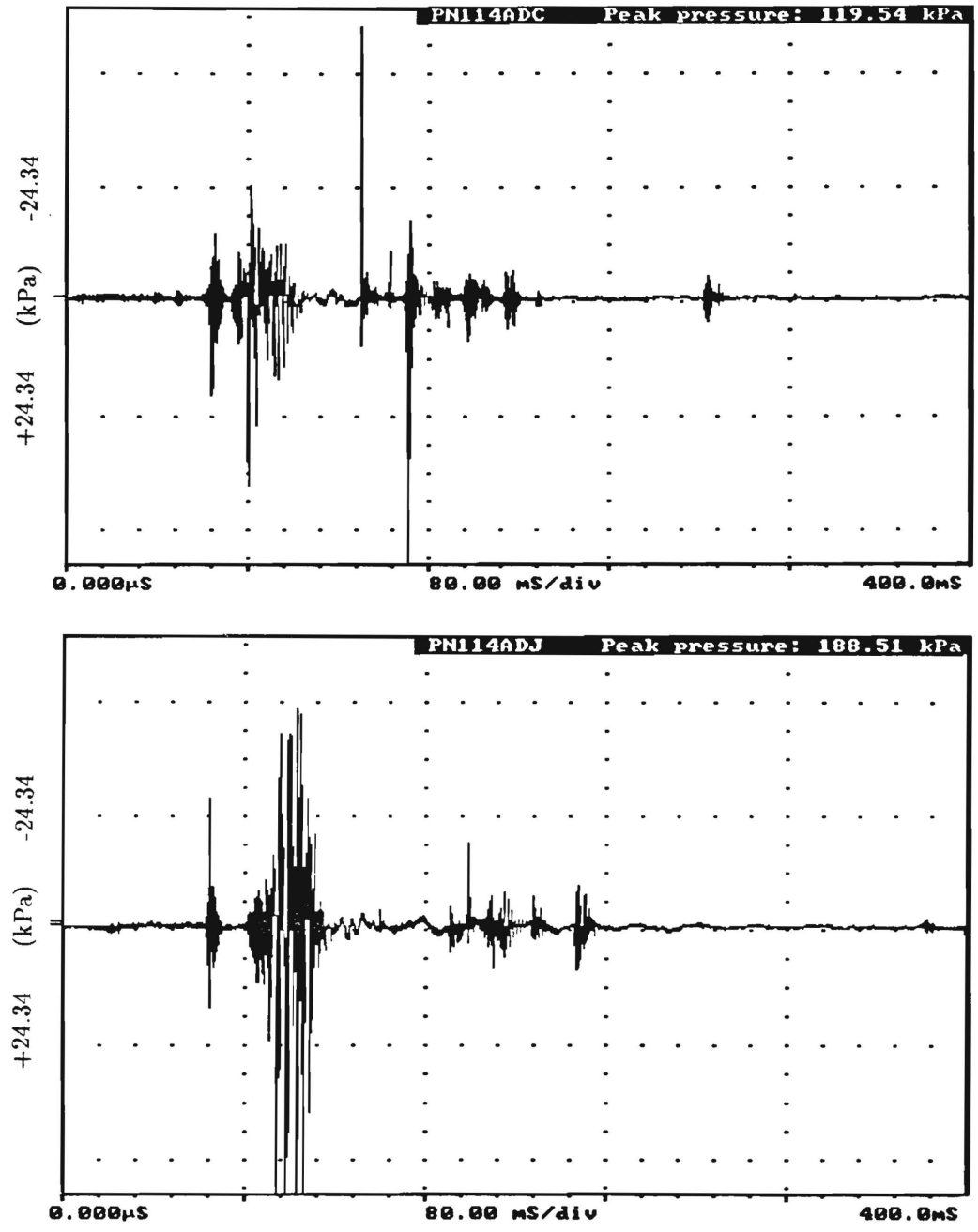

Figure D.16: Transient pressure signals for two experiments using poly(ethylene oxide) with η_r=1.01 and T_{tin}=1000°C. The vertical scale for each graph is 1 volt/division (24.34 kPa/division). Values of the peak pressures are indicated on each graph.

Poly(ethylene oxide), T_{tin}=1000°C, η_r=1.02

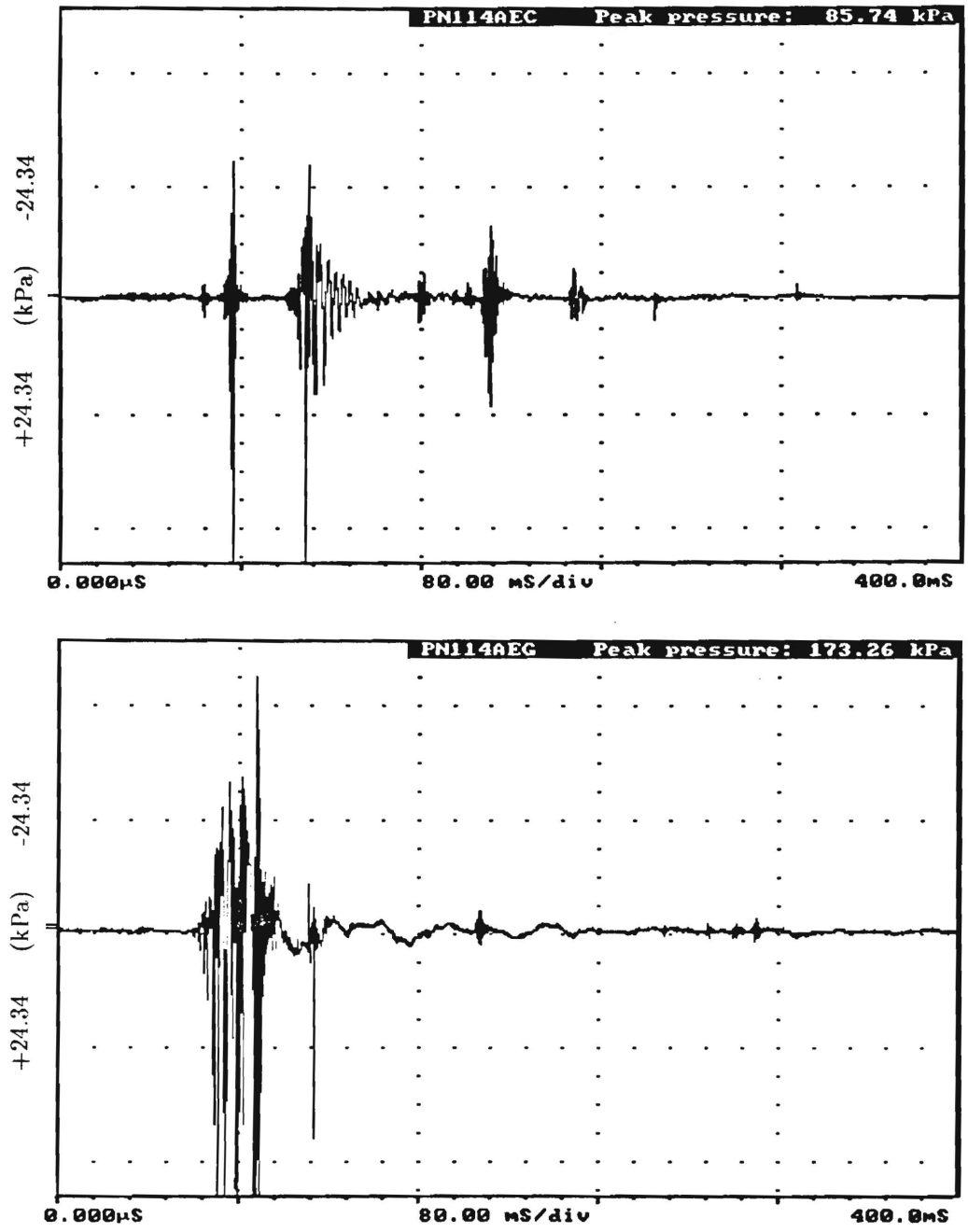

Figure D.17: Transient pressure signals for two experiments using poly(ethylene oxide) with η_r=1.02 and T_{tin}=1000°C. The vertical scale for each graph is 1 volt/division (24.34 kPa/division). Values of the peak pressures are indicated on each graph.

Poly(ethylene oxide), T_{tin}=1000°C, η_r=1.07

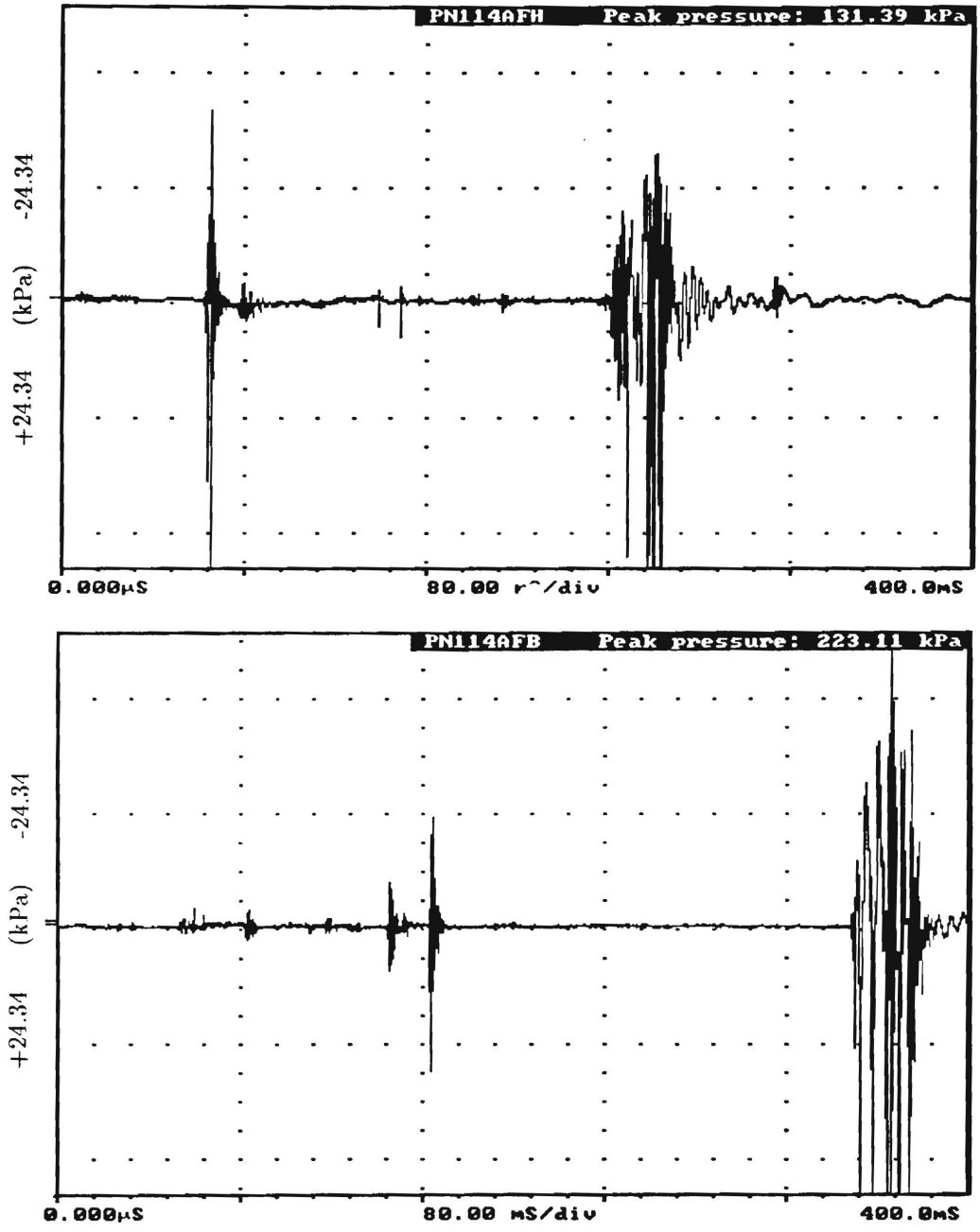

Figure D.18: Transient pressure signals for two experiments using poly(ethylene oxide) with η_r=1.07 and T_{tin}=1000°C. The vertical scale for each graph is 1 volt/division (24.34 kPa/division). Values of the peak pressures are indicated on each graph.

Poly(ethylene oxide), T_{tin}=1000°C, η_r=1.13

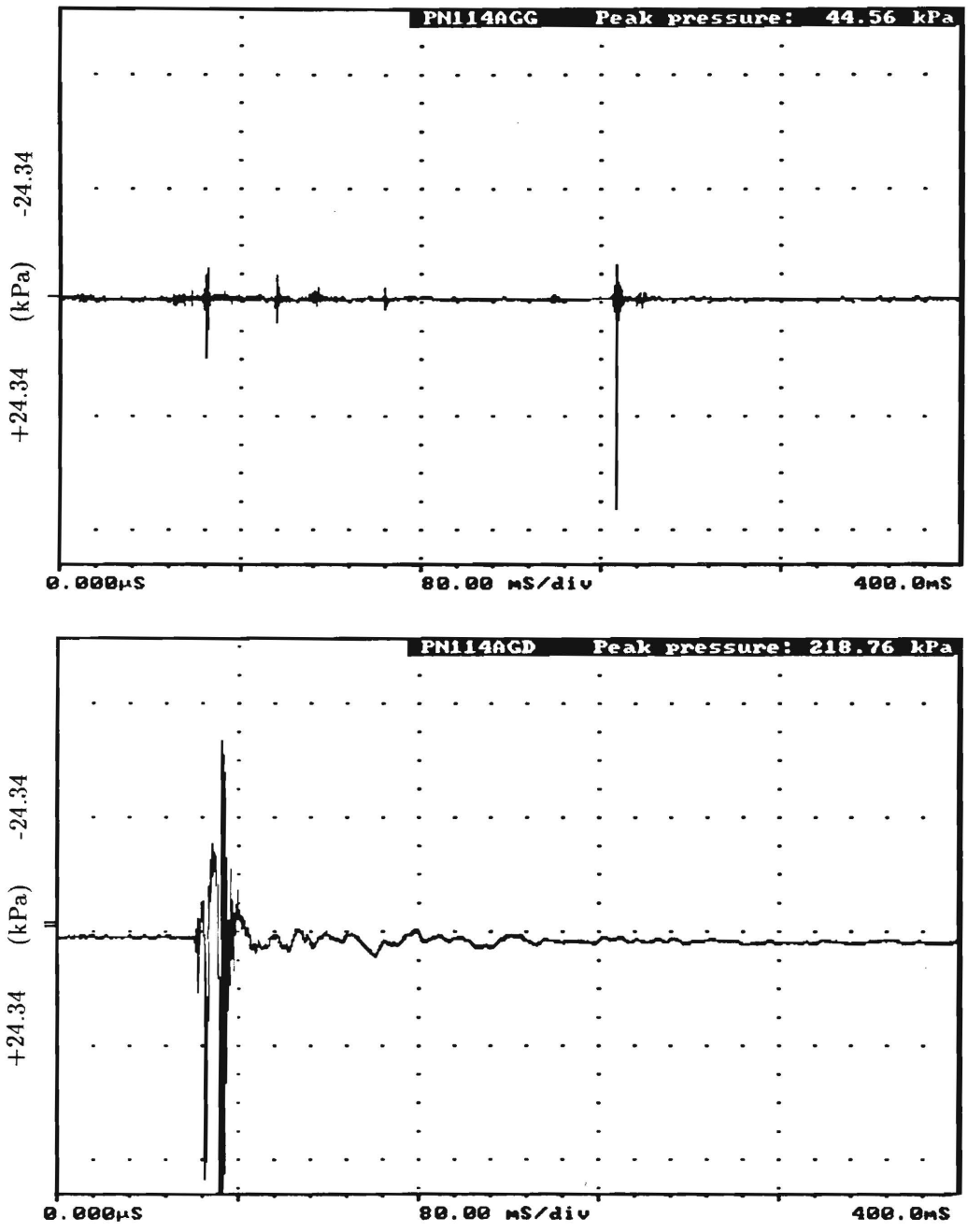

Figure D.19: Transient pressure signals for two experiments using poly(ethylene oxide) with η_r=1.13 and T_{tin}=1000°C. The vertical scale for each graph is 1 volt/division (24.34 kPa/division). Values of the peak pressures are indicated on each graph.

Poly(ethylene oxide), T_{tin}=1000°C, η_r=1.25

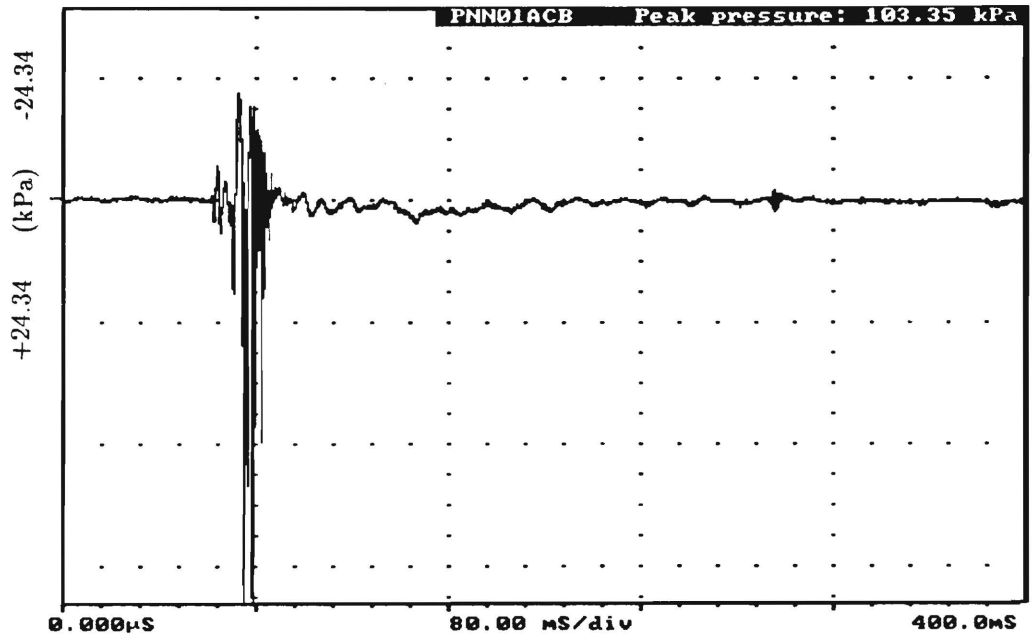

Figure D.20: Transient pressure signals for two experiments using poly(ethylene oxide) with η_r=1.25 and T_{tin}=1000°C. The vertical scale for each graph is 1 volt/division (24.34 kPa/division). Values of the peak pressures are indicated on each graph.

Poly(ethylene oxide), T_{tin}=1000°C, η_r=1.50

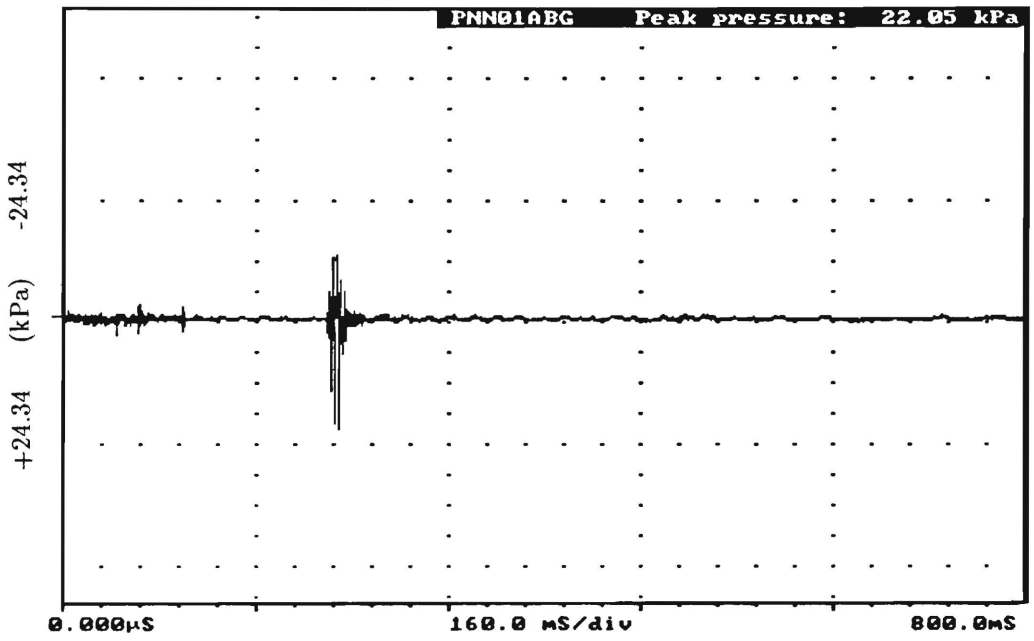

Figure D.21: Transient pressure signals for two experiments using poly(ethylene oxide) with η_r=1.50 and T_{tin}=1000°C. The vertical scale for each graph is 1 volt/division (24.34 kPa/division). Values of the peak pressures are indicated on each graph.

Poly(ethylene oxide), T_{tin}=1000°C, η_r=2.00

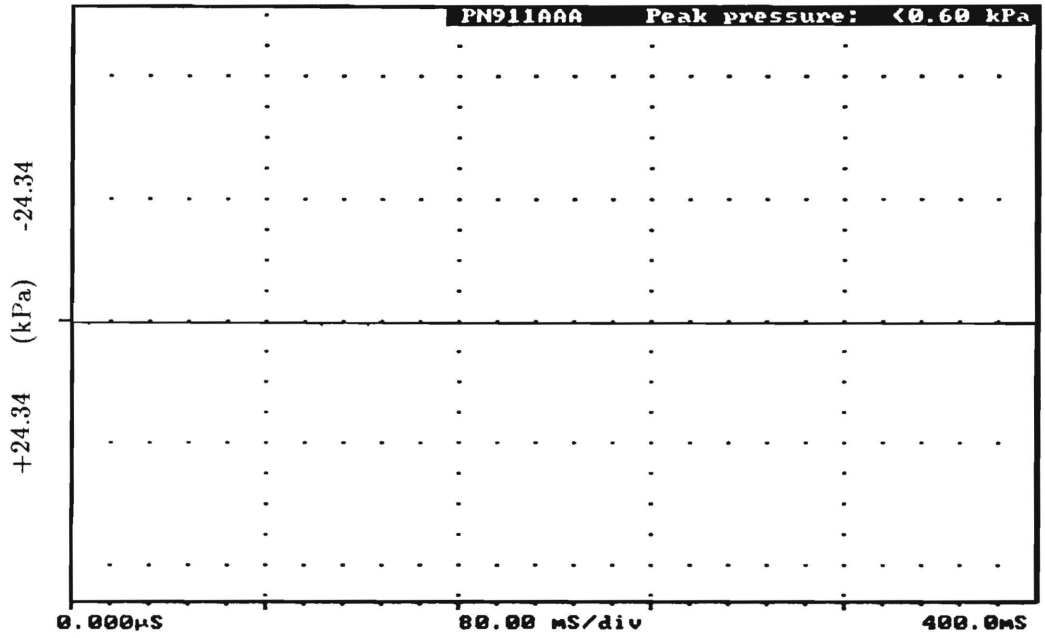

Figure D.22: Transient pressure signals for two experiments using poly(ethylene oxide) with η_r=2.00 and T_{tin}=1000°C. The vertical scale for each graph is 1 volt/division (24.34 kPa/division). Values of the peak pressures are indicated on each graph.

Poly(ethylene oxide), T_{tin}=900°C, η_r=1.25

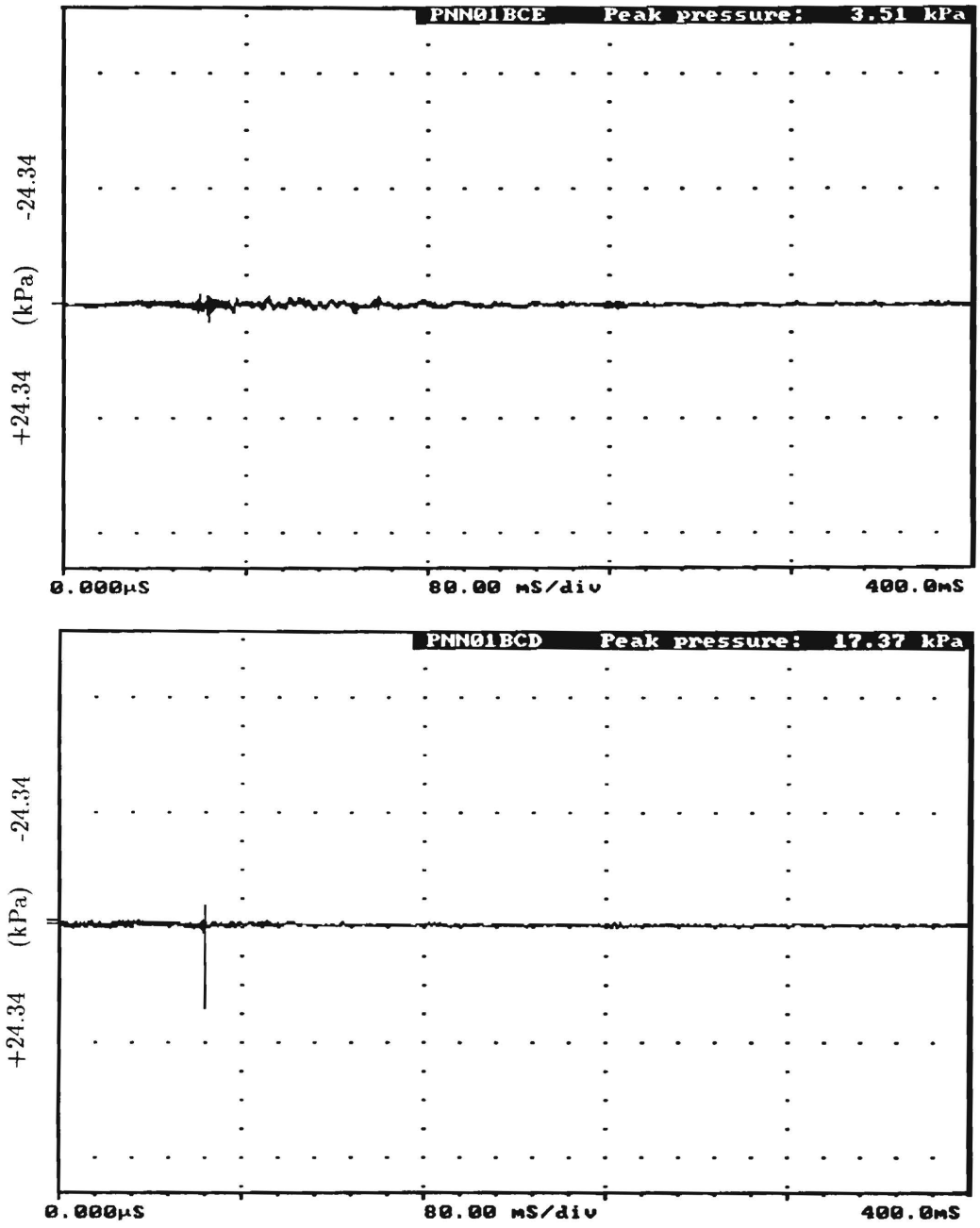

Figure D.23: Transient pressure signals for two experiments using poly(ethylene oxide) with η_r=1.25 and T_{tin}=900°C. The vertical scale for each graph is 1 volt/division (24.34 kPa/division). Values of the peak pressures are indicated on each graph.

Poly(ethylene oxide), T_{tin}=900°C, η_r=1.50

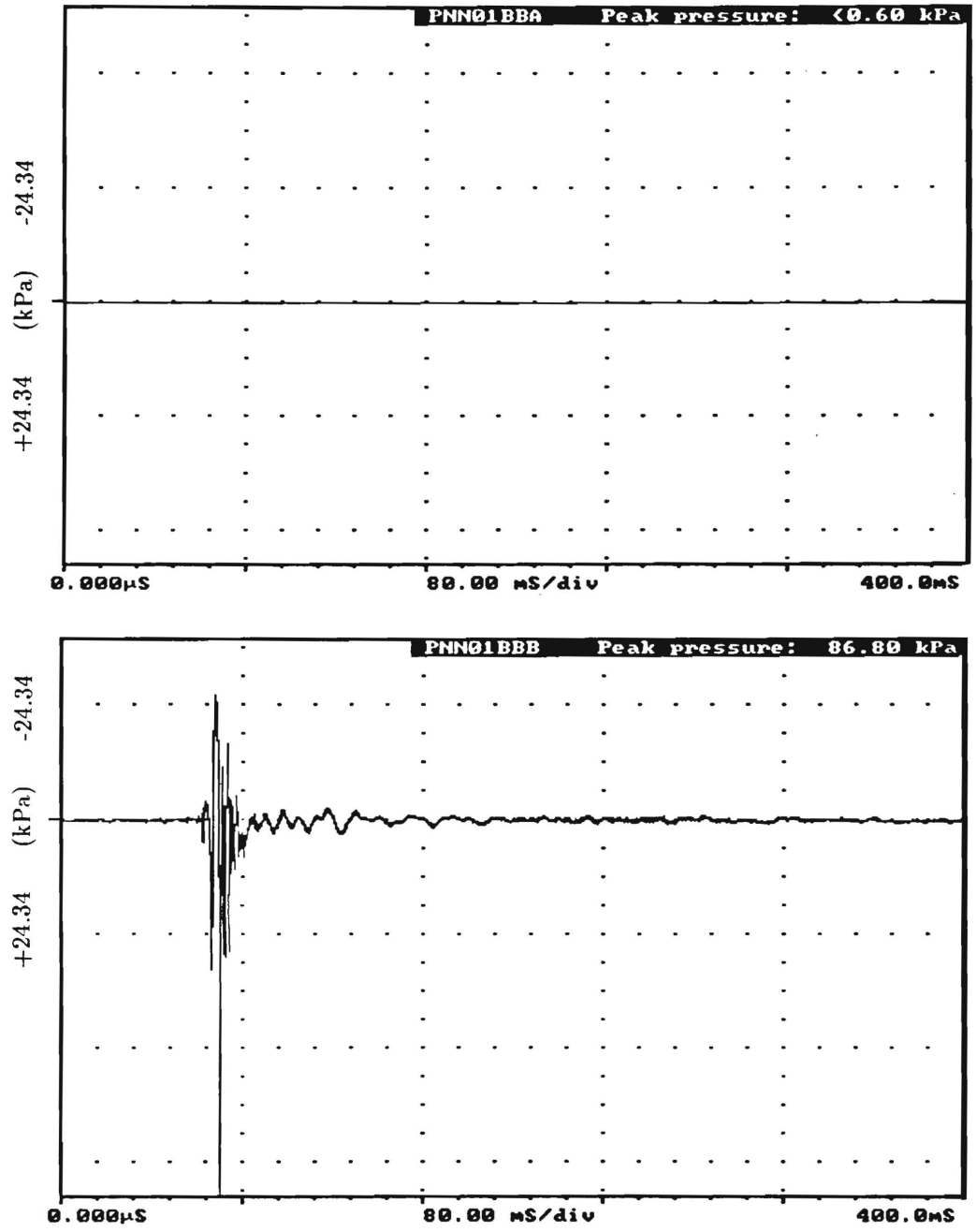

Figure D.24: Transient pressure signals for two experiments using poly(ethylene oxide) with η_r=1.50 and T_{tin}=900°C. The vertical scale for each graph is 1 volt/division (24.34 kPa/division). Values of the peak pressures are indicated on each graph.

Poly(ethylene oxide), T_{tin}=900°C, η_r=2.00

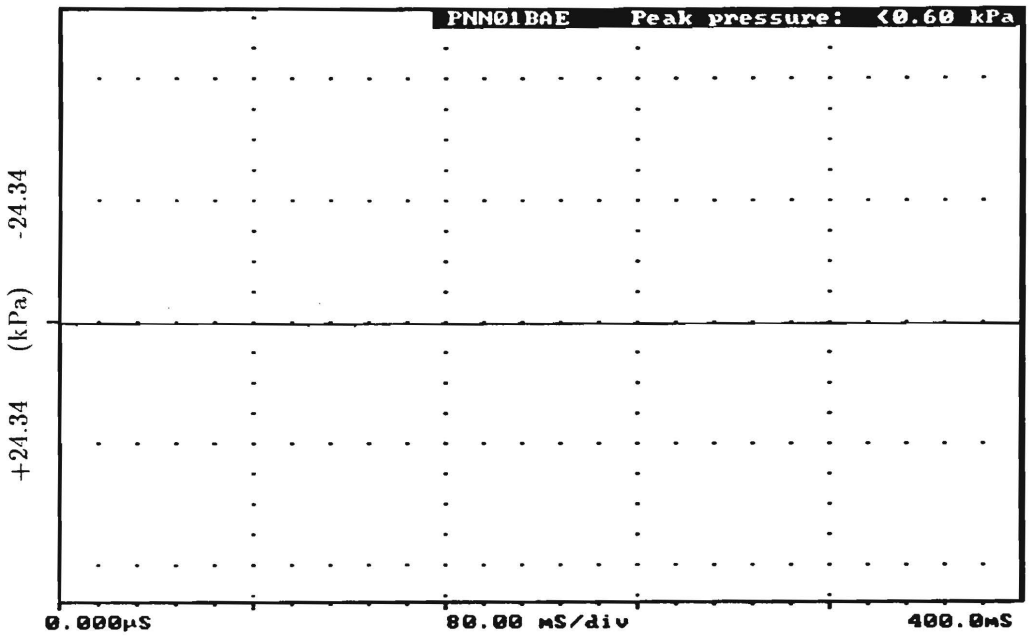

Figure D.25: Transient pressure signals for two experiments using poly(ethylene oxide) with η_r=2.00 and T_{tin}=900°C. The vertical scale for each graph is 1 volt/division (24.34 kPa/division). Values of the peak pressures are indicated on each graph.

Poly(ethylene oxide), T_{tin}=800°C, η_r=1.25

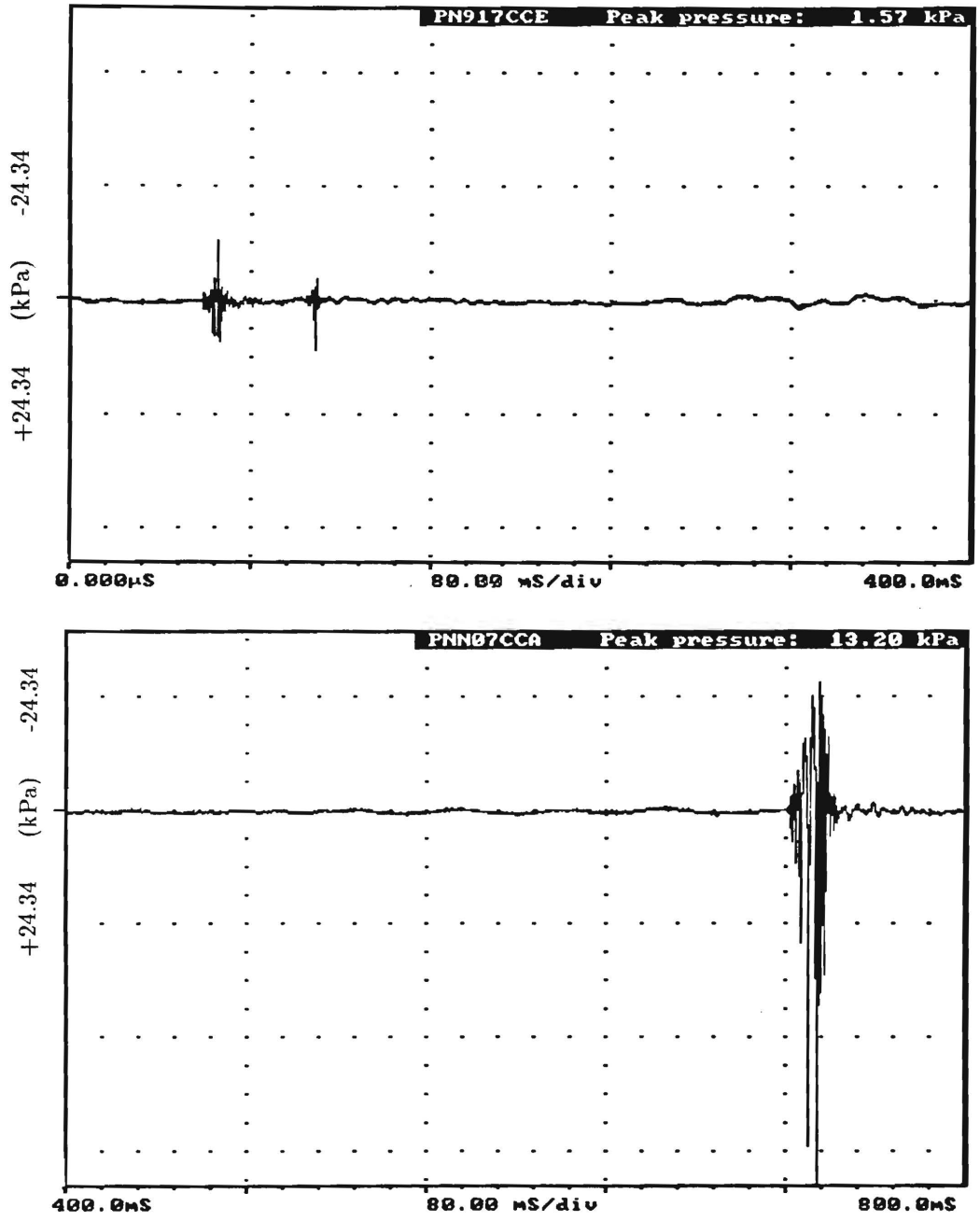

Figure D.26: Transient pressure signals for two experiments using poly(ethylene oxide) with η_r=1.25 and T_{tin}=800°C. The vertical scale for each graph is 1 volt/division (24.34 kPa/division). Values of the peak pressures are indicated on each graph.

Poly(ethylene oxide), T_{tin}=800°C, η_r=1.50

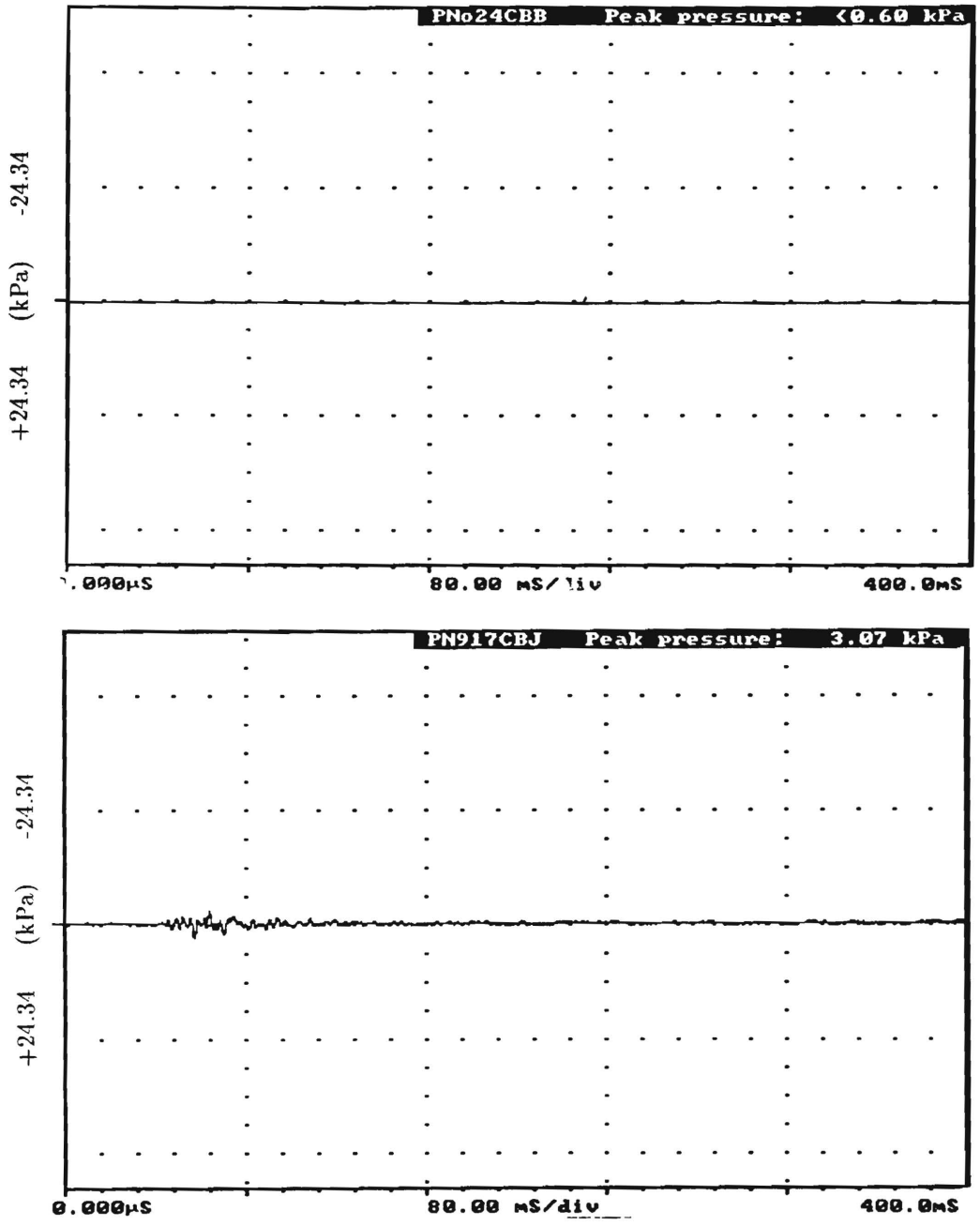

Figure D.27: Transient pressure signals for two experiments using poly(ethylene oxide) with η_r=1.50 and T_{tin}=800°C. The vertical scale for each graph is 1 volt/division (24.34 kPa/division). Values of the peak pressures are indicated on each graph.

Poly(ethylene oxide), T_{tin}=800°C, η_r=2.00

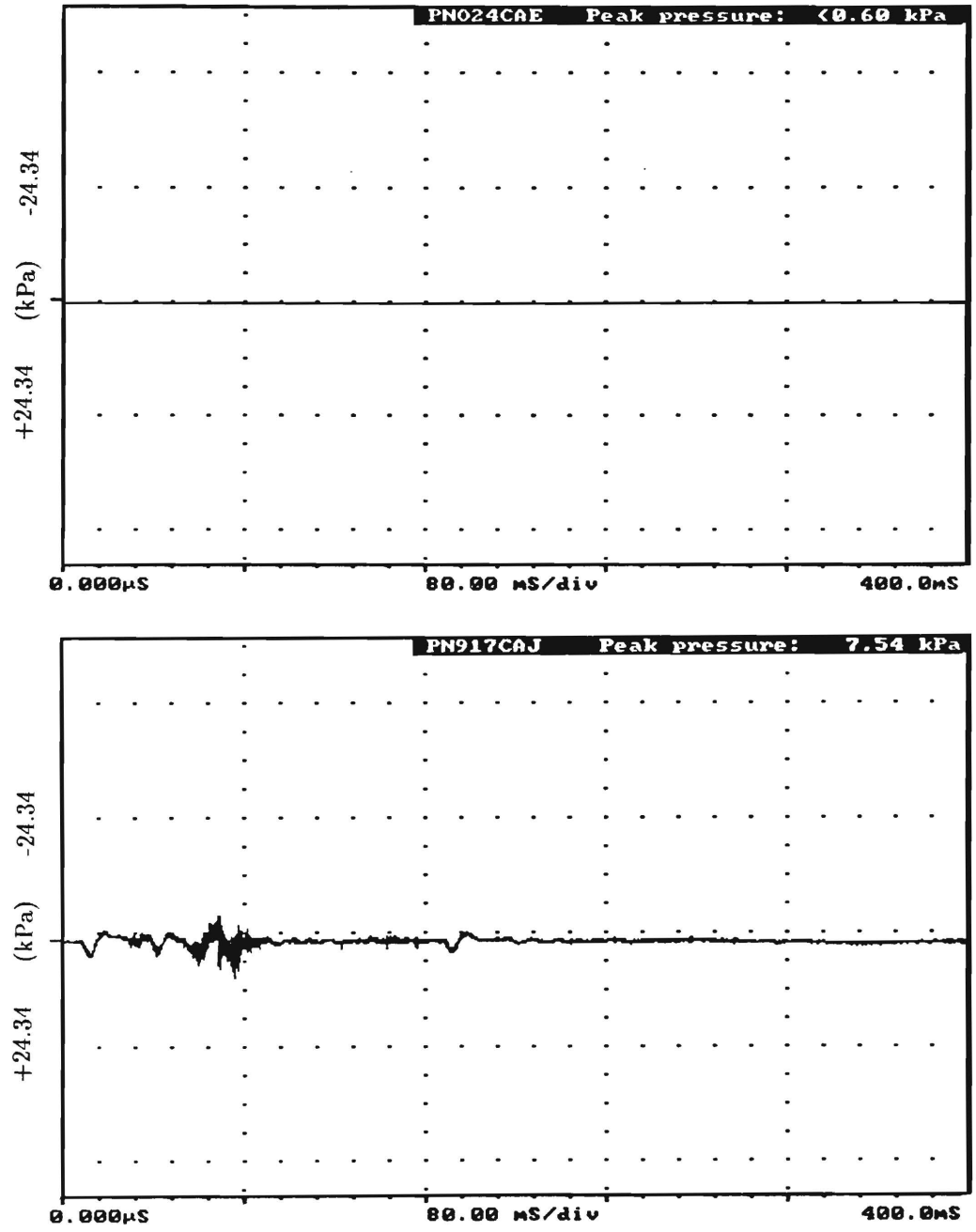

Figure D.28: Transient pressure signals for two experiments using poly(ethylene oxide) with η_r=2.00 and T_{tin}=800°C. The vertical scale for each graph is 1 volt/division (24.34 kPa/division). Values of the peak pressures are indicated on each graph.

Poly(ethylene oxide), T_{tin}=700°C, η_r=1.25

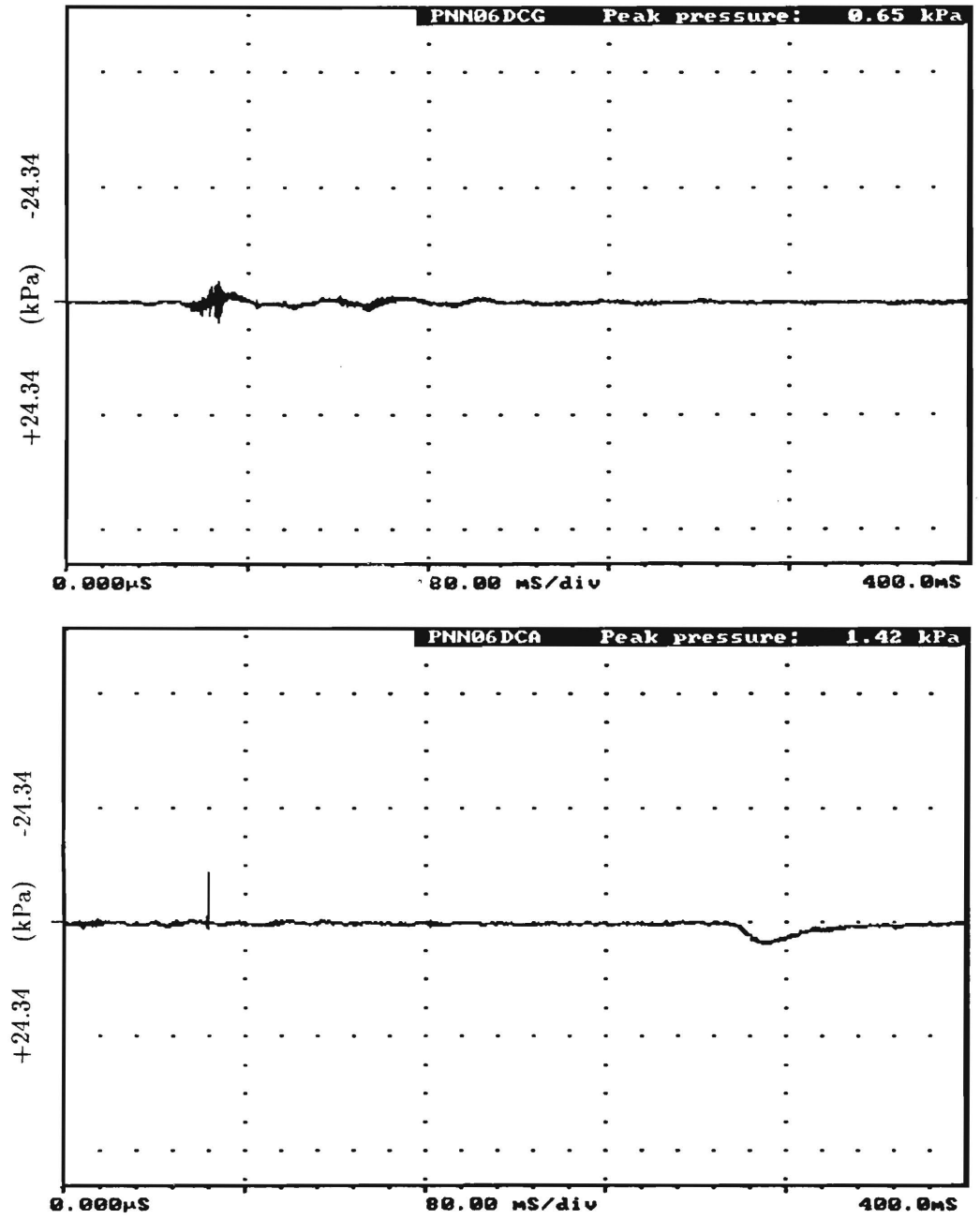

Figure D.29: Transient pressure signals for two experiments using poly(ethylene oxide) with η_r=1.25 and T_{tin}=700°C. The vertical scale for each graph is 1 volt/division (24.34 kPa/division). Values of the peak pressures are indicated on each graph.

Poly(ethylene oxide), T_{tin}=700°C, η_r=1.50

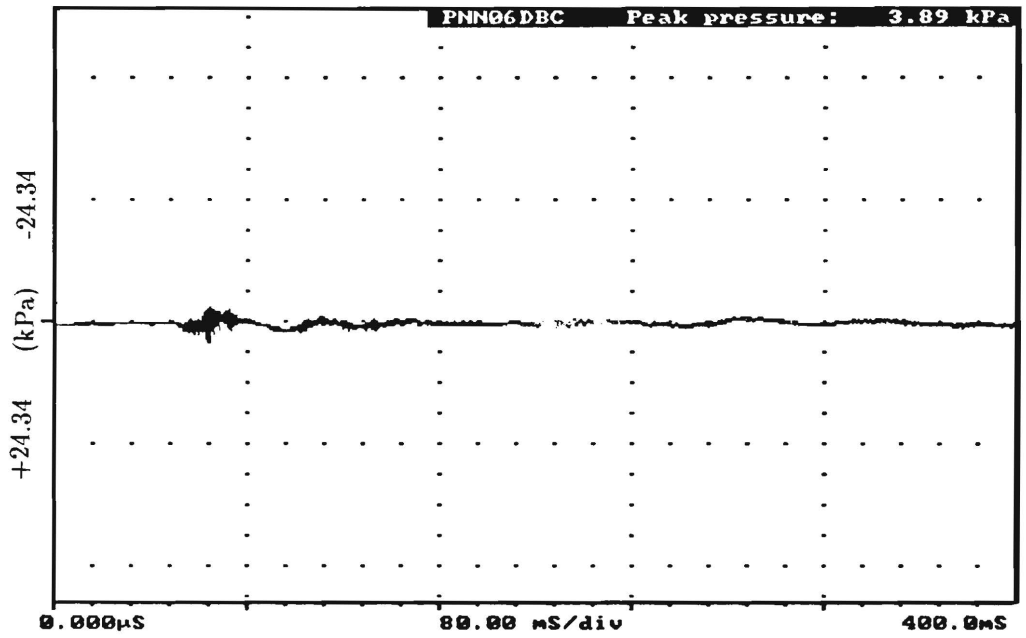

Figure D.30: Transient pressure signals for two experiments using poly(ethylene oxide) with η_r=1.50 and T_{tin}=700°C. The vertical scale for each graph is 1 volt/division (24.34 kPa/division). Values of the peak pressures are indicated on each graph.

Poly(ethylene oxide), T_{tin}=700°C, η_r=2.00

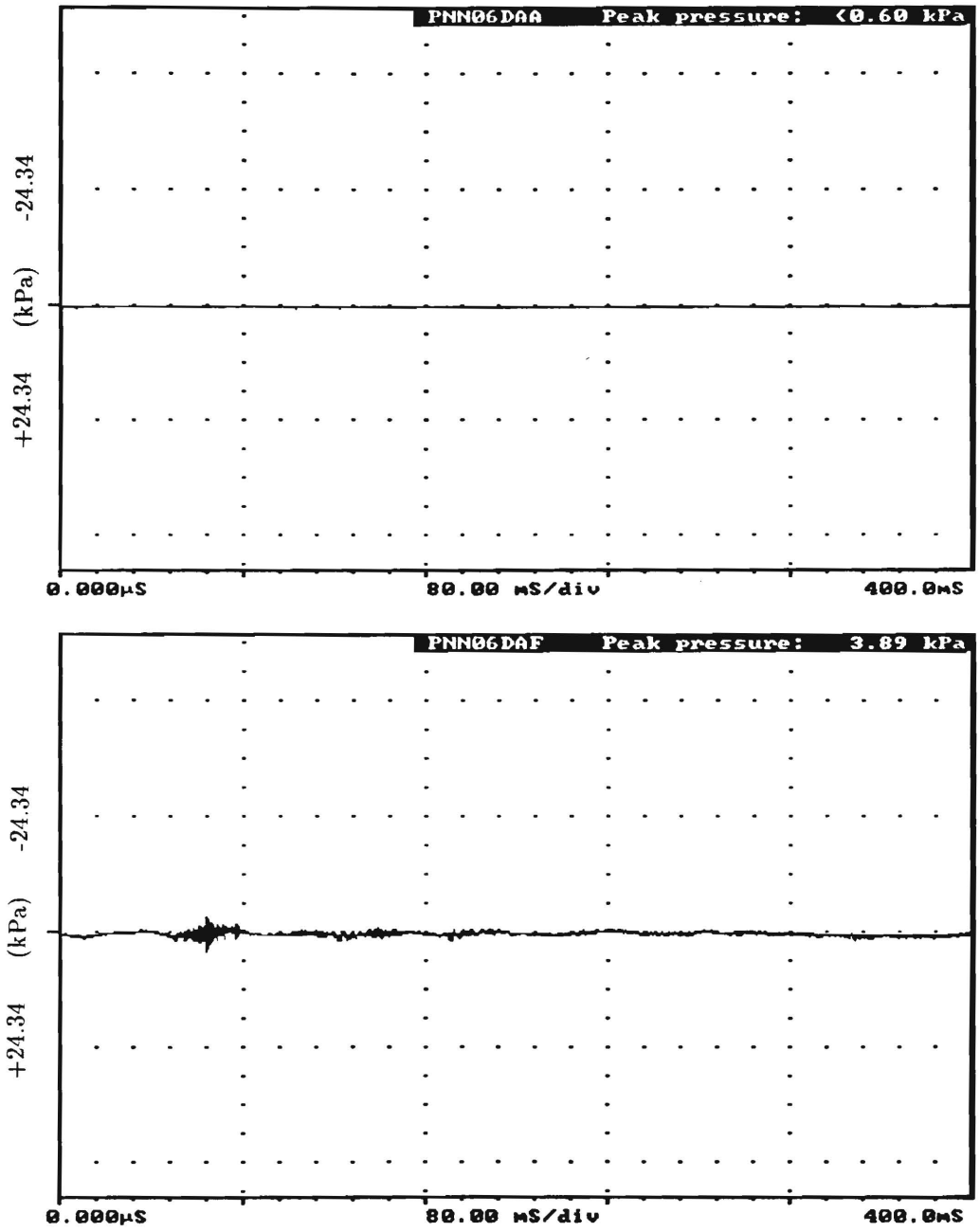

Figure D.31: Transient pressure signals for two experiments using poly(ethylene oxide) with η_r=2.00 and T_{tin}=700°C. The vertical scale for each graph is 1 volt/division (24.34 kPa/division). Values of the peak pressures are indicated on each graph.

Poly(ethylene oxide), T_{tin}=600°C, η_r=1.25

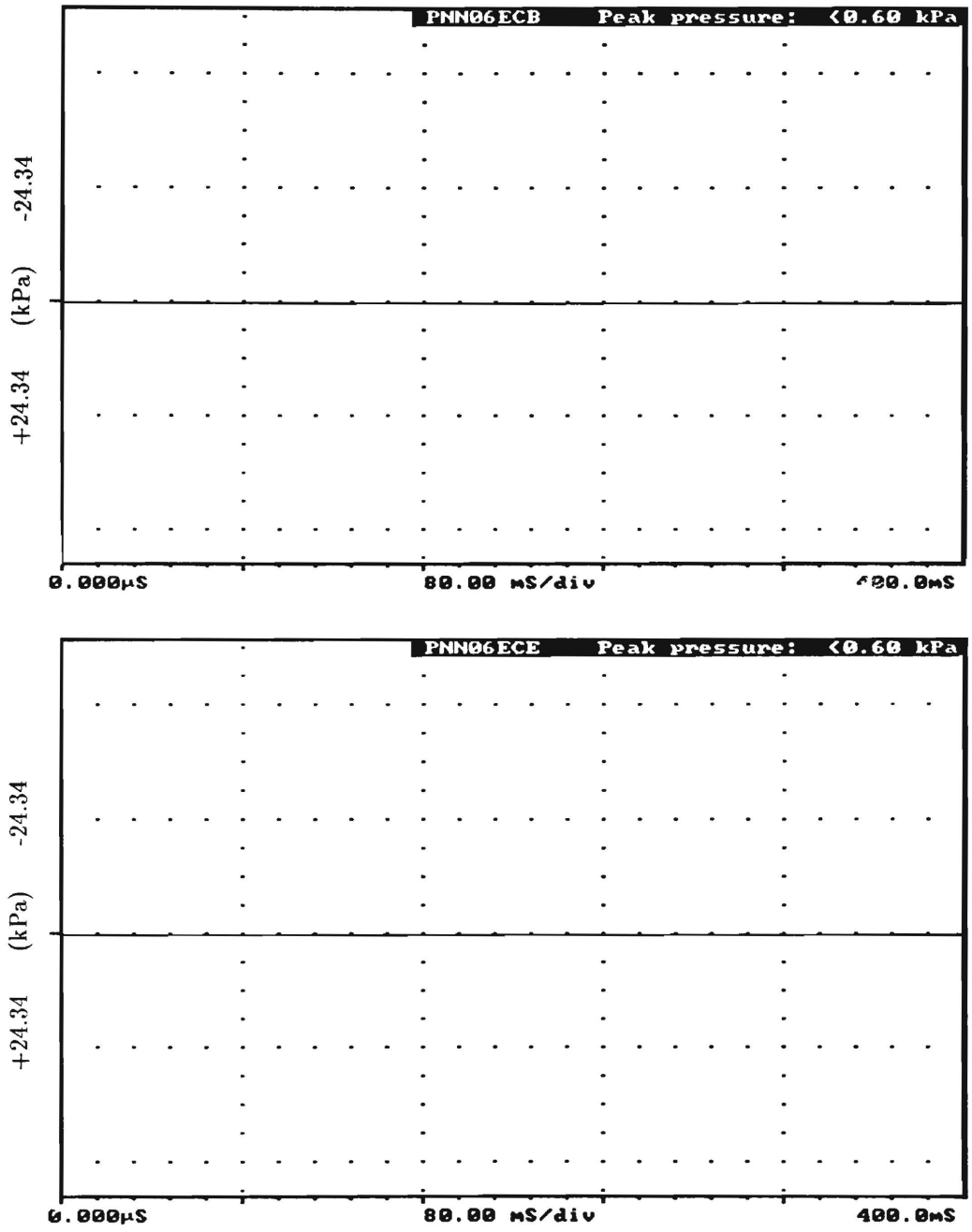

Figure D.32: Transient pressure signals for two experiments using poly(ethylene oxide) with η_r=1.25 and T_{tin}=600°C. The vertical scale for each graph is 1 volt/division (24.34 kPa/division). Values of the peak pressures are indicated on each graph.

Poly(ethylene oxide), T_{tin}=600°C, η_r=1.50

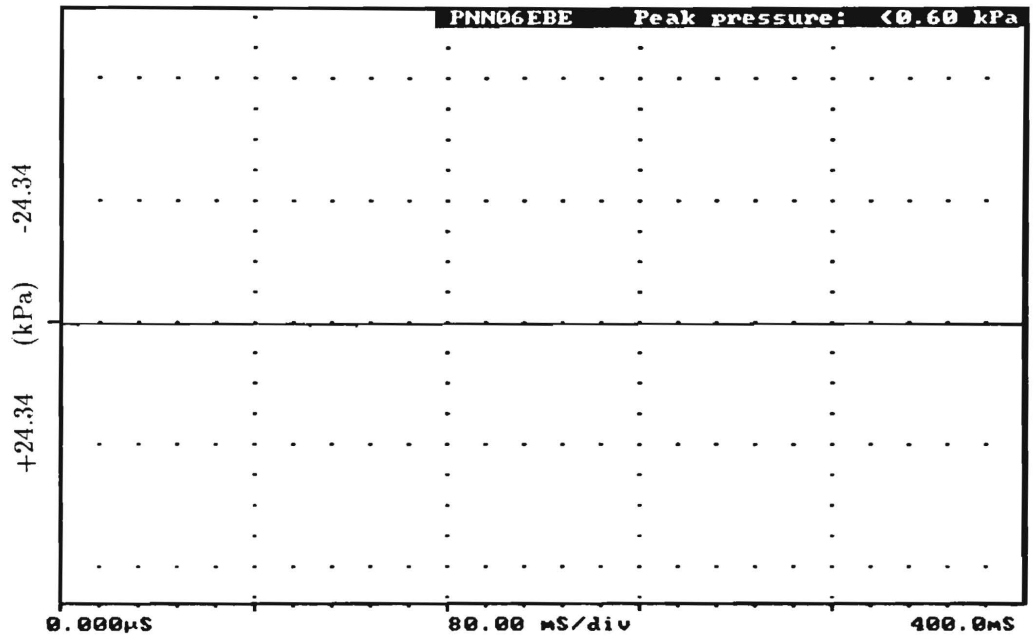

Figure D.33: Transient pressure signals for two experiments using poly(ethylene oxide) with η_r=1.50 and T_{tin}=600°C. The vertical scale for each graph is 1 volt/division (24.34 kPa/division). Values of the peak pressures are indicated on each graph.

Poly(ethylene oxide), T_{tin}=600°C, η_r=2.00

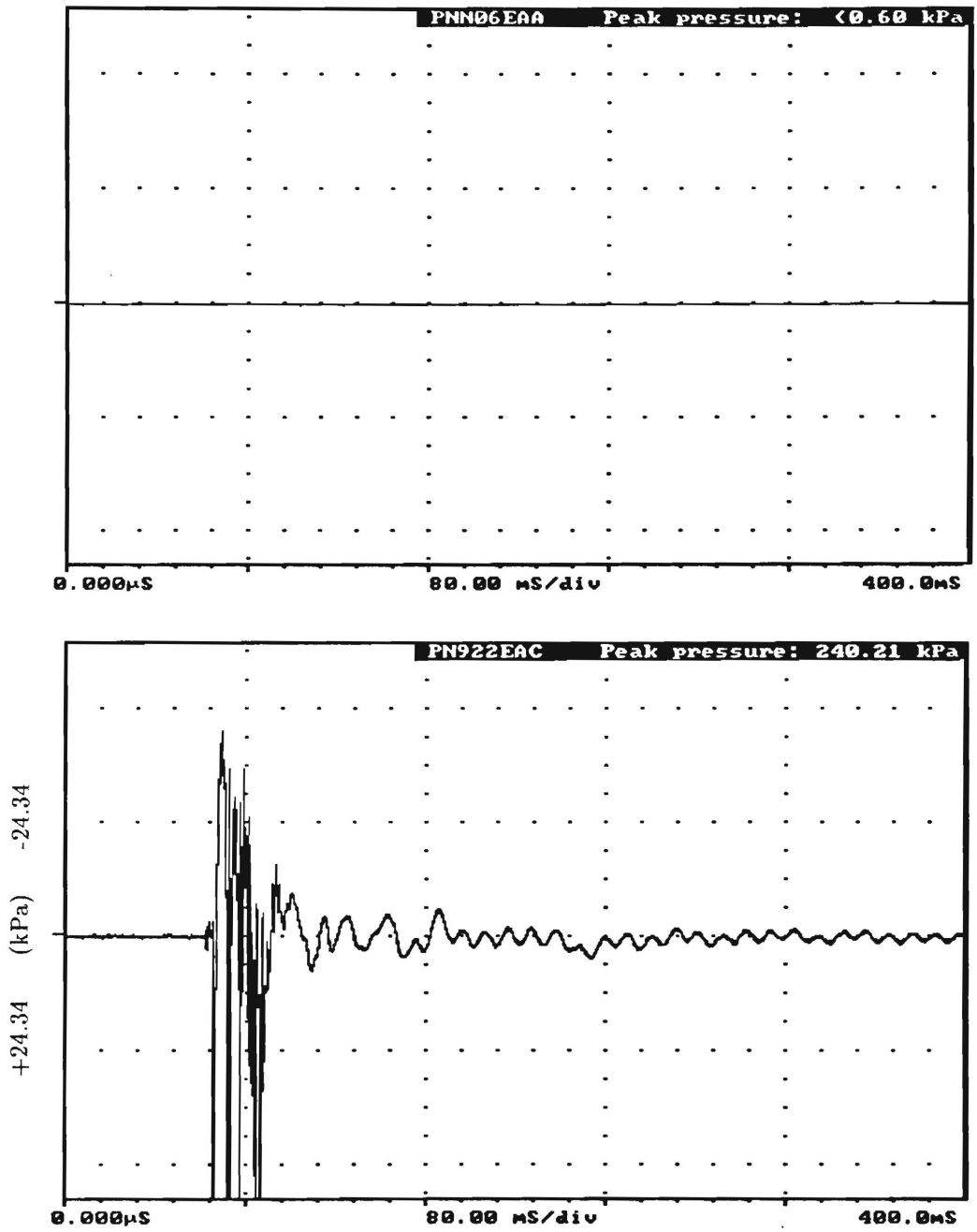

Figure D.34: Transient pressure signals for two experiments using poly(ethylene oxide) with η_r=2.00 and T_{tin}=600°C. The vertical scale for each graph is 1 volt/division (24.34 kPa/division). Values of the peak pressures are indicated on each graph.

Glycerol, T_{tin}=1000°C, η_r=1.68

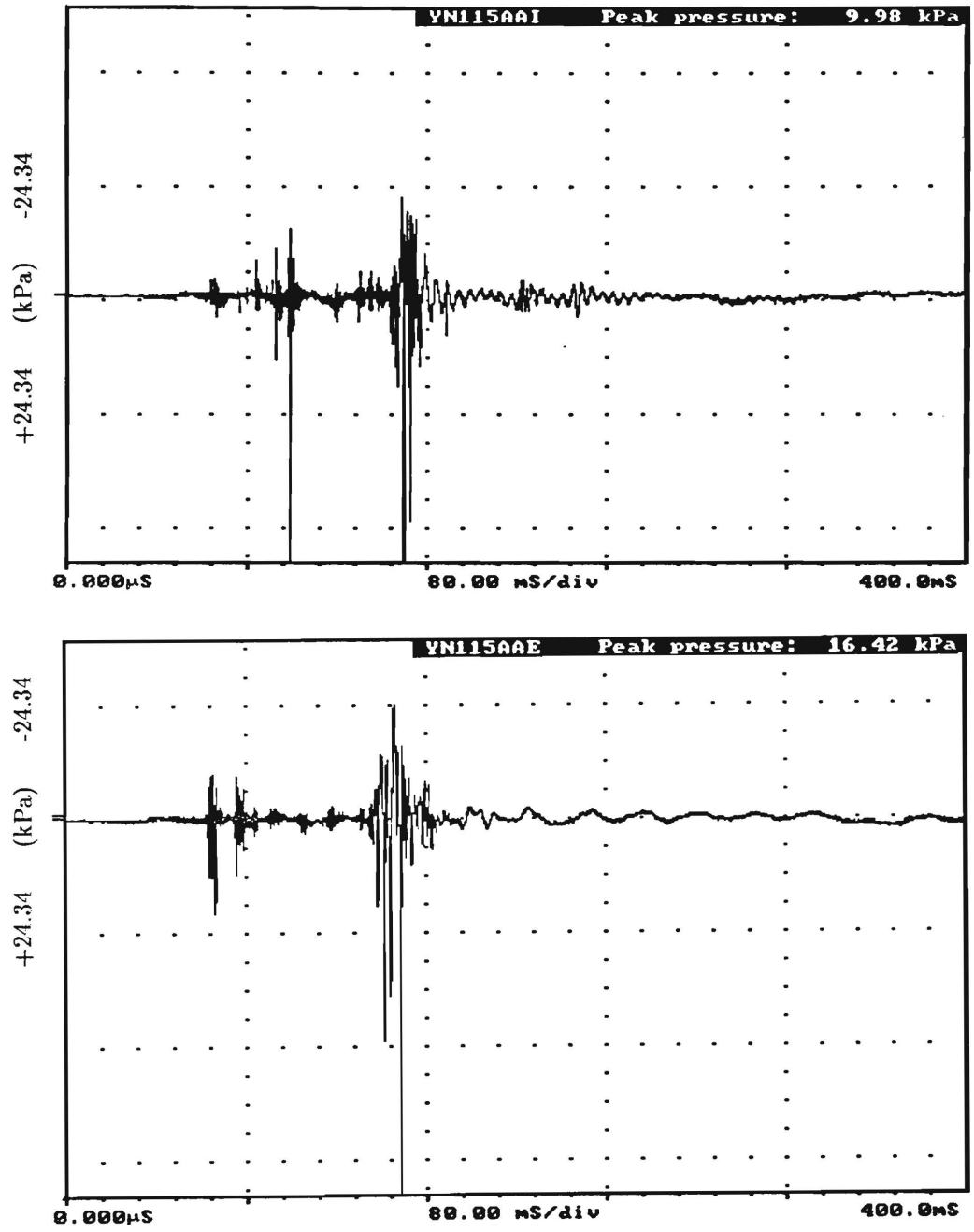

Figure D.35: Transient pressure signals for two experiments using glycerol with η_r=1.68 and T_{tin}=1000°C. The vertical scale for each graph is 1 volt/division (24.34 kPa/division). Values of the peak pressures are indicated on each graph.

Glycerol, T_{tin}=1000°C, η_r=1.94

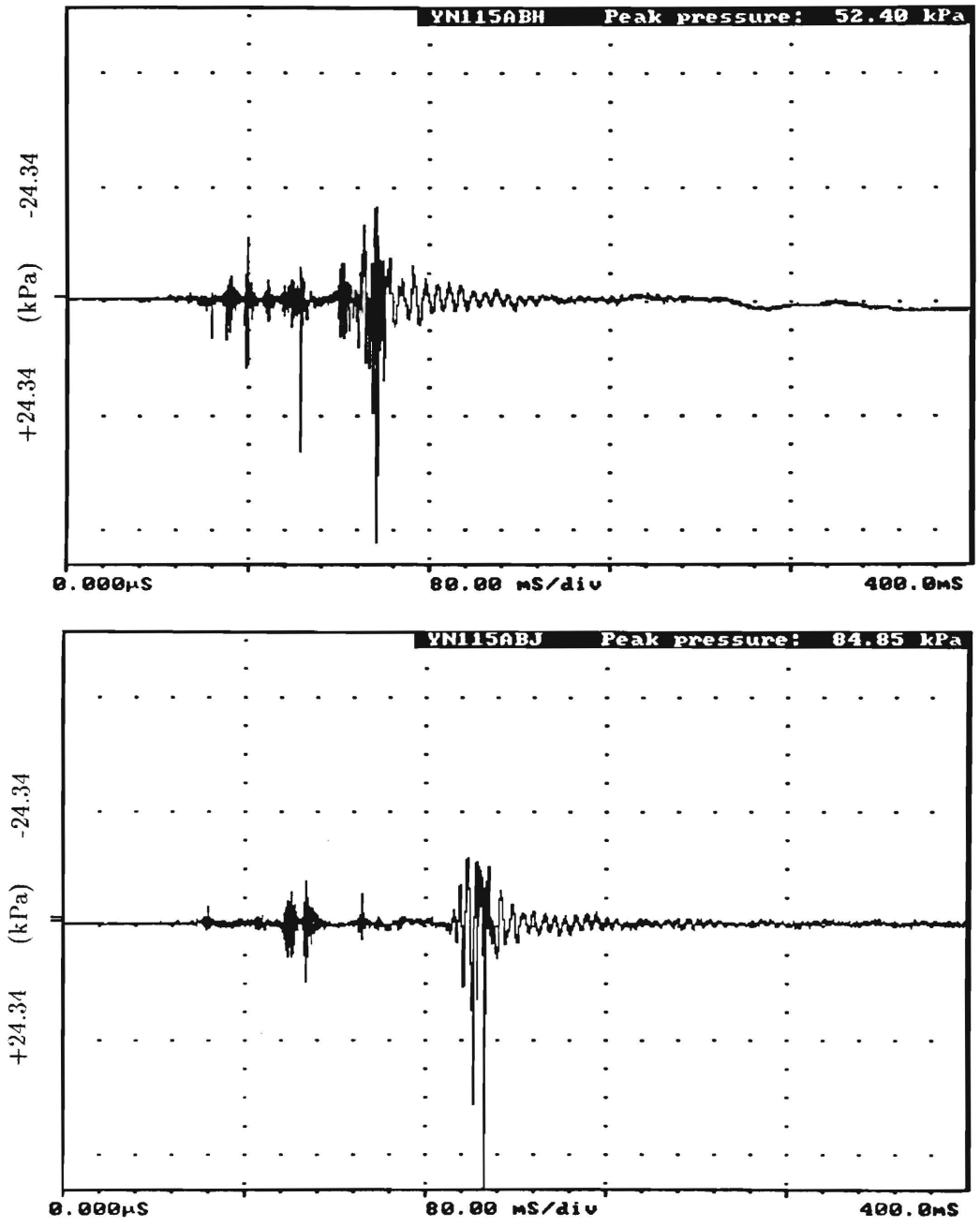

Figure D.36: Transient pressure signals for two experiments using glycerol with η_r=1.94 and T_{tin}=1000°C. The vertical scale for each graph is 1 volt/division (24.34 kPa/division). Values of the peak pressures are indicated on each graph.

Glycerol, T_{tin}=1000°C, η_r=2.97

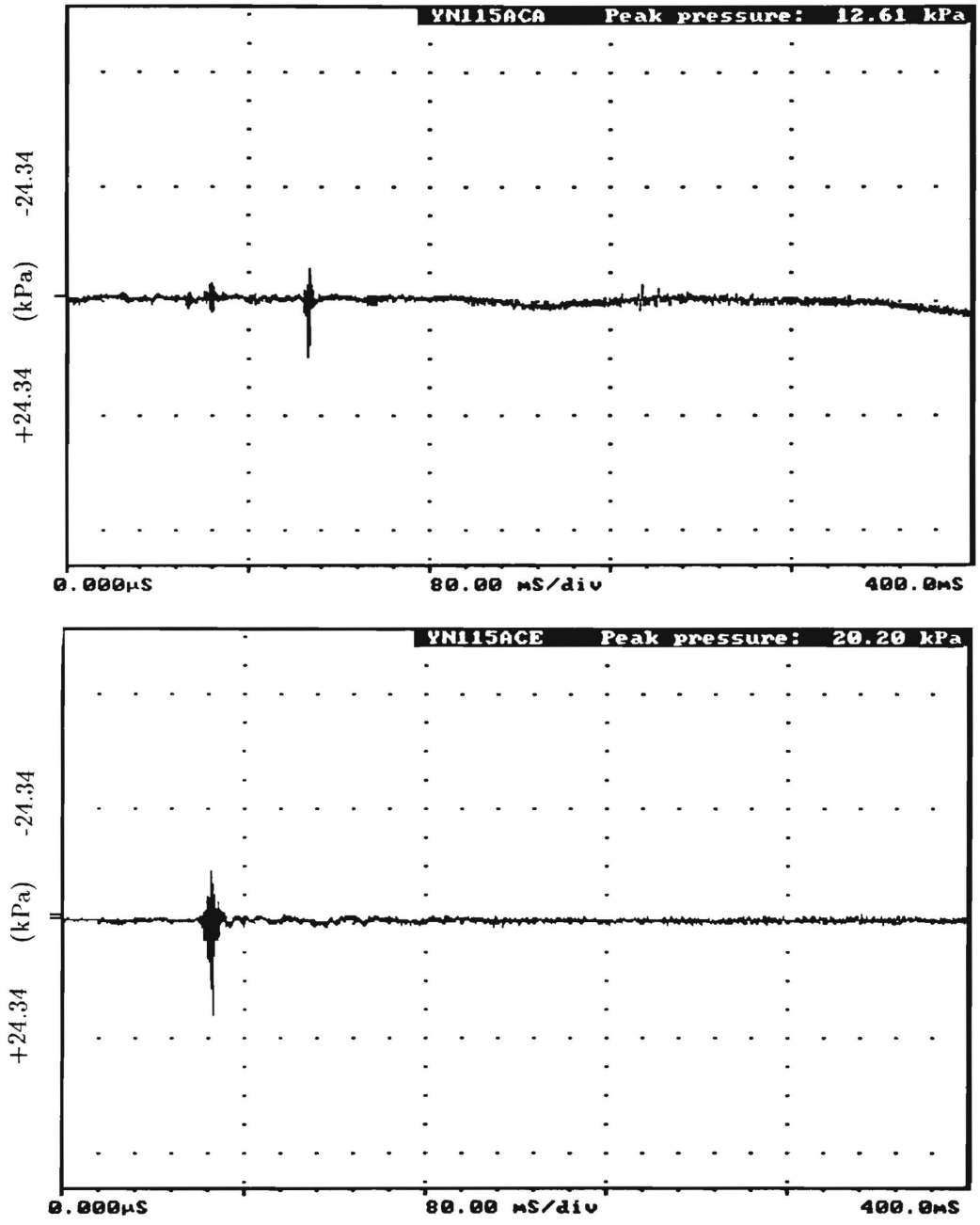

Figure D.37: Transient pressure signals for two experiments using glycerol with η_r=2.97 and T_{tin}=1000°C. The vertical scale for each graph is 1 volt/division (24.34 kPa/division). Values of the peak pressures are indicated on each graph.

Appendix E:
Particle Size Distribution Measurements

E Particle Size Distribution Measurements

NOTES

This appendix contains graphs of the cumulative mass percentage versus debris particle diameter for selected experiments. The transient pressure signals for all of the experiments included in these tests are given in the preceding appendix. In general, two experiments were selected from each of the series of ten experiments performed using a given coolant additive, tin temperature, and viscosity. The two experiments were selected so that the peak pressure for the first was near the average of the ten values for that series and the peak pressure for the second was the maximum obtained for the series. On each graph the results for one of the experiments with water is included as a reference of comparison (the heavy solid line). The peak pressure for the reference experiment was near the average value for its series. The water experiments used as reference lines in the graphs below were:

T_{tin} = 1000°C:	WN911ADD
900°C:	WN914BDC
800°C:	WN917CDC
700°C:	WN919DDI
600°C:	WN922EDH

Peak pressures for the experiments included in this section are given in Appendix C.

Water, T_{tin}=600–1000°C

Experiments with peak pressures near the average value for series:

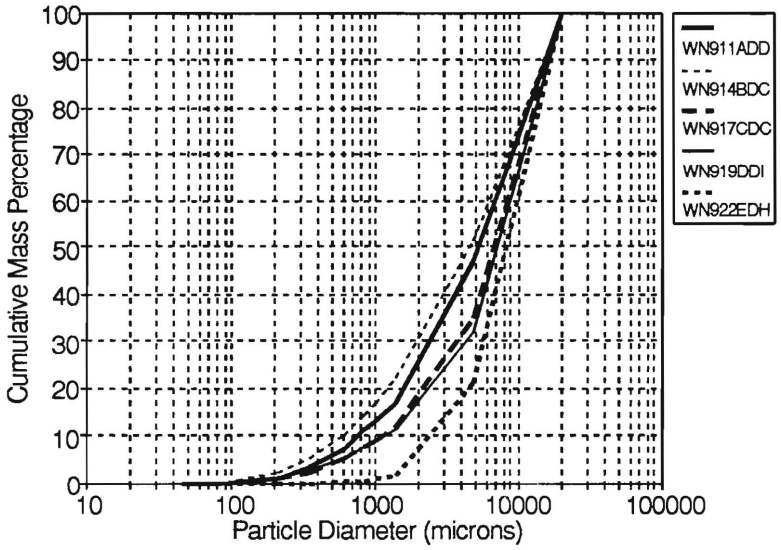

Experiments with peak pressures near the maximum value for series:

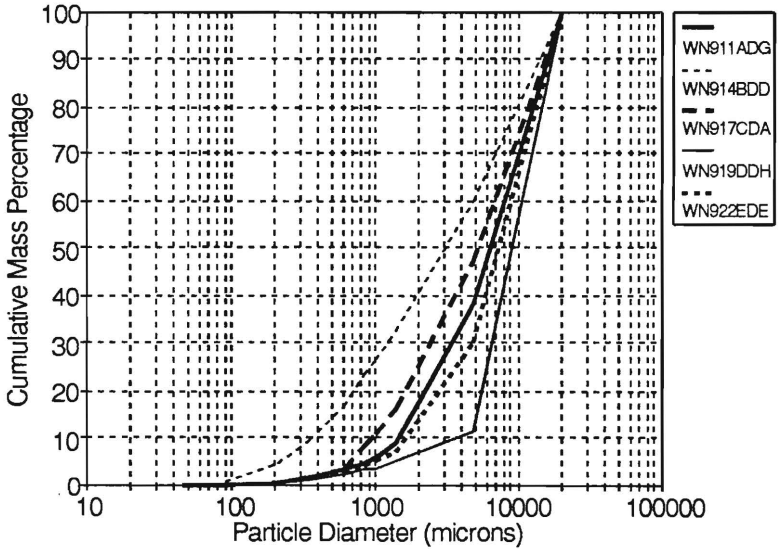

Figure E.1: Particle size distributions for representative experiments in water.

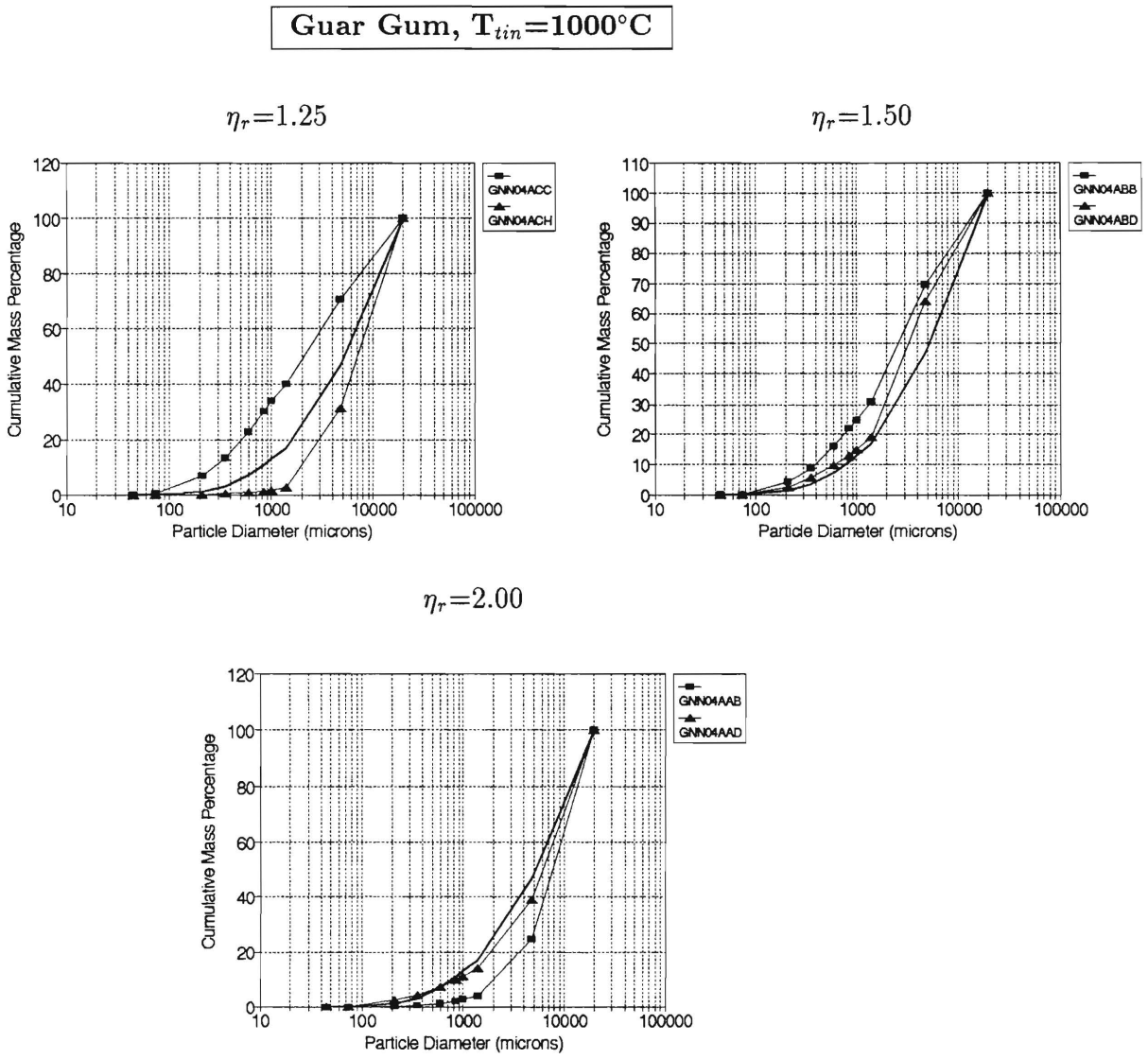

Figure E.2: Particle size distributions for representative experiments in guar gum solutions.

Hydroxyethyl Cellulose, T_{tin}=1000°C

η_r=1.25

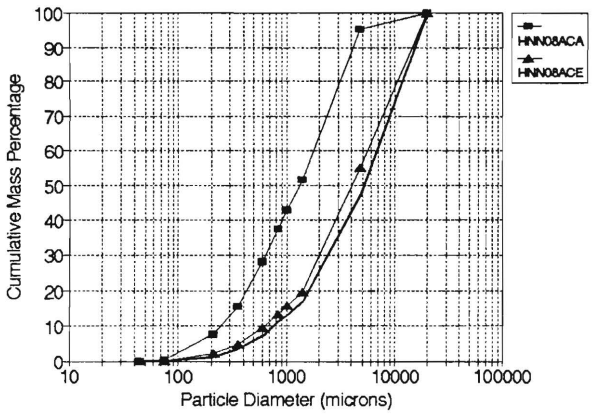

η_r=1.50

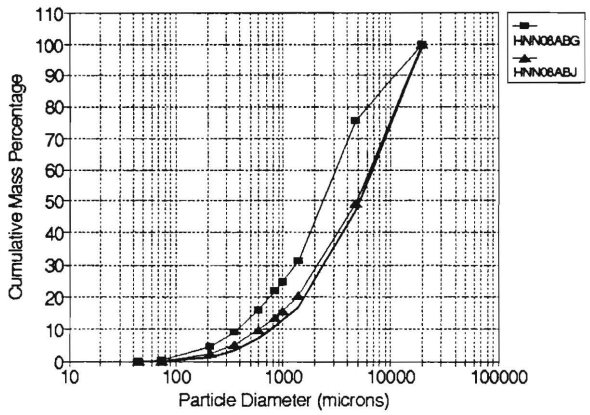

η_r=2.00

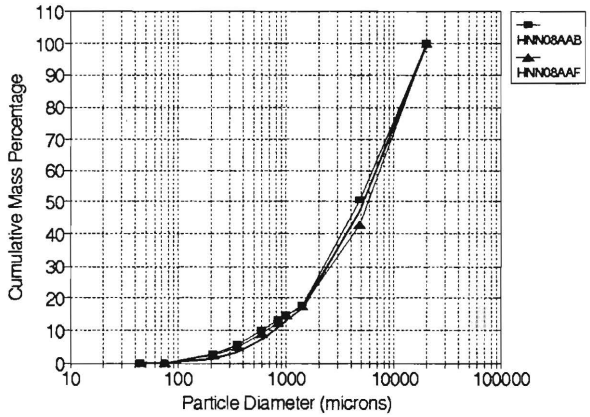

Figure E.3: Particle size distributions for representative experiments in hydroxyethyl cellulose solutions.

Poly(acrylamide/sodium acrylate), T_{in}=1000°C

η_r=1.25

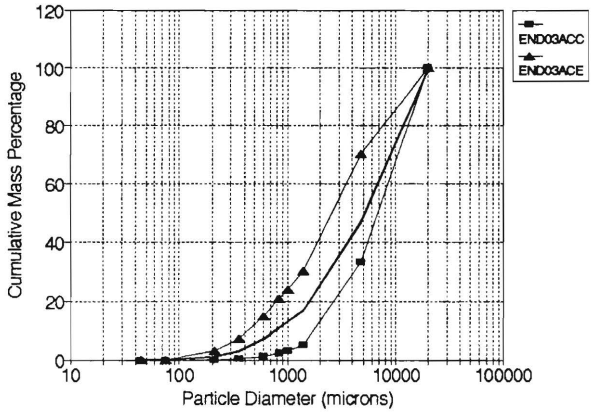

η_r=1.50

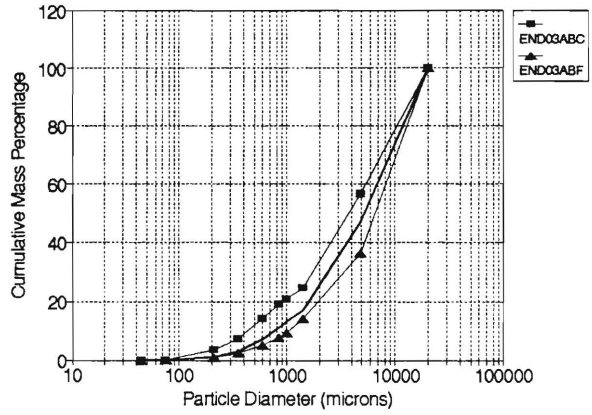

η_r=2.00

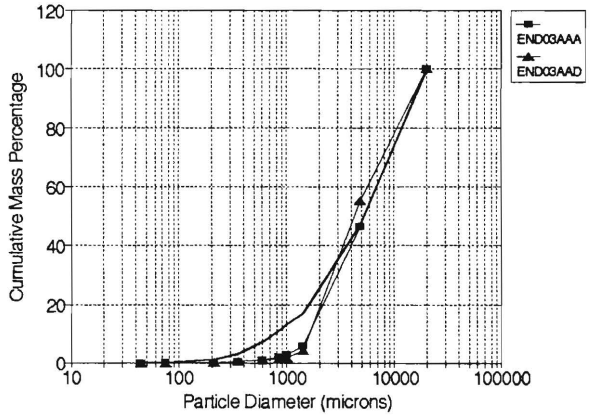

Figure E.4: Particle size distributions for representative experiments in poly(acrylamide/sodium acrylate) solutions.

Poly(ethylene oxide), T_{tin}=1000°C

η_r=1.01

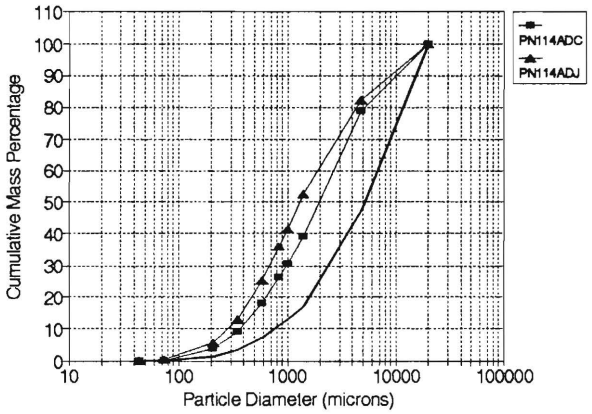

η_r=1.02

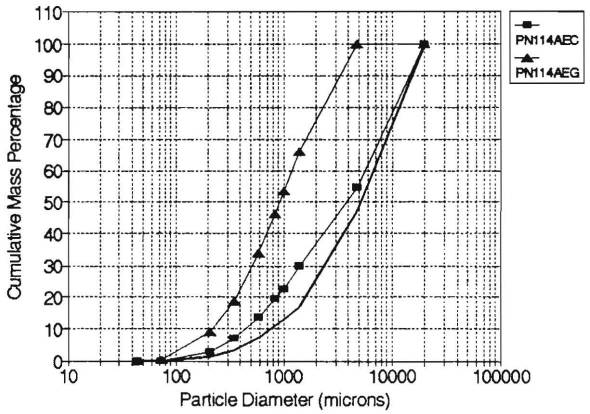

η_r=1.07

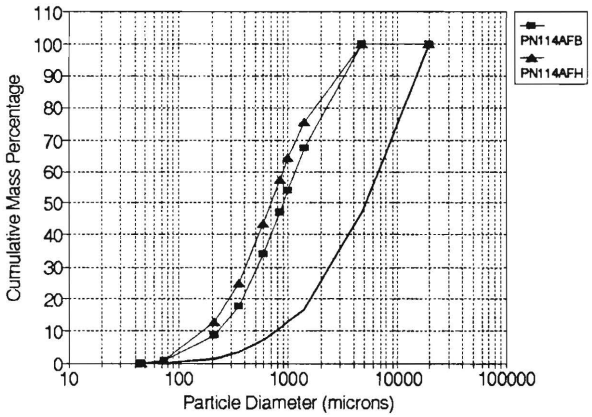

η_r=1.13

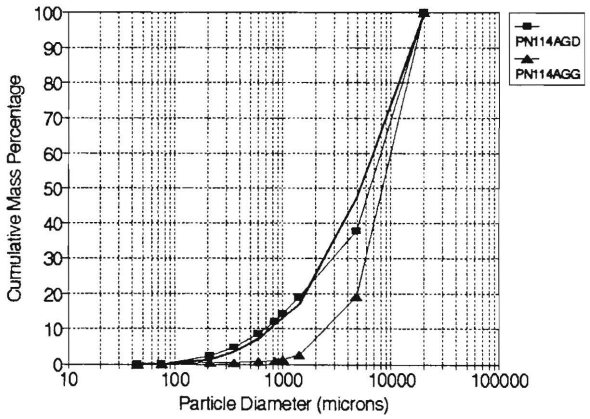

Figure E.5: Particle size distributions for representative experiments in poly(ethylene oxide) solutions.

Poly(ethylene oxide), T_{tin}=1000°C

η_r=1.25

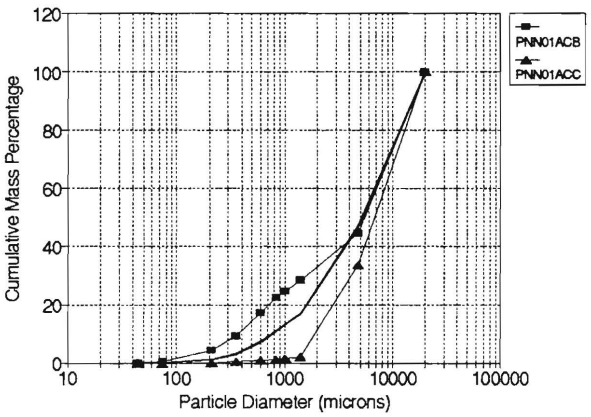

η_r=1.50

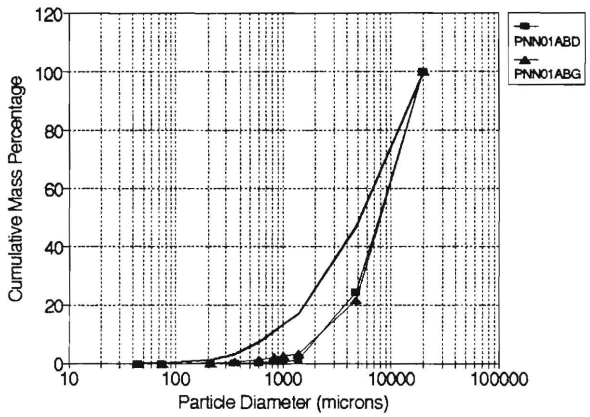

η_r=2.00

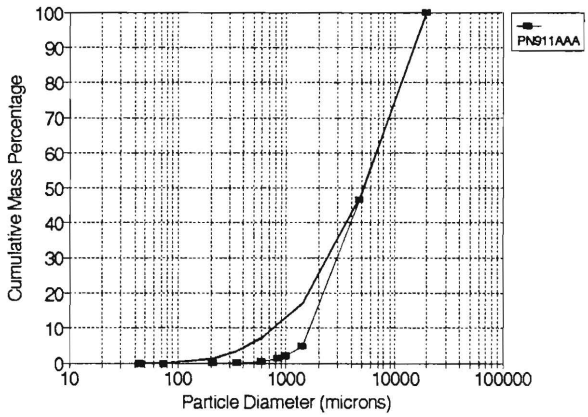

Figure E.6: Particle size distributions for representative experiments in poly(ethylene oxide) solutions.

Poly(ethylene oxide), T_{tin}=900°C

η_r=1.25

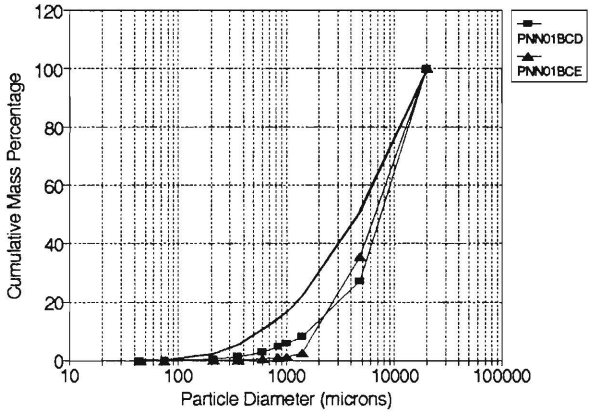

η_r=1.50

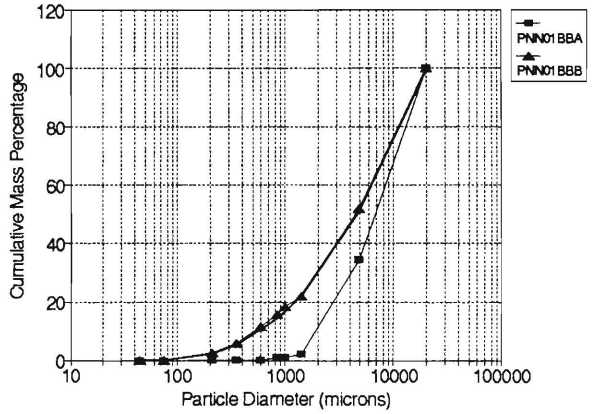

η_r=2.00

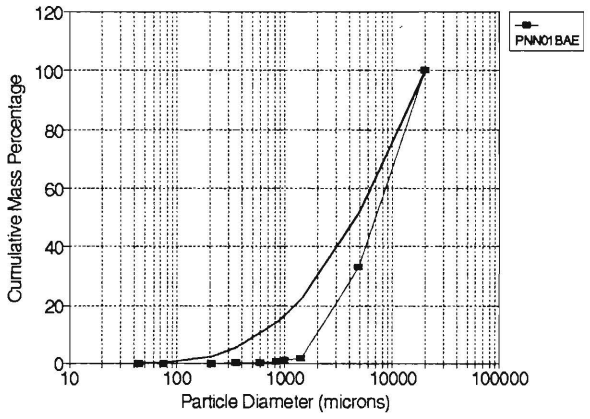

Figure E.7: Particle size distributions for representative experiments in poly(ethylene oxide) solutions.

Poly(ethylene oxide), T_{tin}=800°C

η_r=1.25

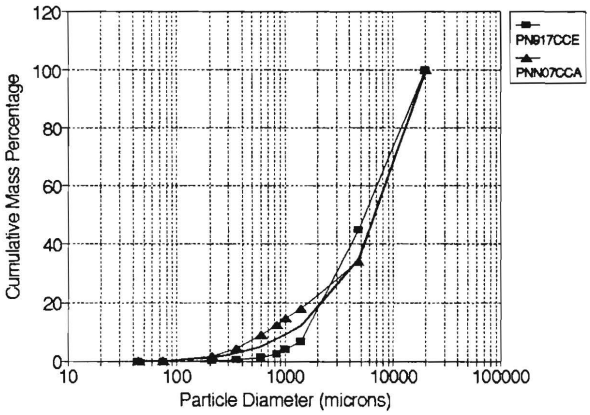

η_r=1.50

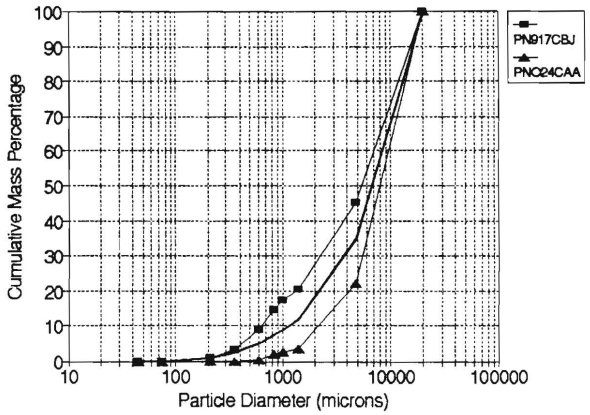

η_r=2.00

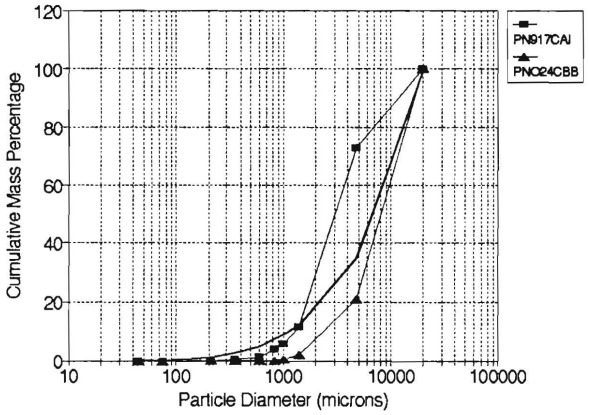

Figure E.8: Particle size distributions for representative experiments in poly(ethylene oxide) solutions.

Poly(ethylene oxide), T_{tin}=700°C

η_r=1.25

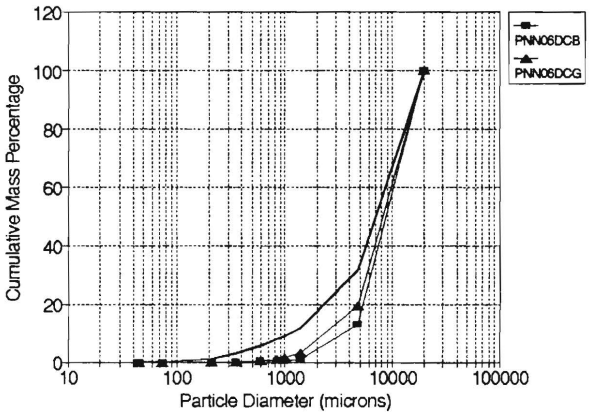

η_r=1.50

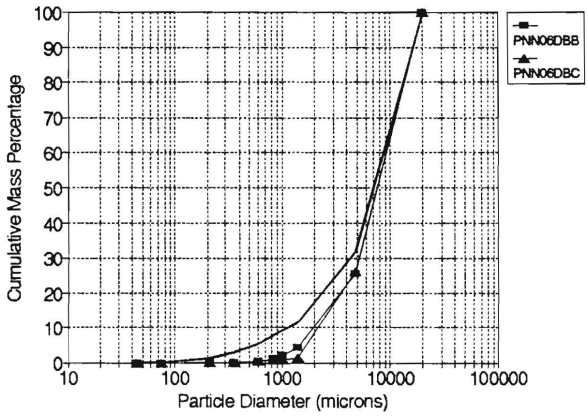

η_r=2.00

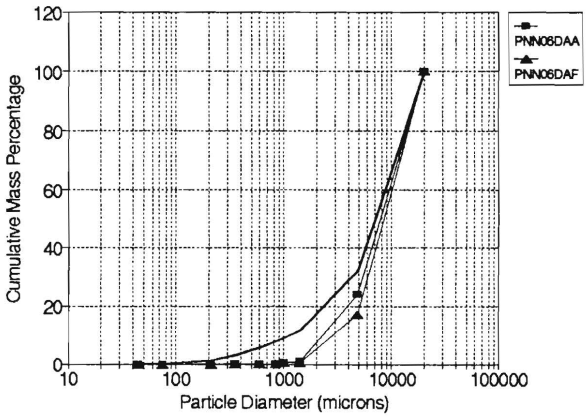

Figure E.9: Particle size distributions for representative experiments in poly(ethylene oxide) solutions.

Poly(ethylene oxide), T_{tin}=600°C

η_r=1.25

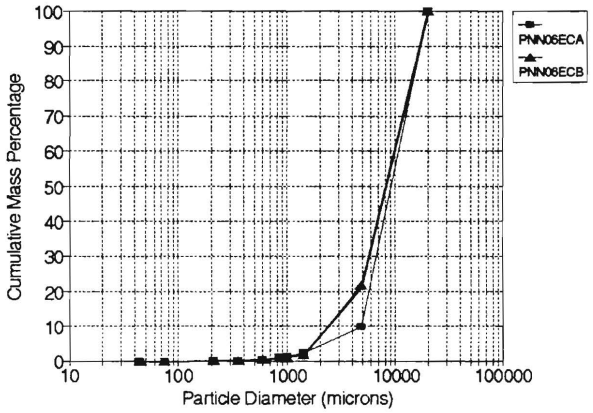

η_r=1.50

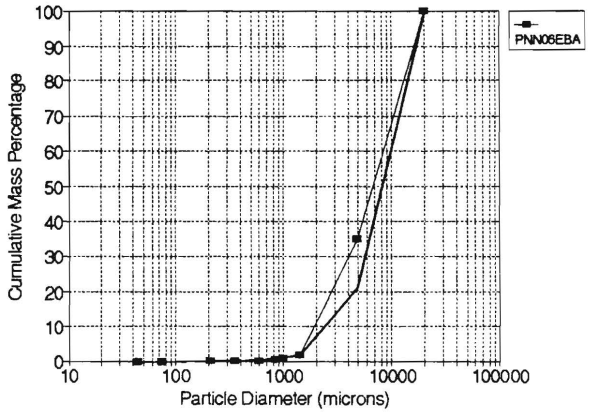

η_r=2.00

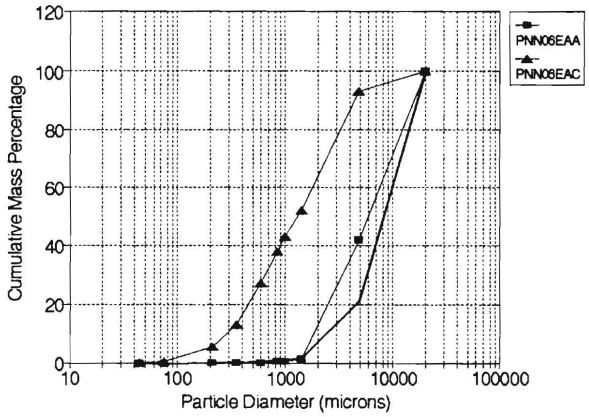

Figure E.10: Particle size distributions for representative experiments in poly(ethylene oxide) solutions.

Glycerol, T_{tin}=1000°C

η_r=1.68

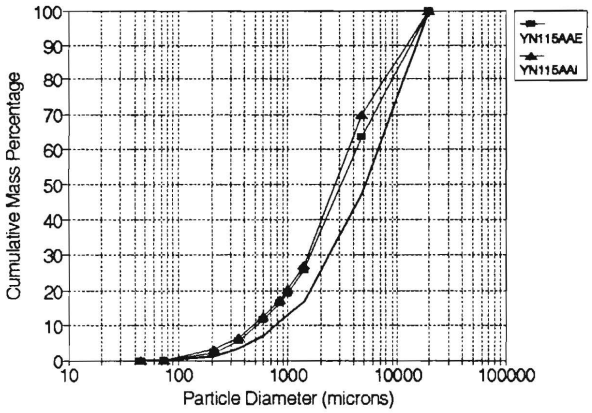

η_r=1.94

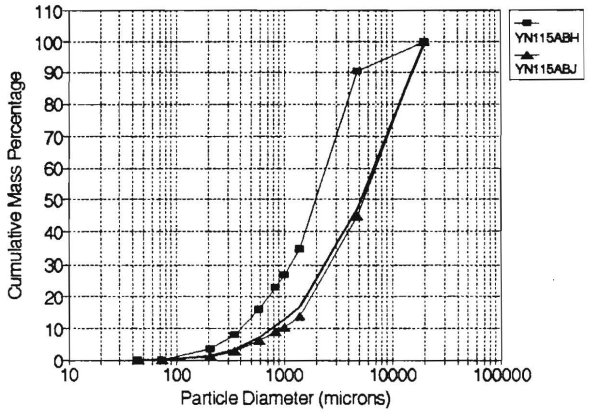

η_r=2.97

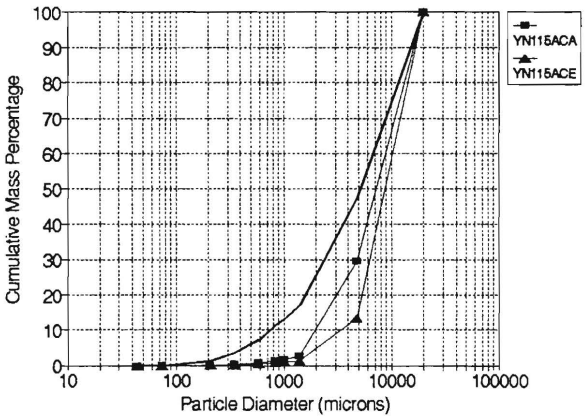

Figure E.11: Particle size distributions for representative experiments in glycerol solutions.

References

[1] Epstein S. G. and Miller R. E. "Causes and Prevention of Molten Aluminum/Water Explosions," *Light Metals 1987*, The Metallurgical Soc. of AIME, Warrendale, PA, p. 693 (1987).

[2] Cronenberg M. L. and Benz R., "Vapor Explosion Phenomena with Respect to Nuclear Reactor Safety Assessment," *Adv. Nucl. Sci. Technol.*, **12**,247 (1980).

[3] Heuser F.W. and Werner W.F., "Final Version of German Phase B," *Nuclear Engineering International*, **35**, 17 (1990).

[4] Farawila, Y.M., Abdel-Khalik, S.I., "A Literature Survey of Vapor Explosion Phenomena," GTRSR-001, Georgia Institue of Technology Report submitted to E.I. duPont Company (1988).

[5] Nelson L., Duda P. M., Frohlich G. and Anderle M. "Photographic Evidence for the Mechanism of Fragmentation of a Single Drop of Melt in Triggered Steam Explosion Experiments", *J. Non-Equilib. Thermodynam.*, **13**, 27 (1988).

[6] Koerber H. and Schuz G., "Contribution of Steam Explosions to the Source Term," *Source Term Evaluation for Accident Conditions*, IAEA, Vienna (1986).

[7] Board S.J., Hall R.W., Hall R.S., "Detonation of Fuel-Coolant Explosions." *Nature*, **254**, 319 (1975).

[8] Kim H. and Corradini M.L., "Modeling of Small-Scale Single Droplet Fuel/Coolant Interactions," *Nuclear Science and Engineering*, **98**, 16 (1988).

[9] Nelson L.S. and Duda P.M. "Steam Explosion Experiments with Single Drops of Iron Oxide Melted with a CO_2 Laser", NUREG/CR-2295, SAND81-1346 R3 (1981).

[10] Nelson L.S. and Duda P.M. "Steam Explosion Experiments with Single Drops of Iron Oxide Melted with a CO_2 Laser," *High Temperatures-High Pressures*, **14**, 259 (1982).

[11] Nelson L.S. "Steam Explosion Studies with Single Drops of Molten Refractory Materials", ANS/European Nuclear Society Topical Meeting: Thermal Reactor Safety, Knoxville, TN., CONF-800403, p. 226 (June 1980).

[12] Nelson L.S. and Duda P.M. "Steam Explosion Experiments with Single Drops of Iron Oxide Melted with a CO_2 Laser. Part II: Parametric Studies", NUREG/CR-2718, SAND82-1105 R3 (1985).

[13] Frölich G. and Anderle M., report IKE2-51, Institut für Kernenenergetik und Energiesysteme, Universität Stuttgart, Stuttgart, FRG (1980).

[14] Corradini M.L., "Analysis and Modelling of Steam Explosion Experiments," Sandia National Laboratories, Albuquerque, NM, NUREG/CR-2072, SAND80-2131 (1981).

[15] Nelson L. and Guay K.P. "Suppression of Stream Explosions in Tin and Fe-Al_2O_3 Melts by Increasing the Viscosity of the Coolant," *High Temperatures-High Pressures*, **18**, 107 (1986).

[16] Kim H. "Single Droplet Vapor Explosion Experiments", Ph.D. Thesis, University of Wisconson-Madison (1987).

[17] Flory K., Paoli R. and Mesler R. "Molten Metal-Water Explosions," *Chem. Eng. Progress*, **65**, 50 (1969).

[18] McCracken G.M. "Investigation of Explosions Produced by Dropping Liquid Metals into Aqueous Solutions", *1972 UKAEA Safety Research Bulletin of the Safety and Reliability Directorate*, **11**, 20 (1973).

[19] Nelson, H.W., and Norton, C.L., "Method of Preventing Smelt-Water Explosions," U.S. Patent No. 3,447,895.

[20] Paul D.D. "Nucleate Boiling in Drag-Reducing Polymer Solution," Ph.D. Thesis, University of Wisconsin-Madison (1983).

[21] Kopchaphakdee, P. and Williams, M.C., "Enhancement of Nucleate Pool Boiling with Polymeric Additives," *Int. J. Heat Mass Transfer*, **13**, 835 (1970).

[22] Rouai, N.M., "Effect of Additives on Pool Boiling of Water," Masters Thesis, UW-Madison (1982).

[23] Bailey, F.E., and Koleske, J.V., *Poly(ethylene oxide)*, Academic Press, Inc. (London) Ltd. (1976).

[24] Georgelos, P. and Torkelson, J.,"The Role of Solution Structure in Apparent Thickening Behavior of Dilute PEO/Water Systems," *J. Non-Newtonian Fluid Mech.*, **25**, 157 (1987).

[25] Dullforce T.A., Buchanan D.J. and Peckover R.S. "Self-Triggering of Small-Scale Fuel-Coolant Interactions: I. Experiments", *J. Physics D.*, **9**, 1295 (1976).

[26] Arakeri V.H., Catton I. and Kastenberg W.E. "Interaction of Molten Tin with Water: Effect of Temperature Stratification in the Coolant", *Trans. Am. Nucl. Soc.*, **22**, 415 (1975).

[27] Anderson R.P. and Armstrong D.R. "Experimental Study of Small Scale Explosions in an Aluminum-Water System", ASME, HTD-Vol. 19, p. 31 (November 1981).

[28] Jeun Gyoodong "Nucleate Boiling in Drag-Reducing Polymer Solutions", Ph.D. Thesis, University of Wisconsin-Madison (1986).